THE ROLE OF APOPTOSIS AND MITOSIS IN LDL TRANSPORT ACROSS ENDOTHELIAL CELL MONOLAYERS

by

LIMARY M. CANCEL

A dissertation submitted to the Graduate Faculty in Biomedical Engineering in partial fulfillment of the requirements for the degree of Doctor of Philosophy, The City University of New York

2010

© 2010

LIMARY MELISSA CANCEL

All Rights Reserved

This manuscript has been read and accepted for the
Graduate Faculty in Engineering in satisfaction of the
dissertation requirement for the degree of Doctor of Philosophy.

	Professor John M. Tarbell
April 27, 2010	
Date	Chair of Examining Committee
	Professor Mumtaz Kassir
April 27, 2010	
Date	Executive Officer

Professor Sheldon Weinbaum

Professor Bingmei Fu

Professor David S. Rumschitkzi
Supervisory Committee

THE CITY UNIVERSITY OF NEW YORK

Abstract

THE ROLE OF APOPTOSIS AND MITOTIS IN LDL TRANSPORT ACROSS ENDOTHELIAL CELL MONOLAYERS

by

Limary M. Cancel

Adviser: Professor John M. Tarbell

We have previously shown that leaky junctions associated with dying or dividing cells are the dominant pathway for LDL transport under convective conditions in vitro, accounting for more than 90% of the transport. To explore the role of apoptosis in the leaky junction pathway, TNFα and cycloheximide (TNFα/CHX) were used to induce an elevated rate of apoptosis in cultured bovine aortic endothelial cell (BAEC) monolayers and the convective fluxes of LDL and water were measured. Control monolayers had an average apoptosis rate of 0.30%. Treatment with TNFα/CHX induced a 18.3-fold increase in apoptosis and a 4.4-fold increase in LDL permeability (P_e). Increases in apoptosis and permeability were attenuated by treatment with the caspase inhibitor Z-VAD-FMK. Water flux (J_v) increased by 2.7-fold after treatment with TNFα/CHX, and this increase was not attenuated by treatment with Z-VAD-FMK. Immunostaining of the tight junction protein ZO-1 showed that TNFα/CHX treatment disrupts the tight junction in addition to inducing apoptosis. This disruption is present even when Z-VAD-FMK is used to inhibit apoptosis, and likely accounts for the increase in water flux. We found a

strong correlation between the rate of apoptosis and the permeability of BAEC monolayers to LDL.

To explore the role of mitosis in the leaky junction pathway, the microtubule stabilizing agent paclitaxel was used to alter the rate of mitosis and the fluxes of LDL and water were measured. Control monolayers had an average mitosis rate of 0.029%. Treatment with paclitaxel (2.5mM) for 1.5, 3, 4.5 or 6 hours yielded increasing rates of mitosis ranging from 0.099% to 1.03%. P_e increased up to 5-fold, while J_v increased up to 3-fold over this range of mitosis rates. We found a strong correlation between the mitosis rate and both the convective LDL permeability and the water flux. These results demonstrate the potential of manipulating endothelial monolayer permeability by altering the rates of apoptosis and mitosis pharmacollogicaly. This has implications for the treatment of atherosclerosis.

Acknowledgements

I would like to thank my mentor, John M. Tarbell, for his guidance and support throughout my years in graduate school. I would also like to thank my colleagues at the BME department, especially my labmates Danielle Berardi, Veronica Lopez, ZD Shi, Maria Nikmanesh, Henry Qazi, Rishi Mathura, Ronny Amaya and Dr. Eno Ebong. Our lively scientific discussions have been a constant source of inspiration throughout my years of research work. For their friendship and moral support, a special thanks to Tieuvi Nguyen, Tabitha Kot, Suzy Bendezu, and Stewart Russell. Finally, I would like to thank my family for their love and support.

This work was supported by NIH Grant HL 57093.

Table of contents

List of Tables

List of Figures

Chapter 1: Introduction

I. Specific Aims

Atherosclerosis is a disease of the arteries in which fatty lesions develop within the blood vessel walls. It is characterized by the infiltration and accumulation of cholesterol into the subendothelial space. This is followed by a complex sequence of events involving platelets, macrophages, smooth muscle cells, and growth factors that produces growing lesions that eventually calcify. The lesions can narrow or completely occlude vessels leading to heart attack or stroke. According to the American Heart Association 2007 Heart and Stroke Statistical Update, cardiovascular diseases accounted for 36.3% of all deaths in the United States in 2004, and atherosclerosis constituted 75% of these (Rosamond, Flegal et al. 2007).

The initiating event in atherosclerosis is the transport of lipid, specifically low density lipoprotein (LDL), into the subendothelial space. There are three potential pathways for transport of macromolecules, such as LDL, across the endothelium: transcytosis in vesicles, paracellular transport through the breaks in the tight junction strand, and the so-called leaky junction pathway associated with cells undergoing mitosis or apoptosis. Previous in vivo (Chien, Lin et al. 1988; Lin, Jan et al. 1988; Lin, Jan et al. 1990) and theoretical (Weinbaum, Tzeghai et al. 1985) studies have supported the importance of the leaky junction pathway in LDL and albumin transport across the endothelium. In a recent study, our lab used an *in vitro* model consisting of bovine aortic endothelial cells (BAEC) plated onto porous, polyester filters to measure the fluxes of water, albumin and LDL through BAEC monolayers (Cancel, Fitting et al. 2007). The results of that study showed that leaky junctions are the dominant transport pathway for LDL under convective conditions, accounting for more than 90% of the transport.

In the present study we propose to use the same *in vitro* model to directly probe the role of cell turnover in LDL transport under convective conditions and assess the potential for reducing LDL permeability by reducing the rates of apoptosis and mitosis. This could lead to new approaches for treating atherosclerosis.

The specific aims of the proposed research are:

1. To test the hypothesis that apoptosis rate dictates, in part, the permeability of endothelial monolayers to LDL under convective conditions. We will measure the rate of apoptosis in endothelial monolayers *in vitro*. We will increase and reduce the rate of apoptosis pharmacologically and measure the effect of these manipulations on the permeability of LDL under pressure.
2. To test the hypothesis that mitosis rate dictates, in part, the permeability of endothelial monolayers to LDL under convective conditions. We will measure the rate of mitosis in endothelial monolayers *in vitro*. We will alter the rate of mitosis pharmacologically and measure the effect of these manipulations on the permeability of LDL under pressure.

II. Background and Significance

The first event in the cascade of processes leading to atherosclerotic lesion formation is lipid infiltration and accumulation within the arterial wall of lesion-prone sites (Schwenke and Carew 1989). Once it has penetrated the endothelium, the LDL binds to the intimal matrix and accumulates, forming liposomes. The LDL may become oxidized, either by endothelial cells (ECs) during uptake, or by interaction with smooth muscle cells (SMCs), macrophages or matrix components in the subendothelial space (Simionescu 2007). Oxidized LDL (oxLDL) acts as a chemotatic agent for monocytes, which adhere to the surface of the endothelium. As a result of lipid accumulation, ECs express vascular adhesion molecules (VCAM) which promote monocyte

adhesion (Li, Cybulsky et al. 1993). The monocytes then migrate through the endothelium and mature into macrophages. These macrophages express receptors that recognize modified forms of LDL including oxLDL. As macrophages ingest and accumulate lipids they become foam cells and form a fatty streak (Ross 1993). The release of growth factors and chemotactic factors from accumulating foam cells, platelets and ECs results in the recruitment of SMCs to the intima and their proliferation. The SMCs themselves also secrete chemotactic factors that recruit additional monocytes (Lefkowitz and Willerson 2001). As this process continues the lesion accumulates lipid, foam cells, macrophages, SMCs and connective tissue, expanding until it impinges on the flow of blood (Ross 1993).

As described above, the progression of atherosclerosis is a complex process and many questions remain unanswered. For the proposed research, however, we shall focus our attention on the first step of the process: lipid infiltration into the subendothelial space. In 1973 Ross formulated the response-to-injury hypothesis which stated that increased transport of LDL into the artery occurred in areas with a denuding endothelial injury (Ross and Glomset 1976). However, scanning electron microscopic studies demonstrated a continuous endothelial monolayer, even in areas of increased permeability to horseradish peroxidase (HRP) (Stemerman 1981) and LDL (Stemerman, Morrel et al. 1986). This led Ross to modify the response-to-injury hypothesis. Endothelial denudation was replaced with the idea that different risk factors (such as hypercholesterolemia, oxLDL, hypertension, diabetes and cigarette smoking) somehow lead to endothelial dysfunction (Ross 1993).

A relationship between enhanced endothelial permeability to LDL and the localization of atherosclerotic plaques is well established. Radiolabelled LDL injected intravenously was found to enter the aortic wall of dogs in a pattern similar to the accumulation of cholesterol in

experimental atherosclerosis (Duncan, Buck et al. 1963). Nielsen et al. found a strong correlation between LDL permeability of a certain aortic segment in normal rabbits and the cholesterol accumulation in the same segment after cholesterol feeding (Nielsen, Nordestgaard et al. 1992). In animal studies, lesion prone areas have been consistently detected before plaques become visible by their uptake of the protein-binding dye Evans Blue (Schwartz, Kelley et al. 1989). These lesion prone (blue) areas have also been shown to exhibit an enhanced permeability to albumin, LDL and cholesterol (Somer and Schwartz 1971; Bell, Somer et al. 1972; Fry, Herderick et al. 1993).

Despite the documented association of enhanced LDL permeability with the formation of atherosclerotic plaques, controlling endothelial permeability to LDL pharmacologically is not currently a strategy in the treatment of atherosclerosis. Current strategies involve the reduction of blood cholesterol levels using statins. The aims of the proposed research represent a fundamental step towards determining the feasibility of developing drugs that reduce endothelial permeability to LDL.

III. Low Density Lipoproteins (LDL)

All cells use and rely on cholesterol as building blocks to create the multiple membranes which cells use to both control internal water content, internal water soluble elements and to organize their internal structure and protein enzymatic systems (Alberts, Johnson et al. 2002). As it is insoluble in plasma, cholesterol in the blood is carried in the form of lipoproteins. The general structure of a lipoprotein includes a core consisting of a droplet of triacylglycerols and/or cholesteryl esters, and a surface monolayer of phospholipid, unesterified cholesterol and specific proteins (apolipoproteins).

LDL (Figure 1.1) is the cholesterol carrier most commonly found in the blood and in atherosclerotic lesions. High plasma levels of LDL have been causally linked to the development of atherosclerosis (Nielsen 1996). The LDL particle is spherical with an average diameter of 22 nm and a molecular weight of 3000kDa. It consists of a core of some 1,500 cholesteryl esters and 170 triglycerides surrounded by 800 molecules of phospholipids, 500 molecules of unesterified cholesterol, and a single apolipoprotein B-100 protein (Esterbauer, Gebicki et al. 1992). The apolipoprotein B-100 is necessary to bind to the cell surface receptors.

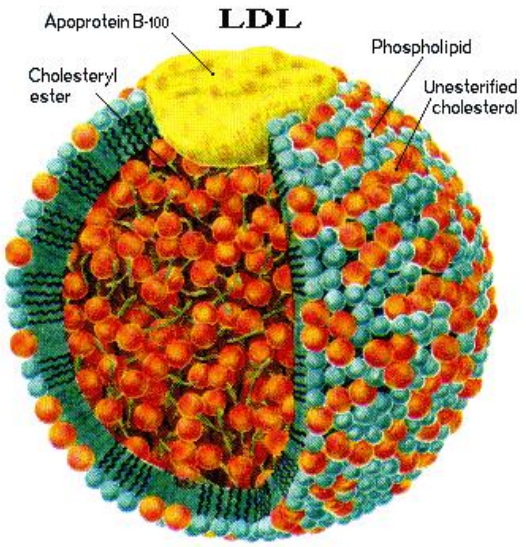

Figure 1.1 Structure of the LDL molecule. Image from http://bioch.szote.u-szeged.hu/astrojan/prot/Ldl.jpg

IV. Endothelium

The inner lining of all blood vessels is a thin layer of endothelial cells called endothelium. Endothelial cells play important roles in the regulation of blood pressure, blood vessel growth, and absorption of materials. Figure 1.2 shows a cross section of a normal arterial wall. The endothelial cell monolayer is directly in contact with the flowing blood and forms the first and principal barrier to the transport of nutrients and other components from the blood to the underlying tissue.

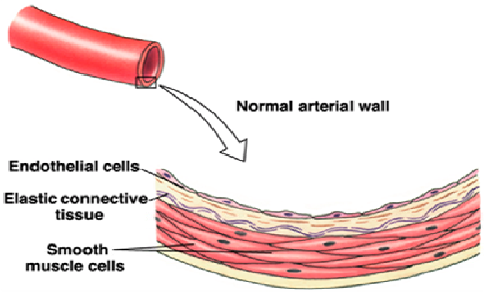

Figure 1.2. Cross-section of normal arterial wall. From (Silverthorn 2000).

The junctional complexes between endothelial cells give the endothelium its barrier characteristics and provide means of communication between the cells. Figure 1.3 is a schematic of the intercellular junction showing the three main types of junctions between endothelial cells: tight junctions, gap junctions and adherens junctions.

Tight junctions form the major barrier to the paracellular transport of solutes. This junction is the closest to the lumen side of the vessel and is formed by integral membrane adhesion proteins claudin and occludin. Occludin is a 65-kDa protein and claudin is a 22-kDa protein. Both contain two extracellular loops and four membrane-spanning regions. The cytoplasmic domain of claudins and occludins bind to ZO-1, which in turn binds to ZO-2. ZO-2 links the tight junction to cytoskeletal filaments including actin. Gap junctions are composed of arrays of small channels that permit small molecules to shuttle from one cell to another and thus directly link the interior of adjacent cells. The major proteins in gap junctions are the connexins. Six connexin molecules arranged into a hexagonal tube are called a connexon, which forms an aqueous pore roughly 2 nm in diameter between two cells. The main function of gap junctions is communication between cells (Alberts, Johnson et al. 2002).

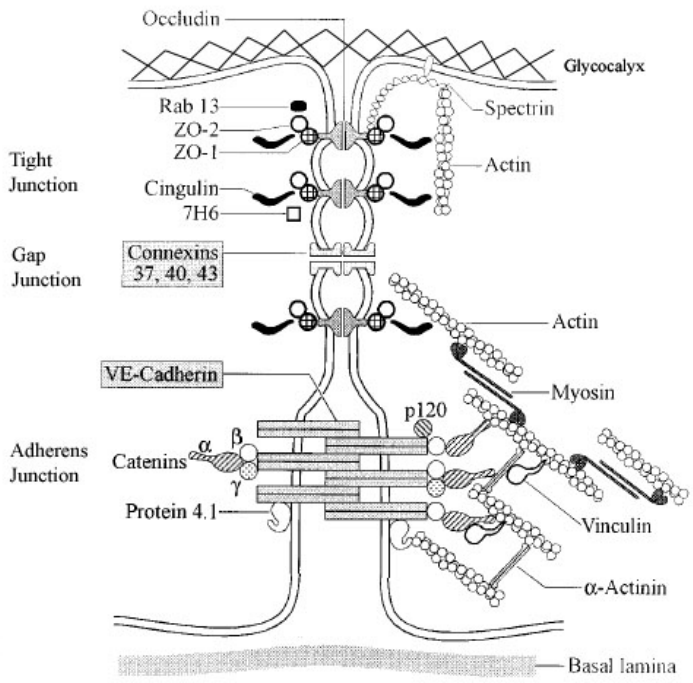

Figure 1.3. Endothelial juntional complexes. Adapted from (Michel and Curry 1999).

The adherens junction is an anchoring junction that binds cells together and connects the actin cytoskeleton to the plasma membrane. The calcium-dependent adhesion molecule VE-cadherin is the major transmembrane protein in this junction and consists of five extracellular 110-amino acid repeats, a transmembrane domain and a highly conserved cytoplasmic region. VE-cadherin attaches to actin cytoskeleton via the cytoplasmic proteins α, β, and γ-catenin (Dejana, Lampugnani et al. 2000).

In addition to the junctional complexes described above, the glycocalyx that covers the surface of endothelial cells and is believed to extend to the entrance of the intercellular junction also offers resistance to the transport of macromolecules. The glycocalyx is composed of glycosaminogycans (GAG), proteoglycans (PG), and glycolipids. Besides serving as a molecular filter restricting the passage of macromolecules, the glycocalyx also has a role in resisting the flow of water across the endothelium and in the transmission of fluid shear stress to endothelial cells. A review of the functions of the glycocalyx is given in (Weinbaum, Tarbell et al. 2007). An extensive description of the biochemical structure of the glycocalyx and its role in mechanotransduction is given in (Tarbell and Pahakis 2006).

V. Transport Pathways

There are three pathways for potential transport of macromolecules across the endothelium (reviewed in (Tarbell 2003)): transcytosis in vesicles, paracellular transport through the breaks in the tight junction strand, and the leaky junction pathway associated with cells undergoing mitosis or apoptosis. Figure 1.4 is a schematic of these three pathways or pores. The pathways are discussed in detail below. The tight junction itself is not an available transport pathway for macromolecules, but could carry small molecules. In addition to paracellular transport, water could also cross the endothelium through aquaporin channels. Aquaporin-1 water channels are expressed in microvascular endothelia of kidney, lung and skin, among others, as well as in tumor microvessels (Verkman 2006). Aquaporin-1 has also recently been found in rat aortic tissue and in bovine aortic endothelial cells *in vitro* (Nguyen, Toussaint et al. 2007). However, the physiological importance of water transport through aquaporins in the large vasculature remains uncertain.

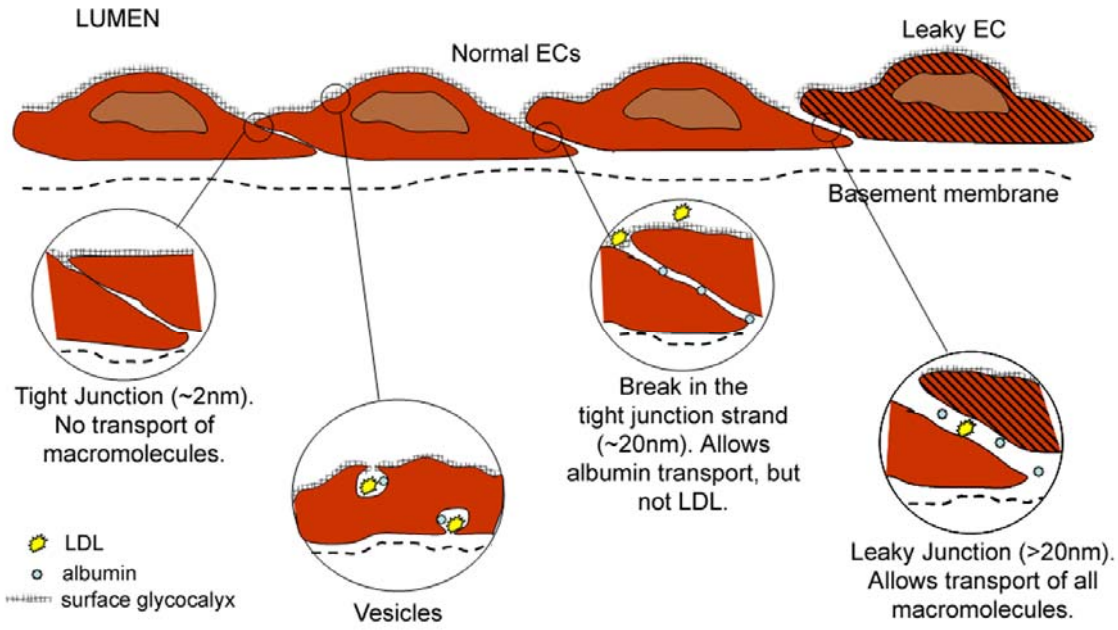

Figure 1.4. Endothelial transport pathways. Macromolecules can cross the endothelium through three pathways, or "pores". Pore 1 – vesicles allow both albumin (red) and LDL (yellow) transport and potentially include both non-specific and receptor-mediated transcytosis. Pore 2 – the break in the tight junction strand restricts passage of molecules larger than the width of the adherens junction. Pore 3 – the leaky junction allows passage of all macromolecules.

Vesicles

A major feature of continuous endothelium is the abundance of membrane-bounded vesicles in continuity with either the luminal or abluminal plasma membrane. Figure 1.5 is a TEM micrograph of our cultured endothelial cell monolayers showing numerous vesicles on the luminal side of the layer. These vesicles are known as caveolae and range in size from 50-70 nm diameter (Tuma and Hubbard 2003). The flask shape of caveolae is due in part to the structural protein caveolin, which coats the surface facing the cytosol. Caveolae may play a role in trancytosis, the transport of macromolecules from one side of the cell to the other within a membrane-bounded vesicle. In transcytosis, caveolae from the luminal side pinch off into the

cytoplasm, taking with them proteins and extracellular fluid. They then traverse the cytoplasm, fuse with the abluminal plasma membrane and release their contents outside the cell. In some cases, two or more caveolae fuse together to form a channel that directly connects the luminal and abluminal side of the endothelium and could serve as means of macromolecular transport (Simionescu, Siminoescu et al. 1975).

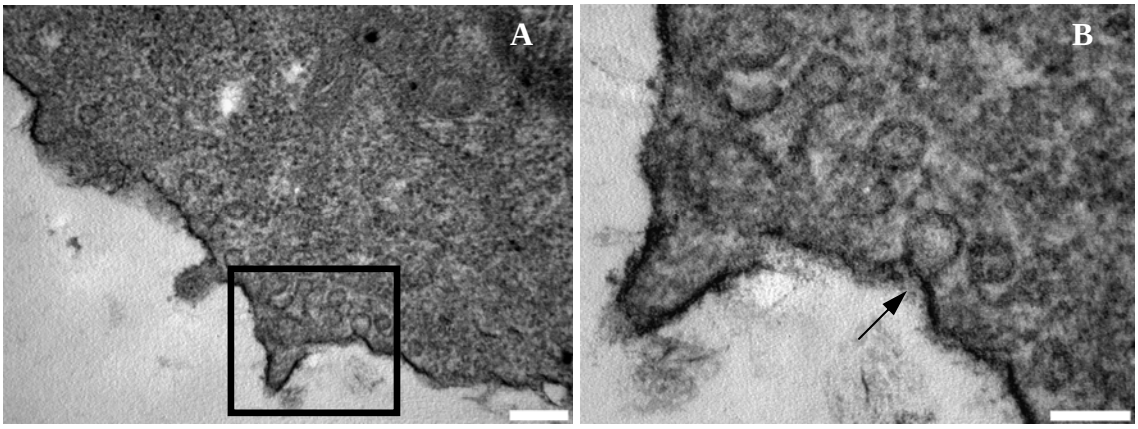

Figure 1.5. TEM micrographs of cultured endothelial cells. A) Vesicles on the luminal side of a cell. *bar = 200nm* B) Higher magnification of the boxed section in A showing a typical flask-shaped caveolae (arrow). *bar = 100nm*.

Endocytic vesicles may also play a role in macromolecular transport. These vesicles differ from caveolae in that they possess a thick coating of the protein clathrin and they contain specific receptors for different macromolecules. They also tend to be larger, with diameters up to 100 nm (Rippe, Rosengren et al. 2002). Endocytic vesicles are responsible for the uptake of cholesterol into endothelial cells. The cholesterol is bound to the LDL molecule, which in turn can bind to a receptor in the clathrin-coated vesicle. Once the vesicle is endocytosed, the cholesterol is delivered to endosomes and the receptors return to the plasma membrane (Alberts, Johnson et al. 2002).

Breaks in the Tight Junction Strand

Adamson and Michel (Adamson and Michel 1993) studied the ultrastructure of the intercellular junction in frog mesentery capillaries using serial sections and found discontinuities or "breaks" in the tight junction strand. The breaks had a mean length of 150 nm and a width in the order of 20 nm, similar to the wide part of the cleft. They also confirmed previous studies by Ward et al.(Ward, Bauman et al. 1988) and Bungaard (Bundgaard 1984) showing that even in the tight regions of the cleft the cell membranes are not fused, but separated by a small gap. Ward et al. and Bungaard, working with rat heart capillaries, observed a gap width of 4 and 5 nm, respectively. In frog mesentery capillaries, Adamson and Michel measured the gap at 2.3 nm. This gap could allow the passage of small molecules, but would restrict pressure driven water flux due to the large hydrodynamic resistance of small channels.

Figure 1.6 (adapted from (Fu, Curry et al. 1997)) is a conceptual model of the junction between endothelial cells. In this model, the cells are represented by two planes separated by a distance 2B (~20 nm). In the middle of the channel formed by the two cells is the tight junction strand, represented by solid walls that are separated by a small gap of height 2b (~1.5 nm). The break in the tight junction strand is seen as an opening of width 2d (~150 nm) in the middle of the strand. A fiber matrix representing the glycocalyx fills the lumen side of the channel between the cells. The fibers are spaced 7 nm apart and have a radius of 0.6 nm. The fiber matrix therefore serves as the primary molecular filter, and allows solutes up to the size of albumin to pass through. The model predicts that most of the water and macromolecule (up to the size of albumin) flux pass through the breaks in the tight junction strand.

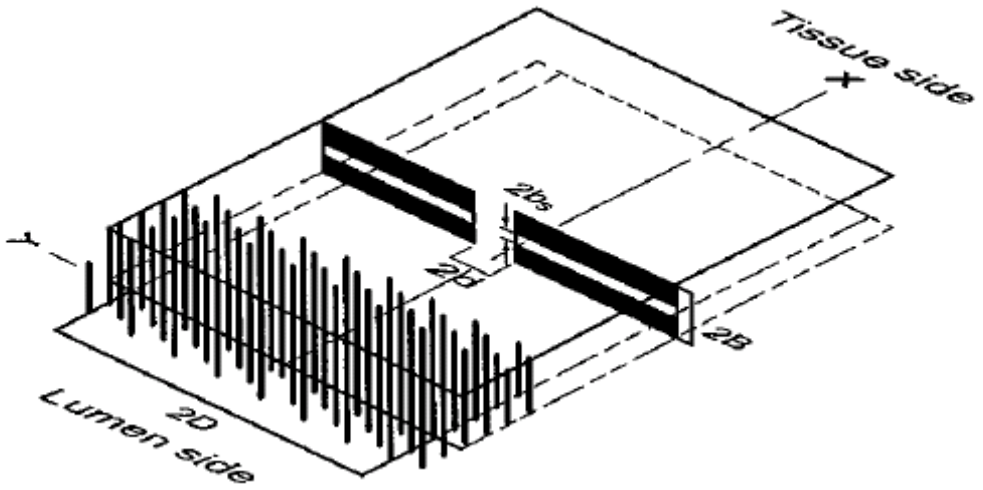

Figure 1.6. Conceptual model of the endothelial cell-cell junction. From (Fu, Curry et al. 1997)

Leaky Junction

It is unlikely that a normal endothelial junction, as described above, would permit the passage of LDL (22 nm diameter), even without the glycocalyx as a molecular filter, because the widest part of the junction is expected to be about 20 nm. Disruption to the endothelial junction can occur when cells are undergoing mitosis or when they are dying. Weinbaum et al. (Weinbaum, Tzeghai et al. 1985) proposed that these disrupted junctions were the primary pathway for LDL transport. Using a quantitative model, they showed that a small fraction of cells in the process of turnover (mitotic or dying) could account for a significant increase in permeability. Chen et al. (Chen, Jan et al. 1995) studied the ultrastructure of leaky endothelial junctions associated with mitotic or dying cells using electron microscopy. Leaky junctions around mitotic cells had a minimum width of 80 nm and a maximum width of 1330 nm. Around dying cells, leaky junctions had a minimum width of 15 nm and a maximum width of 1000 nm.

Another possible source of leaky junctions is the tricellular corner, where the borders of three endothelial cells intersect. Freeze-fracture (Walker, MacKenzie et al. 1994) and immunofluorescence (Burns, Walker et al. 1997) microscopy show that tight junctions are discontinuous at tricellular corners. Walker et al. (Walker, MacKenzie et al. 1994) studied the structure of tricellular corners in pulmonary capillaries using freeze-fracture electron microscopy and found intramembranous gaps with an average width of 27.4 nm and an average length of 1.1 μm. The tricellular regions were organized such that an overlapping flap provided by one of the cells covered the other two adjacent cells. In studies with human umbilical vein endothelial cells (HUVEC), immunofluorescence analysis revealed discontinuous staining of junction proteins, including occludin, ZO-1, cadherin and β-catenin, around the tricellular corner. In addition, transendothelial migration of neutrophils was found to occur preferentially at the tricellular corner (Burns, Walker et al. 1997). These studies suggest that tricellular corners might also constitute a leaky junction.

VI. Endothelial Transport Equations

Water flux across the endothelium is characterized by the following membrane transport equation (Kedem and Katchalsky 1958)

$$J_V = L_P\left(\Delta P - \sigma\Delta\pi\right) \quad (1)$$

where J_V is the volume flux across the endothelium, L_P is the hydraulic conductivity, ΔP is the pressure differential across the endothelium, σ is the reflection coefficient and $\Delta\pi$ is the osmotic pressure differential. Equation (1) is generally referred to as Starling's Law. It expresses Starling's hypothesis that fluid movement across capillaries is determined by the differences in hydrostatic and osmotic pressure across the capillary wall. Equation (1) predicts that when the

osmotic pressure gradient exceeds capillary pressure, such as in the venous end of the microcirculation, the net force driving water flux changes from positive (filtration) to negative (reabsorption). However, studies (Michel and Phillips 1987; Hu, Adamson et al. 2000; Pang and Tarbell 2003) have shown that reabsorption can occur transiently, but not on steady state basis. Michel (Michel 1997) and Weinbaum (Weinbaum 1998) proposed that the pressure and osmotic gradients (ΔP and $\Delta\pi$ in Equation (1), respectively) that determine water flux are not the global differences between plasma and tissue, but the local differences across the glycocalyx layer, which serves as the primary filter for plasma proteins. The theoretical model (Hu and Weinbaum 1999) shows that the protein concentration just behind the glycocalyx layer differs from that in the tissue because the convective flow through the break in the junction strand prevents back diffusion of protein from the tissue to the lumen.

Solute transport through a single pathway can be described using the following relationships (Patlak, Goldstein et al. 1963)

$$P_e = P_0 Z + (1-\sigma) J_V \quad (2)$$

where P_0 is the diffusive permeability, P_e is the apparent permeability and it has been assumed that the concentration in the abluminal side of the endothelium is much less than that on the luminal side. The first term is the diffusive contribution and the second term is convective. The relative importance of diffusion to convection is determined by Z, defined as

$$Z = \frac{N_{P_e}}{\exp N_{P_e} - 1} \quad (3)$$

where N_{Pe} is the Peclet number defined as

$$N_{P_e} = \frac{J_V (1-\sigma)}{P_0} \quad (4)$$

If we allow for vesicular transport that is strictly diffusive (i.e. no water flux through vesicles), and two convective pathways (a pathway through the breaks in the tight junction and a leaky junction pathway) then the following 3-pore model equations arise

$$J_V = J_{V2} + J_{V3} \qquad (5)$$

$$P_e = P_{0v} + P_{02}Z_2 + J_{V2}(1-\sigma_2) + P_{03}Z_3 + J_{V3}(1-\sigma_3) \quad (6)$$

J_{vi} is the water flux through pore i ; P_{ov} is the diffusive permeability of the vesicular pathway ; P_{oi} is the diffusive permeability of pore i ; σ_i is the reflection coefficient of pore i and Z_i is defined by equations (3) and (4) with the appropriate subscripts for pore i. This model will be used in Chapter 4 to determine the contribution of each pore to the overall water and LDL transport for control experiments, as well as experiments in which apoptosis and mitosis rates are altered pharmacologically.

VII. Previous Studies of Macromolecular Transdendothelial Transport

In 1951, Pappenheimer et al. (Pappenheimer, Renkin et al. 1951) developed the pore theory of capillary permeability. The theory predicts that diffusion of small solutes across capillaries occurs through water-filled pores with a radius of ~4 nm. In 1956, Grotte (Grotte 1956) observed that the transport of dextrans larger than 4.5 nm in radius was only slightly affected by increases in molecular size. This led to the conclusion that a few large pores, with radius of 25-60 nm and representing 1 in 30,000 of the small pores, accounted for the transport of the larger molecules. The physiological equivalent to this large pore system is still the subject of controversy. As discussed earlier, the two main pathways available to a molecule the size of LDL are transcellular transport through vesicles (transcytosis), and paracellular transport through leaky junctions.

The evidence in favor of transcytosis is mostly based on morphological studies. Vasile et al. first studied the transport of LDL through vesicles in the rat aorta and coronary artery using electron microscopy (Vasile, Simionescu et al. 1983). By looking at tissue sections at increasing time intervals after LDL administration, they concluded that LDL was taken up by either receptor-mediated endocytic vesicles which delivered it to lysosomes for use by the ECs, or by plasmalemmal vesicles which delivered the LDL to the abluminal side. These processes occurred simultaneously and were distinguished only by the morphological features of the structures involved in each (e.g. coated pits, endosomes and lysosomes for endocytosis). It seems unlikely that receptor-mediated endocytosis plays a role in transendothelial transport of LDL, because a number of studies have shown LDL permeability is not affected by methylation of the apolipoprotein B in LDL, which makes it unrecognizable to receptors (Wiklund, Carew et al. 1985), or by saturation of the receptors (Bratzler, Chisolm et al. 1977; Wiklund, Carew et al. 1985).

Studies by Bungaard (Bundgaard 1984) and later by Huang et al. (Huang, Jan et al. 1992) revealed that a vast majority of the apparently free plasmalemmal vesicles seen in routine electron-microscopic sections were actually part of complex invaginations of the endothelial cell membrane. More recently, Rosengren et al. (Rosengren, Carlsson et al. 2004) studied the effect of cooling on the transport of LDL into the peritoneal cavity of rats *in vivo*. Because it is an active process, transcytosis is sensitive to temperature, whereas paracellular transport is not. Rosengren et al. found that the reduction in LDL transport was only slightly higher than what could be expected from the cooling-induced changes in mean arterial pressure and viscosity. They concluded that while a portion of LDL transport may occur through vesicles, most of the transport is paracellular in nature. While it is now generally accepted in the literature that

transcytosis in endothelial cells does occur, the quantitative significance of this pathway is still the subject of debate (Rippe, Rosengren et al. 2002; Predescu, Predescu et al. 2007).

In 1985, Weinbaum et al. proposed the leaky junction-cell turnover hypothesis, suggesting that the primary pathway for LDL transport was the transiently disrupted junctions around cells in a state of turnover (dying or dividing). The theoretical model (Weinbaum, Tzeghai et al. 1985) showed that although these leaky junctions would occupy less than 10^{-5} of the endothelial surface area, the permeability could increase by 50-100% due to experimentally observed variations in turnover in arteries. In the normal rabbit aorta, Stemerman et al. (Stemerman, Morrel et al. 1986) showed scattered foci with increased permeability to HRP. These foci were found to be less than 1 mm in diameter and have LDL concentration up to 47 times greater than the surrounding area. While the mechanism of leakage was not determined, this study demonstrated that endothelial denudation was not necessary to induce large increases in LDL uptake. Chien and coworkers (Chien, Lin et al. 1988; Lin, Jan et al. 1989; Lin, Jan et al. 1990) later examined the leakage of Evans Blue-albumin (EBA) and Lucifer yellow-LDL (LY-LDL) in association with dying and dividing cells in a series of studies in the rat aorta. Table 1.1 summarizes the results of these studies. In (Lin, Jan et al. 1989) and (Chien, Lin et al. 1988) aortic sections were stained with hematoxylin in order to identify cells in the M phase of the cell cycle using morphological criteria. Roughly 1 in 3000 cells were found to be mitotic, but nearly all of those had a leakage spot associated with it. The percentage of mitotic cells with associated leak is lower for LDL than for albumin. This is expected if the opening and closing of the junction as the cell enters and exits mitosis occurs gradually, from a normal spacing to a gap wide enough to allow passage of LDL. In this scenario, the mitotic cell would be leaky to a smaller molecule such as albumin for a longer period than to LDL (Lin, Jan et al. 1989). Mitotic

cells accounted for 30% of all the EBA leaks and 45% of all LDL leaks. Dying cells occurred with a higher frequency (0.48%) and accounted for 37% of all the EBA leaks (Lin, Jan et al. 1990). In the rabbit aorta, Truskey et al. (Truskey, Roberts et al. 1992) found that mitotic cells accounted for 25% of all regions of increased ^{125}I-LDL permeability, and that these sites had permeabilities 26 to 47% higher than regions of elevated permeability that were not associated with mitotic cells.

Table 1.1. Association of endothelial cell turnover with leakage of EBA and LY-LDL.

Tracer	**Mitotic Cells (%)**	**Mitotic Cells with Leak (%)**	**% of Total Leaks**
EBA[1]	0.014	99	30
LY-LDL[2]	0.032	80	45
Tracer	**Dying Cells (%)**	**Dying Cells with Leak (%)**	**% of Total Leaks**
EBA[3]	0.48	63	37

[1]Chien et al. 1988; [2]Lin et al. 1989; [3]Lin et al. 1990

The studies described above provide direct evidence in support of the leaky junction-cell turnover hypothesis. Indirect evidence comes from the observations that hemodynamic factors usually associated with the development of atherosclerosis, have also been shown to increase cell turnover. Atherosclerotic plaques tend to be localized in regions of low shear stress and disturbed flow (Ku, Giddens et al. 1985; Frangos, Gahtan et al. 1999; Malek, Alper et al. 1999). Several studies have demonstrated that high levels of steady shear stress reduce the rate of endothelial cell proliferation (Levesque, Nerem et al. 1990; Gooch, Dangler et al. 1997). An increase in shear stress has also been shown to reduce the rate of endothelial cell apoptosis (Dimmeler, Haendeler et al. 1996; Cho, Mitchell et al. 1997). Freyberg et al. (Freyberg, Kaiser et al. 2001) have shown that irregular flow conditions increase apoptosis rates. Wang et al. (Wang, Miao et al. 2006) showed that the mRNA level of Krüppel-like factor 2 (KLF-2)

increases after 24 hr exposure to pulsatile shear stress, which has a significant forward component, while it decreases after exposure to reciprocating shear stress, which has a minimal forward direction. KLF-2 has been shown to protect endothelial cells from pro-inflammatory (SenBanerjee, Lin et al. 2004) and apoptotic stimuli (eg. oxidized LDL) (Wang, Miao et al. 2006).

A recent study in our lab (Cancel, Fitting et al. 2007) demonstrated that leaky junctions are the dominant transport pathway for LDL under convective conditions *in vitro*. We used an *in vitro* model consisting of bovine aortic endothelial cells (BAEC) plated onto porous polycarbonate filters and measured the flux of albumin, water and LDL across the endothelial monolayers under diffusive and convective conditions. By comparing the flux of both solutes across normal and chemically fixed monolayers, we established the contribution of the vesicular pathway. Using the 3-pore model equations described above (equations 3 to 6) we determined the relative contribution of each pathway to the overall transport. Leaky junctions accounted for 90.9% of LDL transport, the remainder going through vesicles. Albumin was also preferentially transported through the leaky junction (44%) but had significant contributions from the break in the tight junction pathway (36%) and the vesicular pathway (20%). Water was transported mostly through the break in the tight junction (77.7%) with a portion going through the leaky junction (22.3%). These results are consistent with the *in vivo* observations that vesicles do not contribute significantly to LDL uptake in arteries (Wiklund, Carew et al. 1985; Rosengren, Carlsson et al. 2004) and that regions of enhanced uptake of Evans blue albumin are predictive of regions of enhanced LDL uptake (Schwartz, Kelley et al. 1989). To our knowledge, this remains the only study of LDL transport *in vitro* under convective conditions.

VIII. Molecular Biology of Apoptosis and Mitosis

The results of our previous study (Cancel, Fitting et al. 2007), as well as the documented association of the leaky junction with cell turnover described above, have motivated us to evaluate the potential for reducing LDL transport by manipulating the rates of endothelial cell mitosis and apoptosis pharmacologically. In the following sections a review of the molecular biology of these processes and the pharmacological agents available for their control is presented.

Apoptosis

Apoptosis, also called programmed cell death, is an important process that allows multicellular organisms to tightly control cell number to regulate homeostasis. In contrast to necrosis, in which the cells swell and burst due to acute injury, cells that undergo apoptosis die neatly, without damaging neighboring cells. Morphologically, apoptosis is characterized by cell shrinkage, membrane blebbing, chromatin condensation and DNA fragmentation.

The initiation and regulation of apoptosis is highly controlled by a family of proteolytic enzymes called caspases. Caspases are synthesized in the cell as inactive precursors (procaspases) which are usually activated by cleavage by other caspases. Activated caspases cleave and activate other procaspases, resulting in an amplifying proteolytic cascade. Caspases can be controlled by a variety of inhibitors, some originating from inside the cell, and some artificial inhibitors developed as research tools and as pharmaceutical agents to inhibit cell death *in vivo* (Ekert, Silke et al. 1999).

The process of apoptosis is controlled by a diverse range of cell signals which may originate within the cell (intrinsic or mitochondrial pathway), or outside the cell (extrinsic or death-receptor pathway) (Figure 1.7). The mitochondrial pathway is used in response to internal injury, such as DNA damage, and is regulated by the Bcl-2 family of proteins. Pro and anti

apoptotic Bcl-2 family members meet at the surface of mitochondria where they compete to regulate cytochrome c exit. Cytochrome c associates with Apaf-1 and then procaspase-9 to form the active form of caspase-9, which in turn activates caspase-3. The death-receptor pathway is activated by members of the death-receptor super family such as Fas and tumor necrosis factor (TNF). Once bound to its ligand, Fas forms a death inducing signaling complex which recruits procaspase-8 molecules. These are then activated by induced proximity. The active caspase-8 in turn activates caspase-3. The two pathways converge at the level of caspase-3 activation.

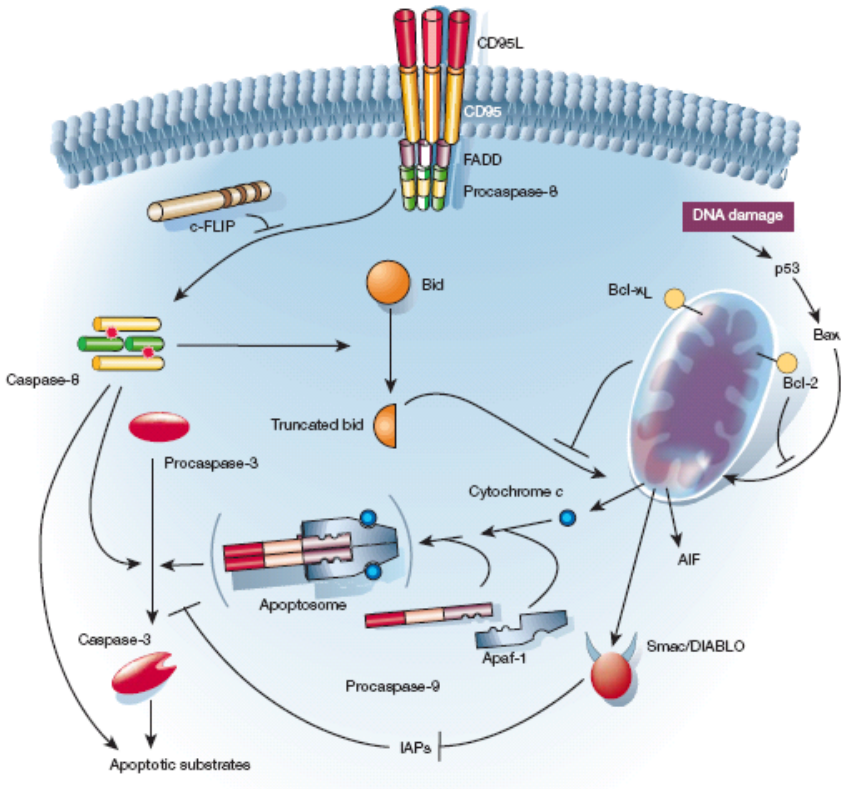

Figure 1.7. The two major apoptotic pathways. Adapted from (Hengartner 2000)

An important family of intracellular apoptosis regulators is the inhibitor of apoptosis (IAP) family. IAPs are believed to prevent apoptosis by binding and inhibiting caspases (Deveraux and Reed 1999). Among the proteins in this family is survivin, which has been

shown to efficiently reduce caspase-3 activity in ECs and block EC apoptosis induced by TNFα/cycloheximide (O'Connor, Schechner et al. 2000).

A number of synthetic caspase inhibitors have been developed for pharmacological use. Among these are Z-VAD-FMK, a broad-spectrum, irreversible inhibitor of caspases 1, 3, 4, and 7, and Ac-DEVD-CHO, a reversible inhibitor of caspase-3. Many more synthetic caspase inhibitors are available, and they differ in their potency, specificity, reversibility and membrane permeability. A review of caspase inhibitors, both cellular and synthetic, is presented in (Ekert, Silke et al. 1999).

Apoptosis agonists for endothelial cells have been described in the literature. Among them are serum deprivation (Hogg, Browning et al. 1999), ox-LDL (Lizard, Monier et al. 1999; Chen, Mehta et al. 2004), hypoxia (Wu, Parungo et al. 2004), transforming growth factor β (Hogg, Browning et al. 1999), TNFα (Polunovsky, Wendt et al. 1994; Spyridopoulos, Brogi et al. 1997; Csiszar, Ungvari et al. 2004) and cycloheximide (Polunovsky, Wendt et al. 1994). TNFα, a proinflammatory cytokine, is one of the most commonly used and studied apoptosis agonists in vascular cells. This is because TNFα has been shown to accumulate in areas of vascular injury (Barath, Fishbein et al. 1990) and may have an important role in the development of atherosclerosis (Choy, Granville et al. 2001).

Mitosis

A cell reproduces by performing a sequence of events in which it duplicates its contents and then divides in two. This cycle of duplication and division is known as the cell cycle (Figure 1.8). The two major phases of the cell cycle are the S phase and the M phase. DNA is duplicated during S phase, which requires 10-12 hours in a typical mammalian cell. Chromosome segregation and cell division occur in M phase, which typically lasts one hour.

Gap phases are inserted into the cell cycle to allow for growth and doubling of the cells proteins and organelles. The G_1 phase, between M phase and S phase, allows time not only for growth, but also for the cell to monitor its internal and external environment to ensure that conditions are suitable for the cell to commit to replication. In the absence of signals to proliferate, the cell cycle arrests. In some cases, cells exit from the cycle to a specialized, nondividing state called G_0. Most cells in our body are in G_0, but the molecular basis and reversibility of this state vary in different cell types (Alberts, Johnson et al. 2002).

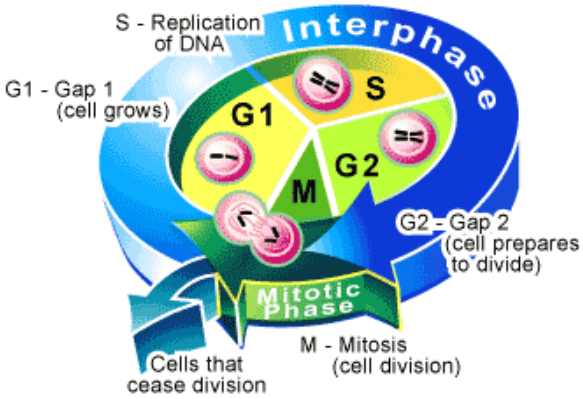

Figure 1.8. The cell cycle. Image from http://www.scq.ubc.ca/the-cell-cycle-a-universal-cellular-division-program/

The cell cycle culminates in M phase, which consists of nuclear division (mitosis) and cytoplasmic division (cytokinesis). M phase is divided into six stages, and mitosis constitutes the first five. The sixth stage is cytokinesis, which overlaps with the end of mitosis. During prophase, the replicated chromosomes condense and the cytoskeleton reorganizes. Prometaphase starts with the breakdown of the nuclear envelope. In metaphase, the chromosomes are aligned at the equator of the mitotic spindle, and in anaphase they are segregated to the two poles of the spindle. During telophase, the two sets of chromosomes arrive at the poles of the spindle and decondense. A new nuclear envelope reassembles around each set, completing the formation of two nuclei and marking the end of mitosis. Finally, during cytokinesis, the cytoplasm is divided in two by a contractile ring of actin and myosin filamens, which pinches the cell in two.

The events of the cell cycle are controlled by the cell-cycle control system, which consists of various cyclin-dependent kinases (Cdks). Cyclins, on which Cdks are dependent for their activity, undergo a cycle of synthesis and degradation in each cell cycle. Changes in cyclin levels result in the cyclic assembly and activation of the cyclin-Cdk complexes, which in turn trigger cell-cycle events. Cyclins are defined by the stage of the cell cycle at which they bind Cdks. There are four classes of cyclins: G_1-cyclins promote passage through the restriction point in late G_1; G_1/S-cyclins commit the cells to DNA replication; S-cyclins are required for the initiation of DNA replication; M-cyclins advance the events of mitosis (Alberts, Johnson et al. 2002).

In most cells there are several points in the cell cycle, called checkpoints, at which the cycle can be arrested if previous events have not been completed. The most important checkpoints are a G_2 checkpoint to enter mitosis, a metaphase checkpoint to exit mitosis, and a G_1 checkpoint to enter S phase. Passage through the G_1 checkpoint is stimulated by extracellular signals in animal cells. Mitogens are molecules that promote cell division, usually by acting in the G_1 phase of the cell cycle. Several growth factors are known to have mitogenic effect on endothelial cells. Among them are vascular endothelial growth factor (VEGF) (Ferrara and Davis-Smyth 1997), epidermal growth factor (EGF) (Raymond, Jumblatt et al. 1986; Shang, Konidari et al. 2001), and keratinocyte growth factor (KGF) (Gillis, Savla et al. 1999). One approach to reducing cell proliferation is through the use of drugs that inhibit growth factor receptors, such as Imatinib, which inhibits platelet derived growth (PDGF) factor receptors, and Gefitinib, which inhibits EGF receptors.

The importance of Cdks in cell cycle regulation and their frequent deregulation in cancer has encouraged an active search for agents capable of disturbing their functions. A variety of

selective low-molecular weight inhibitors of Cdks have been developed (Fabbro, Ruetz et al. 2002; Sridhar, Akula et al. 2006). These compounds reversibly arrest normal cells in either the G_1 phase or in the G_2/M transition, whereas cancer cells would arrest in G_2/M and eventually die by apoptosis.

Other types of cell-cycle arrest drugs act by disrupting microtubule formation and growth. They are termed antimicrotubule drugs (AMDs) and include the cancer therapy drugs Taxol and vincristine, and nocodazole. Because microtubules are essential in the formation of the mitotic spindle, these drugs arrest the cell-cycle in M-phase. However, studies have shown that in some mammalian cells arrest in M-phase is transient and the cells proceed into G_1-phase arrest without dividing (Hong, Chen et al. 1999).

IX. Transport System

Fluorometer

The flux of human LDL tagged with 1,1'-dioctadecyl – 3,3,3',3'-tetramethyl-indocarbocyanine perchlorate (DiI-LDL) was measured using an automated fluorometer system consisting of eight transport chambers, each of which was connected to a laser excitation source and an emission detector via optical fibers arranged in a 45° configuration (Figure 1.9).

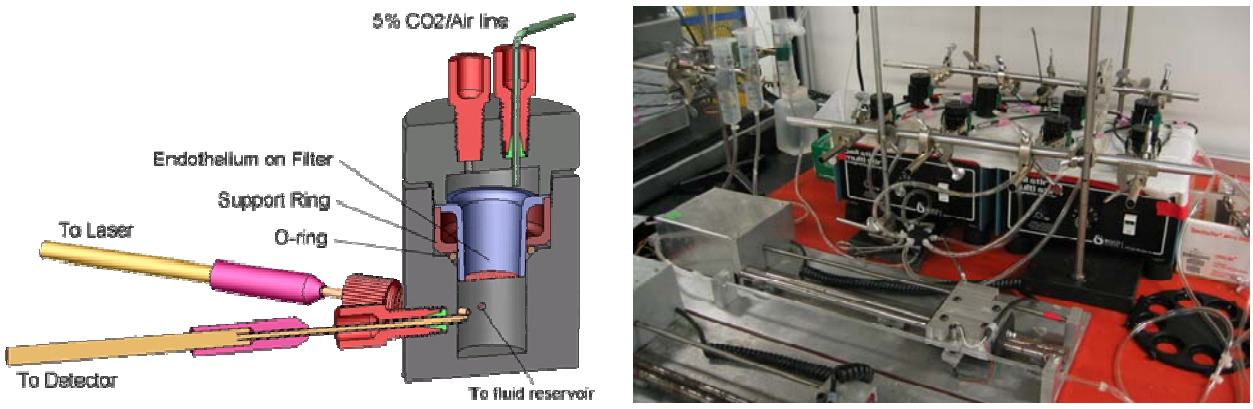

Figure 1.9. (A) Schematic of a transport chamber. (B) The entire transport system consisted of eight of these chambers.

Excitation light at 532 nm was provided by a 10-mW Crystal Laser. The laser beam first impinged on a mirror which deflected the light to one of eight 600-μm excitation fibers going into each chamber. The mirror rotated to sequentially illuminate all eight chambers, with a delay of 1 sec between chambers. The emission fibers were connected to a Model D48 photon counting detector from C&L Instruments (Hummelstown, PA) containing an interference filter that allows light at 571 nm to pass through. The *FluorMeasure* acquisition software and Model PC-DAQ control card (both from C&L Instruments) were used to control the laser exciter and detector, and for data acquisition.

A Transwell filter containing the BAEC monolayer was sealed within each chamber to form a luminal (top) and abluminal (bottom) compartment. An aluminum support ring and an o-ring helped create a tight seal within the chamber, while a magnetic stir bar in the abluminal chamber kept the fluid in this compartment well mixed. The abluminal compartment was connected to a fluid reservoir via tygon tubing. The reservoir could be lowered to apply a hydrostatic pressure differential across the monolayer. Both the luminal compartment and abluminal reservoir were continuously supplied with 5% CO_2-95% air to maintain the media at

physiological pH. The experimental apparatus, excluding the laser source and the emission detector were housed inside a Plexiglas box. A hairdryer attached to a temperature controller maintained the air temperature inside the box at 37°C.

Each filter was rinsed twice with experimental media (1% BSA in phenol red free MEM) prior to inserting into the chambers. A solution of 5μg/mL DiI-LDL was added to the luminal compartment. The abluminal compartment contained a trace amount of DiI-LDL (typically below 0.005 mg/mL) in order to maintain the linear relationship of concentration versus intensity. Each transport experiment consisted of a one hour equilibration period, followed by application of a 10-cm H_2O pressure differential and data collection for one hour, and finally two hours of data collection under diffusive conditions.

Bubble Tracker

The water flux was measured simultaneous to solute flux in two of the eight chambers. Each of these two chambers was connected via tygon tubing and borosilicate glass tubing to an abluminal reservoir. When a 10-cm H_2O differential pressure was applied, the water flux (J_v) was measured by tracking the position of a bubble that was inserted into the glass tube. The bubble was tracked using a spectrophotometer which followed the air-liquid interface in the glass tube (Figure 1.10).

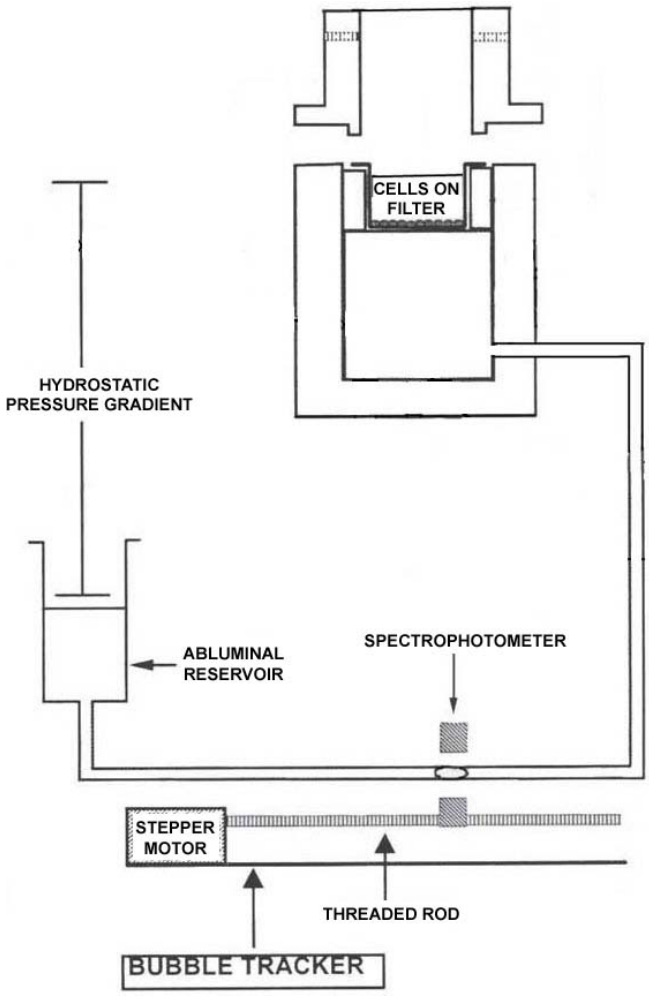

Figure 1.10. Schematic of the experimental setup for water flux measurement.

Calibration of Fluorometer System

To calibrate the fluorometer system, the intensities of ten solutions of known DiI-LDL concentration were measured in each of the eight chambers. Since the abluminal concentration during experiments ranged from 0 to ~0.1 μg/mL, a range of 0 to 0.15 μg/mL was used for the calibration. The intensity of 3 mL of solution was measured for 20 min to ensure that the measurement was stable. A calibration curve was created for each chamber using a linear regression of the concentration vs intensity (averaged over the 20 min) data. The calibration was repeated every time a new vial of DiI-LDL was used.

Calculation of Permeability (Pe) and water flux (Jv) values

The fluorescence intensity in the abluminal compartment was recorded for 10 seconds of every minute for the duration of the experiment. The intensity was converted to concentration by means of a calibration curve, and the permeability was calculated by

$$Pe = \frac{(\Delta C_a / \Delta t) \times V_a}{C_l \times A} \quad (7)$$

where $\Delta C_a / \Delta t$ is the change in abluminal concentration with respect to time, V_a is the fluid volume in the abluminal compartment, C_l is the concentration in the luminal compartment, and A is the area of the filter. $\Delta C_a / \Delta t$ was determined using a linear regression of the concentration versus time data over 50 min for the convective permeability (P_e), and over 100 min for the diffusive permeability (P_o) (Figure 1.11).

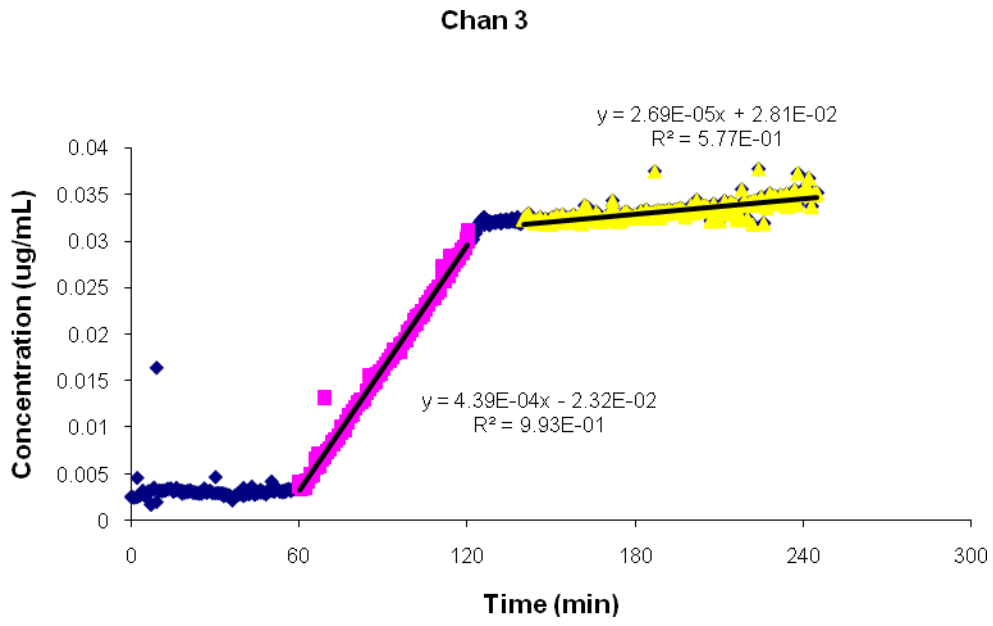

Figure 1.11. Typical concentration versus time plot for DiI-LDL transport experiment. Following a 1 hr equilibration period, a hydrostatic pressure differential was applied for 1 hr. After the pressure differential was taken off, the diffusive flux was measured for 2 hrs. Linear regressions of the data were used to compute the permeability.

The bubble displacement data was used to compute J_v values using the following equation

$$J_V = \frac{\Delta d}{\Delta t} \times \frac{F}{A} \quad (8)$$

where $\Delta d/\Delta t$ is the bubble displacement per unit time, A is the area of the Transwell filter and F is a tube calibration factor (fluid volume per unit length of tubing). The value of F for our glass tube was 0.0302 cm^2. Figure 1.12 shows a typical plot of the data obtained from the bubble tracker. During the first 20-30 minutes $\Delta d/\Delta t$ decreases with time. This is the typical sealing effect previously described by our lab (DeMaio, Tarbell et al. 2004). For J_v calculations, $\Delta d/\Delta t$ was computed for the last 30 minutes of pressure application.

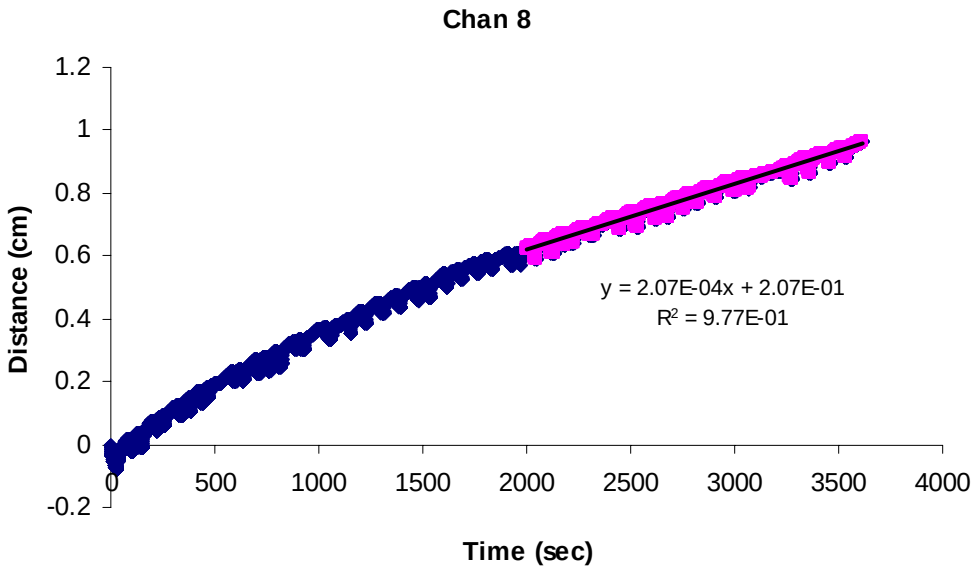

Figure 1.12. Typical distance versus time plot for water flux experiment. A linear regression of the data over the last 30 minutes was used to calculate Jv.

As noted, the aims of this work are to directly probe the role of the leaky junction in LDL transport and to assess the potential for reducing LDL permeability by reducing the rate of cell turnover pharmacologically. In Chapter 2 we investigate the role of apoptosis in LDL transport across endothelial monolayers. We use TNFα and cycloheximide to induce an elevated rate of apoptosis, and the broad caspase inhibitor Z-VAD-FMK to reduce the apoptosis rate. We find a strong correlation between the convective permeability of LDL and the rate of apoptosis. In Chapter 3 we turn our attention to the role of mitosis. Using the microtubule stabilizing agent paclitaxel to induce elevated rates of mitosis, we find strong correlations between mitosis and both the water flux and convective LDL permeability. Finally, in Chapter 4, we use our 3-pore model to analyze the data obtained and gain additional insight into the contribution of each pathway to the overall transport.

Chapter 2: The role of apoptosis in LDL transport through cultured endothelial cell monolayers

I. Introduction

Atherosclerosis is a disease of the large arteries in which fatty lesions develop within the blood vessel walls. The initiating event in atherosclerosis is the transport of lipid, specifically low density lipoprotein (LDL), into the subendothelial space (Schwenke and Carew 1989). Elevated permeability of vascular endothelium to LDL is characteristic of focal sites within the vasculature that are prone to the development of atherosclerosis (Nielsen, Nordestgaard et al. 1992). In animal studies, lesion prone areas have been detected consistently before plaques become visible by their uptake of the protein-binding dye Evans Blue (Schwartz, Kelley et al. 1989). These lesion prone (blue) areas have also been shown to exhibit an enhanced permeability to albumin, LDL and cholesterol (Somer and Schwartz 1971; Bell, Somer et al. 1972; Fry, Herderick et al. 1993). Despite the documented association of enhanced LDL permeability with the formation of atherosclerotic plaques, current strategies for the treatment of atherosclerosis focus on lowering LDL concentration in the blood (statins (1994; Shepherd, Cobbe et al. 1995; 1998)), not controlling endothelial permeability to LDL.

There are three potential pathways for transport of macromolecules, such as LDL, across the endothelium (reviewed in Tarbell (Tarbell 2003)): transcytosis in vesicles, paracellular transport through the breaks in the tight junction strand, and the so-called "leaky junction" pathway associated with cells undergoing mitosis or apoptosis. Weinbaum et al. (Weinbaum, Tzeghai et al. 1985) proposed that these leaky junctions were the primary pathway for LDL transport. Using a quantitative model, they showed that a small fraction of cells in the process of dying or dividing could account for a significant increase in permeability. Previous *in vivo*

(Chien, Lin et al. 1988; Lin, Jan et al. 1988; Lin, Jan et al. 1990) studies have supported the importance of the leaky junction pathway in LDL and albumin transport across the endothelium. Lin et al. (Lin, Jan et al. 1990) examined the leakage of Evans Blue-albumin (EBA) in association with dying cells in the rat aorta using IgG as a marker for cell death. They found that while frequency of dying cells was low (0.48%) a large fraction of these (63%) were associated with EBA leakage spots, accounting for 37% of all leakage sites.

Indirect evidence supporting the importance of apoptosis in atherogenesis comes from observations that hemodynamic factors usually associated with the development of atherosclerosis, have also been shown to affect endothelial cell apoptosis. Atherosclerotic plaques tend to be localized in regions of low shear stress and disturbed flow (Frangos, Gahtan et al. 1999). Irregular flow conditions have been shown to increase apoptosis rates (Freyberg, Kaiser et al. 2001), while increases in shear stress have been shown to reduce the rate of endothelial cell apoptosis (Dimmeler, Haendeler et al. 1996; Cho, Mitchell et al. 1997).

In a recent study, we used an *in vitro* model consisting of bovine aortic endothelial cells (BAEC) plated onto porous, polyester filters to measure the fluxes of water, albumin and LDL through BAEC monolayers (Cancel, Fitting et al. 2007). The results of that study showed that leaky junctions are the dominant transport pathway for LDL under convective conditions, when the pressure differential across the monolayer drives a physiological level of water flux. The leaky junctions accounted for more than 90% of the LDL transport. The vesicular pathway accounted for the remainder (9.1%) of the LDL transport. These results were consistent with *in vivo* observations that vesicles do not contribute significantly to LDL uptake in arteries (Wiklund, Carew et al. 1985; Rosengren, Carlsson et al. 2004). In the present study, the same *in vitro* model was used to probe the role of endothelial apoptosis in LDL transport under

convective conditions and to assess the potential for reducing LDL transport by reducing the rate of apoptosis. BAEC monolayers were treated with a combination of tumor necrosis factor alpha (TNFα) and cycloheximide (CHX) to induce an elevated rate of apoptosis, and with the caspase inhibitor Z-VAD-FMK to inhibit apoptosis. LDL flux was measured using an automated fluorometer system and water flux was measured using a bubble tracker apparatus. BAEC monolayers were assayed to determine apoptosis rates as well as to determine the effects of treatment on the tight junction protein, ZO-1. We observed that the rate of LDL transport across the endothelium was proportional to the apoptosis rate.

II. Material and Methods

Cell Culture

Bovine aortic endothelial cells (BAECs) were purchased from VEC Technologies, Inc. (Rensselaer, NY) and grown in minimum essential medium (MEM) (Sigma, St. Louis, MO) supplemented with 10% fetal bovine serum (FBS) (Hyclone, Logan, UT), 1% l-glutamine and 1% penicillin-streptomycin. For transport experiments, cells were plated onto fibronectin-coated Transwell membranes (Corning, Acton, MA) at a density of 1.25×10^5 cells/cm^2. Experiments were carried out on monolayers 4-6 days post-plating.

Induction, Inhibition and Measurement of Apoptosis

BAEC monolayers were incubated with tumor necrosis factor alpha (TNFα; 20ng/mL) and cycloheximide (CHX; 3μg/mL) in 10% FBS-MEM for 3.5 hrs as described in Polunovsky et al (Polunovsky, Wendt et al. 1994). To inhibit apoptosis, some monolayers were simultaneously treated with the pan-caspase inhibitor Z-VAD-FMK (Calbiochem, La Jolla, CA) at concentrations of 50 or 100μM. The inducer was then removed, and the monolayers were

allowed to recover for 20 hrs in the presence or absence of the inhibitor (recovery phase). In preliminary studies, monolayers that were not allowed to recover after the induction phase appeared disrupted after application of 10cm-H_2O pressure gradient for 1hr, while control monolayers appeared intact and confluent. The recovery time allowed treated monolayers to be pressurized without disruption while maintaining an elevated rate of apoptosis. The reason that monolayers that were not allowed to recover did not hold up well under pressure was hypothesized to be an effect of TNFα on junction proteins (see Discussion below).

Apoptosis rates were determined using the Vybrant Apoptosis assay kit #2 from Molecular Probes (Eugene, OR) following manufacturer's instructions. This assay uses the high affinity binding of annexin V to phosphatidylserine to identify apoptotic cells. Propidium iodide (PI) was used to identify necrotic cells, which also bind annexin V, virtually eliminating the possibility of false positive results. The apoptosis rate is defined as the number of apoptotic cells in a field divided by the total number of cells in the field, and presented as a percent.

For co-staining of apoptosis and junction proteins, the In situ cell death detection kit (TMR red) from Roche (Indianapolis, IN) was used. This assay uses the TdT-mediated dUTP nick end labeling (TUNEL) technique to identify apoptotic cells. While sensitive and fast, the TUNEL method is subject to false positives from necrotic cells and cells undergoing DNA repair. To ensure reliable results TUNEL positive cells should be examined for other morphological hallmarks of apoptosis (e.g. cells shrinkage, membrane blebbing). Cells were first stained for ZO-1 or VE-cadherin as indicated below, re-fixed with 4% paraformaldehyde for 1hr, permeabilized with 0.1% Triton X-100 in 0.1% sodium citrate for 2min, then incubated with the TUNEL reaction mixture for 1hr at 37 ºC. Cells were then washed 3X with PBS and imaged under a fluorescent microscope.

Immunostaining of Junction Proteins

BAEC monolayers were grown in the same manner as for transport experiments. Monolayers were washed 2X with PBS, fixed in 1% paraformaldehyde for 10 min, permeabilized with 0.2% Triton X-100 in PBS for 10 min and blocked with 10% bovine serum albumin (BSA) and 0.1% Triton X-100 in PBS for 1 hr. After washing with PBS, the monolayers were incubated with primary antibody for ZO-1 (Zymed, San Francisco, CA) or VE-cadherin (Cell Signaling, Beverly, MA) for 3 hrs at room temperature or overnight at 4°C. The monolayers were then washed 5X with PBS and incubated with secondary antibody, Alexa Fluor 488 donkey anti-rabbit IgG (Invitrogen, Carlsbad, CA), for 1 hr at room temperature. The monolayers were washed 4X in PBS before imaging.

All imaging was conducted with a Nikon Eclipse TE2000-E microscope. Images were taken with a Photometrics Cascade 650 CCD camera from Roper Scientific (Tucson, AZ).

Measurement of solute and water flux

The flux of human LDL tagged with 1,1'-dioctadecyl – 3,3,3',3'-tetramethyl-indocarbocyanine perchlorate (DiI-LDL) (Biomedical Technologies, Stoughton, MA) was measured using an automated fluorometer system previously developed in our laboratory (Antonetti, Wolpert et al. 2002), consisting of eight transport chambers, each of which was connected to a laser excitation source and an emission detector via optical fibers arranged in a 45° configuration. Excitation light at 532 nm was provided by a 10-mW Crystal Laser. The emission fibers were connected to a Model D48 photon counting detector from C&L Instruments (Hummelstown, PA). The *FluorMeasure* acquisition software and Model PC-DAQ control card (both from C&L Instruments) were used to control the laser exciter and detector, and for data acquisition.

A Transwell filter containing the BAEC monolayer was sealed within each chamber to form a luminal (top) and abluminal (bottom) compartment. The abluminal compartment was connected to a fluid reservoir via tygon tubing. The reservoir could be lowered to apply a hydrostatic pressure differential across the monolayer. Both the luminal compartment and abluminal reservoir were continuously supplied with 5% CO_2-95% air to maintain the medium at physiological pH. The experimental apparatus, excluding the laser source and the emission detector were housed inside a temperature-controlled Plexiglas box maintained at 37°C.

Each filter was rinsed twice with experimental medium (1% BSA in phenol red-free MEM) prior to inserting into the chambers. A solution of 5μg/mL DiI-LDL was added to the luminal compartment. Each transport experiment consisted of a one hour equilibration period, followed by application of a 10-cm H_2O pressure differential (to drive convective flux) and data collection for one hour, and finally two hours of data collection under diffusive conditions (no pressure differential).

The water flux was measured simultaneously with solute flux in two of the eight chambers. These two chambers were connected via tygon tubing and borosilicate glass tubing to an abluminal reservoir. When a 10-cm H_2O differential pressure was applied, the water flux (J_v) was measured by tracking the position of an air bubble that was inserted into the glass tubing. The bubble was monitored using a spectrophotometer which followed the air-liquid interface in the glass tube.

Calculation of Permeability (P_e or P_o) and water flux (J_v) values

The fluorescence intensity in the abluminal compartment was recorded for 10 seconds of every minute for the duration of the experiment. The intensity was converted to concentration by means of a calibration curve, and the permeability was calculated by

$$P_e, P_o = \frac{(\Delta C_a / \Delta t) \times V_a}{C_l \times A} \quad (1)$$

where P_e (P_o) is the convective (diffusive) permeability, $\Delta C_a / \Delta t$ is the change in abluminal concentration with respect to time, V_a is the fluid volume in the abluminal compartment, C_l is the concentration in the luminal compartment, and A is the area of the filter.

The bubble displacement data was used to compute J_v values using the following equation

$$J_V = \frac{\Delta d}{\Delta t} \times \frac{F}{A} \quad (2)$$

where $\Delta d/\Delta t$ is the bubble displacement per unit time, and F is a tube calibration factor (fluid volume per unit length of tubing).

Statistical Analysis

Permeability and water flux values were normalized with respect to control and presented as mean ± SEM. Data sets were analyzed for statistical significance by a Student's *t*-test and $p<0.05$ was considered statistically significant. Where multiple comparisons were made, the Bonferroni correction was used. The Bonferroni correction gives a conservative significance level of p/m, where m is the number of comparisons. For example, when comparing four groups $p<0.05$ is replaced with $p<0.05/6$ or 0.008.

III. Results

Effect of TNFα/CHX and Z-VAD-FMK on apoptosis rate and LDL permeability

BAEC monolayers were incubated with the apoptosis inducers TNFα/CHX for 3.5 hrs in the presence or absence of the inhibitor Z-VAD-FMK then allowed to recover for 20 hrs without the inducer as described in the Methods. The baseline apoptosis rate was 0.3% $\pm$ 0.036%.

TNFα/CHX-treated monolayers had an apoptosis rate of 5.9% ± 0.356%, an 18.3-fold increase over baseline. While the inhibitor had no effect on the baseline rate of apoptosis (control = 0.45% ± 0.05%, Z-VAD-FMK = 0.678% ± 0.14%; $p>0.09$) it did inhibit TNFα/CHX-induced apoptosis in a dose-dependent manner. When the cells were treated with 50μM and 100μM Z-VAD-FMK, the apoptosis rate was increased by 9.2-fold and 5.6-fold, respectively (Figure 2.1A). Necrotic cells were occasionally found, usually in an annular area midway between the center and the edge of a filter. However, the number and pattern of necrotic cells were not affected by treatment with TNFα/CHX or with the caspase inhibitor. Instead, we found that careful handling of the filter during the apoptosis assay eliminated necrotic cells.

The diffusive permeability (P_o) of control monolayers was $2.6 \times 10^{-7} \pm 3.7 \times 10^{-8}$ cm/s, similar to our previous measurements (Cancel, Fitting et al. 2007). P_o increased to $4.52 \times 10^{-7} \pm 4.94 \times 10^{-8}$ cm/s when monolayers were treated with TNFa/CHX alone. When 50μM and 100μM Z-VAD-FMK was added, P_o was $4.56 \times 10^{-7} \pm 4.48 \times 10^{-8}$ cm/s and $3.22 \times 10^{-7} \pm 5.18 \times 10^{-8}$ cm/s, respectively. There was no significant difference between the P_o of control and any of the treated monolayers. Figure 2.1B shows the effect of TNFα/CHX and Z-VAD-FMK on the convective permeability (P_e) of BAEC monolayers to LDL. Control monolayers had a baseline P_e of $2.07 \times 10^{-6} \pm 3.18 \times 10^{-7}$ cm/s. Treatment with TNFα/CHX alone increased the permeability by 4.4-fold. Addition of Z-VAD-FMK attenuated the increase in permeability to 3.5-fold when 50μM Z-VAD-FMK was added, and to 2.2-fold when 100μM Z-VAD-FMK was added.

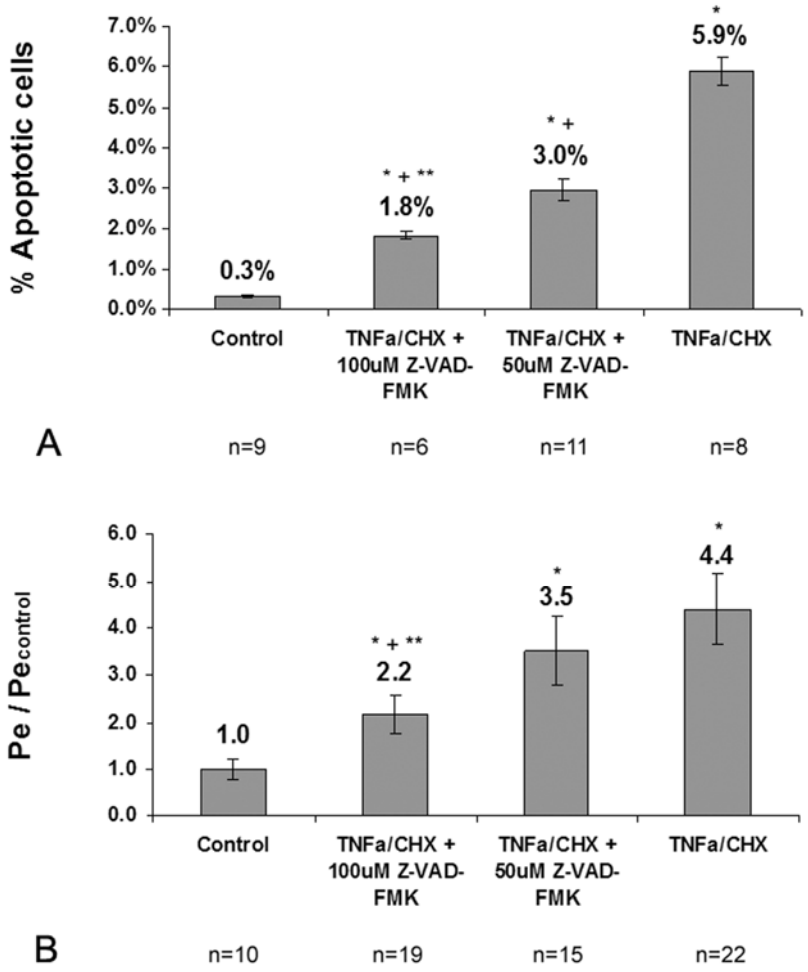

Figure 2.1. Effect of TNFα/CHX and Z-VAD-FMK on (A) apoptosis rate and (B) convective LDL permeability (P_e). BAEC monolayers were treated for 3.5hrs followed by a 20-hr recovery period. Control monolayers had an average P_e of $2.07 \times 10^{-6} \pm 3.18 \times 10^{-7}$ cm/s. Mean ± SEM shown. *p<0.008 vs control, **p<0.008 vs 50μM Z-VAD-FMK, +p<0.008 vs TNFα/CHX.

BAEC monolayers were incubated with CHX alone to control for the effects of protein inhibition on apoptosis and LDL permeability. At the concentration and duration used in this study, CHX had no significant effect on apoptosis rate (0.21% ± 0.029%, p>0.048 vs. control) or on LDL permeability ($1.47 \times 10^{-6} \pm 1.69 \times 10^{-7}$ cm/s, p>0.012 vs. control).

Effect of TNFα/CHX and Z-VAD-FMK on water flux (J_v)

The water flux of treated monolayers was measured to assess the effect of TNFα/CHX treatment on paracellular transport through the breaks in the tight junction strand, the main pathway for water transport (Cancel, Fitting et al. 2007). Control monolayers had a J_v of 5.05 x 10^{-6} ± 4.41 x 10^{-7} cm/s. Figure 2.2 shows that treatment with TNFα/CHX increased J_v by a factor of 2.7. Treatment with the caspase inhibitor Z-VAD-FMK did not significantly attenuate the increase in J_v at any concentration. Treatment with CHX alone had no significant effect on the J_v (3.53 x 10^{-6} + 2.06 x 10^{-7} cm/s, p>0.010 vs. control).

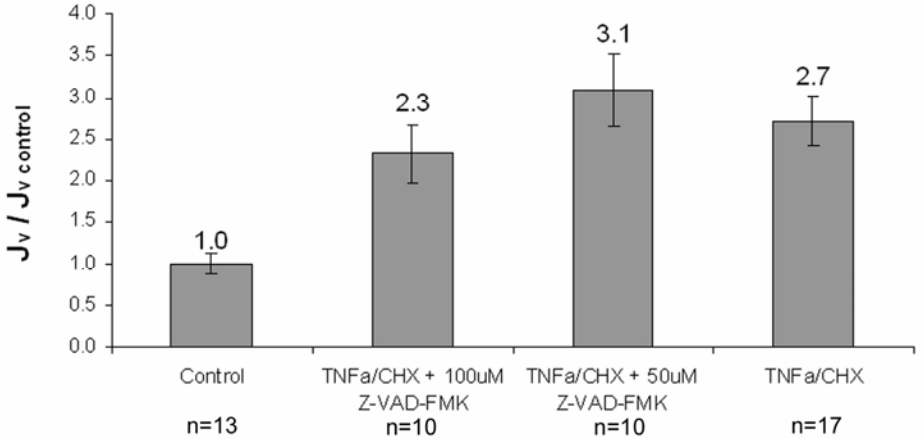

Figure 2.2. Effect of TNFα/CHX and Z-VAD-FMK on water flux (J_v). BAEC monolayers were treated for 3.5hrs followed by a 20-hr recovery period. Control monolayers had an average J_v of 5.05 x 10^{-6} ± 4.41 x 10^{-7} cm/s. Mean ± SEM shown. All conditions are statistically different ($p<0.008$) from control, but not from each other.

Effect of TNFα/CHX and Z-VAD-FMK on tight junction proteins

The results of water flux measurements suggest that TNFα/CHX may be affecting the paracellular pathway through the breaks in the tight junction strand in ways unrelated to the induction of apoptosis. Since previous studies (Wojciak-Stothard, Entwistle et al. 1998; Petrache, Birukova et al. 2003; McKenzie and Ridley 2007) have shown that TNFα disrupts the junctional complex of endothelial cells independent of its apoptotic effects, we performed

immunostaining of the tight junction protein ZO-1 in order to assess junctional integrity under the treatment conditions of this study.

BAEC monolayers were incubated with TNFα/CHX in the presence or absence of Z-VAD-FMK for 3.5 hrs then allowed to recover for 20 hrs in the presence or absence of Z-VAD-FMK. The monolayers were then exposed to a 10-cm H_2O pressure gradient for 1 hr, as in the transport experiments, before being stained for ZO-1 as indicated in the methods. Figure 2.3 shows representative photomicrographs of ZO-1 immunostating.

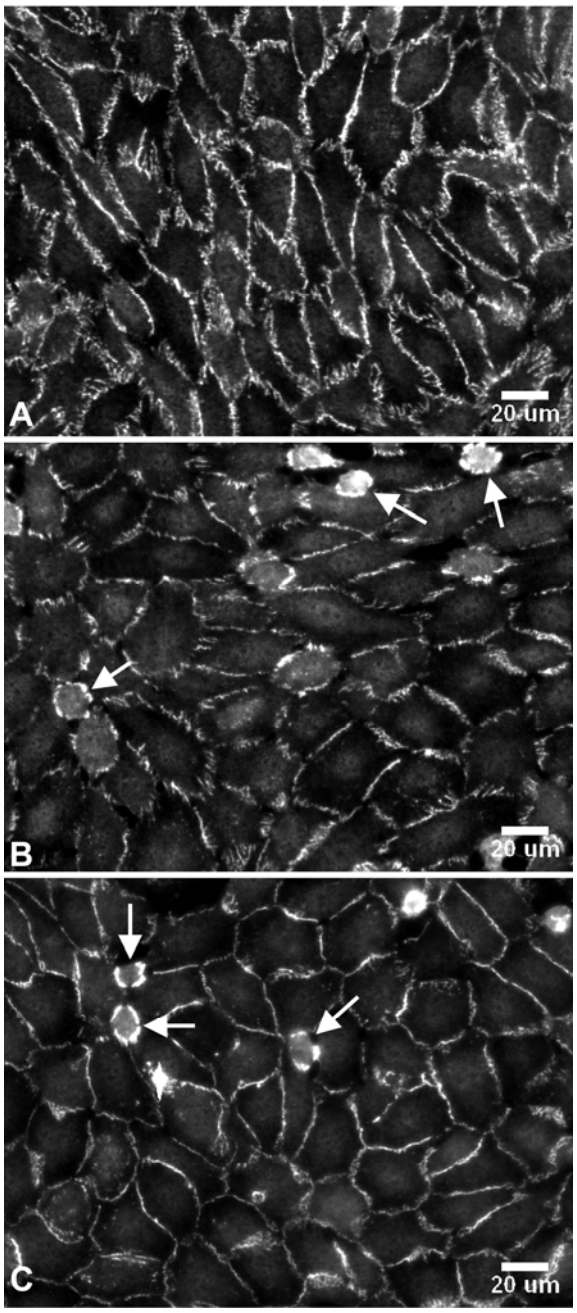

Figure 2.3. ZO-1 immunostaining of BAEC monolayers after treatment with TNFα/CHX in the presence or absence of the caspase inhibitor Z-VAD-FMK for 3.5hrs followed by a 20-hr recovery period. A) control. B) TNFα/CHX. C) TNFα/CHX + 100μM Z-VAD-FMK. Arrows denote detaching cells.

Immunoreactivity in treated and untreated monolayers is concentrated at the cell-cell border, with negligible cytoplasmic staining. Control monolayers show a broad, continuous band of ZO-1 staining around the perimeter of each cell (Figure 2.3A). The staining appears predominantly in spikes that are oriented perpendicular to the perimeter of the cell. Monolayers

treated with TNFα/CHX show a narrower and weaker band of ZO-1 around the perimeter with numerous discontinuitites (Figure 2.3B). Monolayers treated with TNFα/CHX + 100μM Z-VAD-FMK also show a narrow and discontinuous band of staining around the perimeter (Figure 2.3C). Several cells appear to be detaching from the treated monolayers (arrows in Figures 2.3B and 2.3C). Gaps between cells are visible around or near the detaching cells. These gaps likely account for the increased permeability of treated monolayers.

BAEC monolayers immunostained for ZO-1 were co-stained for apoptosis using the TUNEL technique as described in the methods to assess whether detaching cells were apoptotic. Representative photomicrographs from control and treated monolayers are shown in Figure 2.4. The nucleus in TUNEL positive (apoptotic) cells stained red as the TMR-labelled dUTP incorporated into damaged DNA. Apoptotic cells were found in all monolayers. In most cases, the apoptotic cell was found to be balling up and detaching from the monolayer, creating gaps between it and its neigboring cells (arrows in Figures 2.4A, C, D, E and F). In other cases, the apoptotic cell was still attached and spread with small gaps beginning to form (arrowheads in Figures 2.4B and 2.4C). There was no distinguishable difference in the TUNEL staining between control and treated monolayers, aside from the frequency of TUNEL postitive cells found.

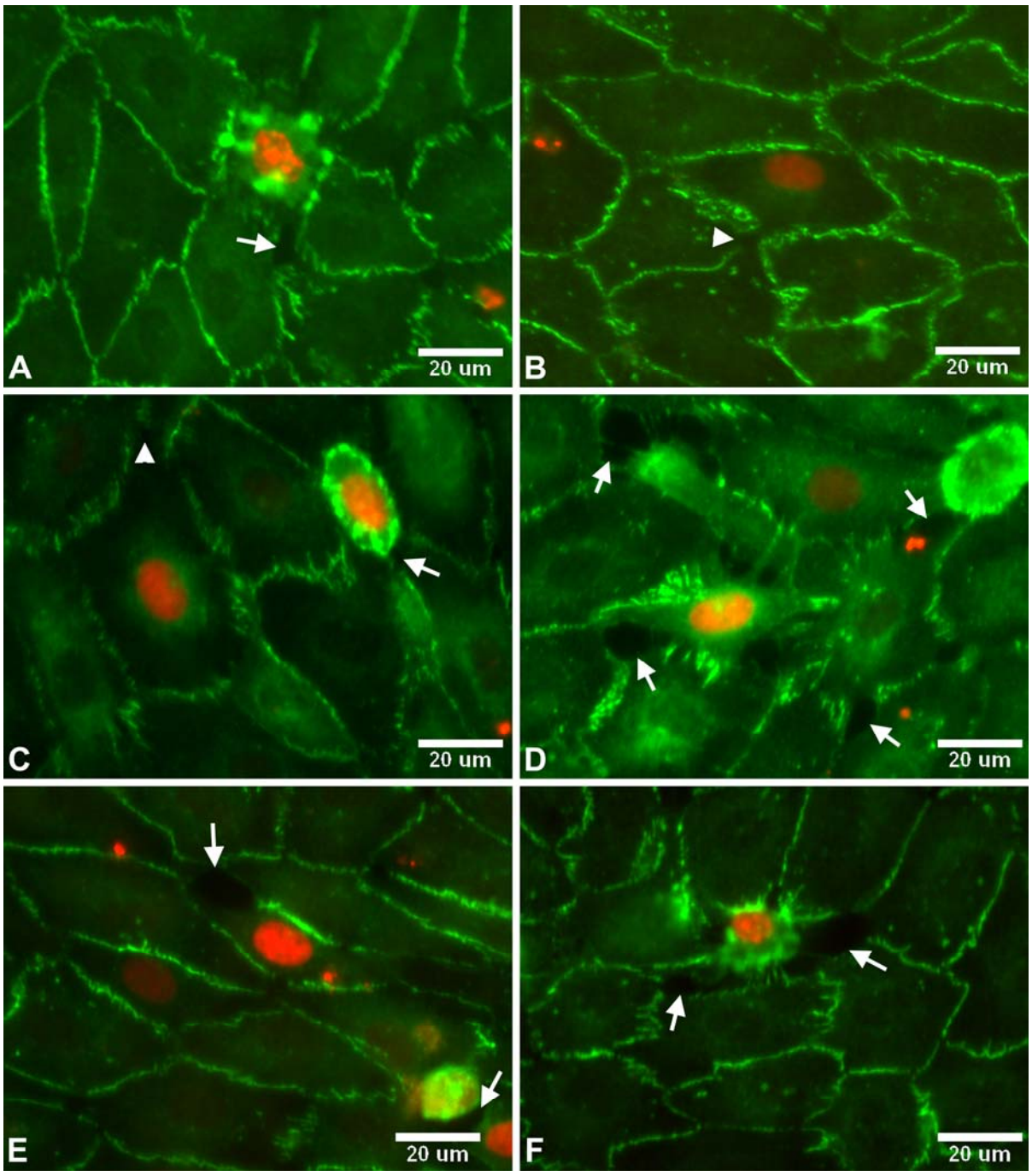

Figure 2.4. Co-localization of endothelial cell detachment and gap formation with apoptosis. BAEC monolayers were immunostained for ZO-1 (green) and apoptotic cells were identified using the TUNEL method (red). A) and B) control. C) and D) TNFα/CHX. E) and F) TNFα/CHX + 100μM Z-VAD-FMK. Arrows denote gaps around apoptotic cells that are balling up and detaching from the monolayer. Arrowheads denote small gaps starting to form around apoptotic cells that are still attached and spread.

Quantification of endothelial gap formation in association with apoptosis

In a separate set of experiments, BAEC monolayers were immunostained for the adherens junction protein VE-cadherin and subsequently co-stained using the TUNEL technique to identify apoptotic cells. We chose to conduct these experiments with VE-cadherin instead of ZO-1 staining to minimize confusion between gaps related to apoptosis and those related to the effects of TNFα on the tight junction. One control and one TNFα/CHX-treated filter were analyzed. The total number of apoptotic cells and gaps in 15 fields per filter (0.044mm^2 per field) was quantified. A gap was defined as a clear opening in the cell-cell junction, normally appearing as a dark region between cells (arrows in Figure 2.5). In addition to quantifying gaps associated with apoptotic cells, we also identified tricellular corners, which occur where three cells meet (arrowheads in Figure 2.5). Tight junctions have been shown to be discontinuous at tricellular corners (Walker, MacKenzie et al. 1994; Burns, Walker et al. 1997), and transendothelial migration of neutrophils was found to occur preferentially at the tricellular corner (Burns, Walker et al. 1997) suggesting that tricellular corners might also constitute a leaky junction. The results are shown in Table 2.1 for a control monolayer and Table 2.2 for a monolayer treated with TNFα/CHX.

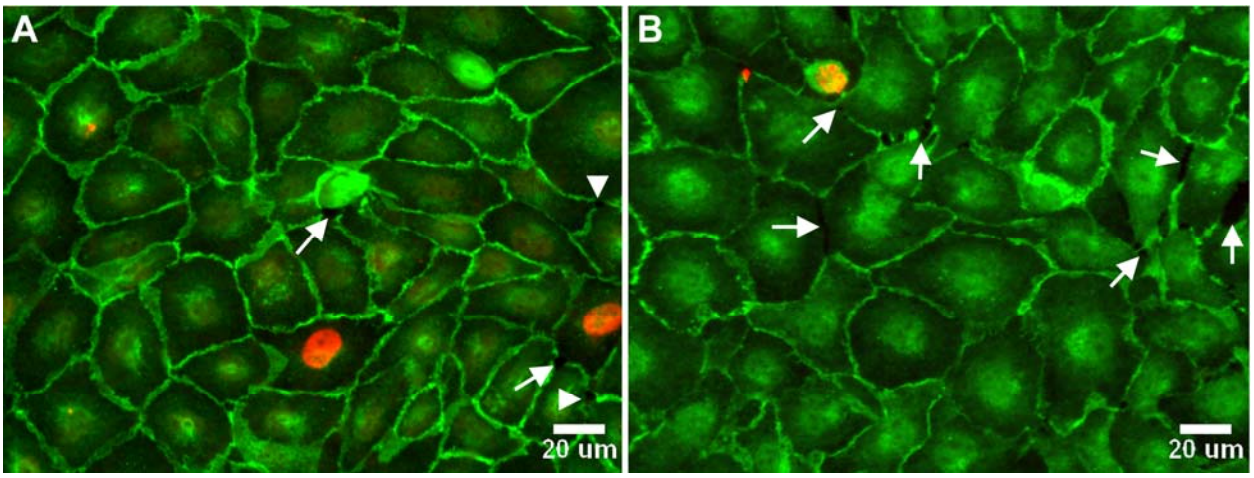

Figure 2.5. Co-localization of endothelial cell detachment and gap formation with apoptosis. BAEC monolayers were immunostained for VE-cadherin (green) and apoptotic cells were identified using the TUNEL method (red). A) shows an area containing two apoptotic cells from a control monolayer. B) shows an area with one apoptotic cell from a TNFα/CHX-treated monolayer. Arrows denote gaps around cells. Arrowheads denote tricellular gaps. Note that gaps are not regularly distributed but instead tend to lie around a cell or group of cells.

The apoptosis rate for each monolayer was obtained from a count of the apoptotic cells in the center field of the filter using the microscope eyepiece (~1400 cells). Since most camera fields (~60 cells) analyzed contained at least one apoptotic cell, the rate obtained by adding up these fields is artificially high. In control monolayers, 43% of the apoptotic cells had a gap associated with them, while this number increased to 89% for treated monolayers. Most gaps were not directly associated with an apoptotic cell, i.e. they were not between the apoptotic cell and one of its neighbors. Some of these gaps could be leaky junctions associated with mitotic cells, which we would not be able to identify without specific staining unless they were in the late stages of cytokinesis. These gaps could also be associated to early apoptotic cells that do not yet show DNA damage and therefore are not stained by the TUNEL technique. Corfe et al. showed that changes in cell-cell junctions in apoptotic cells occur before nuclear condensation and even before phosphatidylserine (PS) exposure at the cell surface (Corfe, Dive et al. 2000).

One final possibility is that some of these gaps are left over by apoptotic cells that have just detached from the monolayer (or have been washed away during the immunostaining process) while the surrounding cells have not yet closed all the gaps.

Note also the difference in cell density between control and treated monolayers. The lower cell density for treated monolayers along with the fact that the apoptosis rate is an order of magnitude higher than the mitosis rate (see Lin et al. (Lin, Jan et al. 1990) for in vivo rates; see Chapter 3 for mitosis rates in BAECs) suggests that neighboring cells stretch to push out and take the place of the dying cell. Rosenblatt et al. showed in epithelial cell (MDCK) monolayers that an apoptotic cell signals its neighbors to form an actin and myosin ring that contracts to extrude the apoptotic cell (Rosenblatt, Raff et al. 2001). They observed that the surrounding cells stretched as much as two cells diameters to take up the space left by the dying cells. This stretching could create gaps in the monolayer that, while not directly associated with an apoptotic cell, are a consequence of the apoptosis process.

Table 2.1. Quantification of gaps in association with apoptosis and tricellular corners in a control monolayer.

	Cells			Gaps			
Field	**Apoptotic**	**Total**	**Cell Density (cells/cm^2)**	**Apoptotic**	**Tricellular**	**Other**	**Total**
1	2	66	1.5 x10^5	0	1	6	7
2	1	64	1.5 x10^5	1	2	5	8
3	1	57	1.3 x10^5	0	1	2	3
4	1	64	1.5 x10^5	1	1	1	3
5	1	60	1.4 x10^5	0	0	8	8
6	2	67	1.5 x10^5	0	2	2	4
7	0	56	1.3 x10^5	0	0	2	2
8	0	62	1.4 x10^5	0	0	8	8
9	2	52	1.2 x10^5	2	1	10	13
10	0	57	1.3 x10^5	0	0	0	0
11	2	61	1.4 x10^5	1	1	2	4
12	1	62	1.4 x10^5	0	1	5	6
13	1	63	1.4 x10^5	1	0	5	6
14	0	62	1.4 x10^5	0	1	7	8
15	0	65	1.5 x10^5	0	2	6	8
Total	14	918	-	6	13	69	88

Apoptosis rate: 0.58%
Apoptotic cells with gap: 43%

Gaps associated with apoptotic cells: 7%
Gaps associated with tricellular corners: 15%
Other gaps: 78%

Table 2.2. Quantification of gaps in association with apoptosis and tricellular corners in a TNFα/CHX-treated monolayer.

	Cells			Gaps			
Field	**Apoptotic**	**Total**	**Cell Density (cells/cm^2)**	**Apoptotic**	**Tricellular**	**Other**	**Total**
1	3	55	1.2 x10^5	3	0	10	13
2	1	46	1.0 x10^5	1	0	11	12
3	1	49	1.1 x10^5	0	1	18	19
4	1	47	1.1 x10^5	1	0	11	12
5	0	48	1.1 x10^5	0	0	15	14
6	3	51	1.2 x10^5	3	0	12	15
7	4	53	1.2 x10^5	4	2	13	19
8	1	49	1.1 x10^5	1	0	18	19
9	0	49	1.1 x10^5	0	1	7	8
10	0	38	8.6 x10^4	0	1	10	11
11	1	45	1.0 x10^5	1	4	12	17
12	3	39	8.9 x10^4	2	3	8	13
13	0	45	1.0 x10^5	0	0	10	10
14	1	42	9.5 x10^4	1	0	16	17
Total	19	656	-	17	12	170	199

Apoptosis rate: 6.7%
Apoptotic cells with gap: 89%

Gaps associated with apoptotic cells: 9%
Gaps associated with tricellular corners: 6%
Other gaps: 85%

While there seem to be a large number of gaps in all these fields, most of them lie around the same cell or group of cells (Figure 2.5B). In order to compare our gap counts to leakage spot co-localization studies in the literature, we estimated the number of distinct spots that would be produced from the gaps in our monolayers. Lin et al. (Lin, Jan et al. 1989) reported Lucifer Yellow LDL leakage spots around mitotic cells to be slightly larger than the size of one cell. Truskey et al. (Truskey, Roberts et al. 1992) observed focal regions of increased ^{125}I-LDL permeability, some around mitotic cells, to be two or three cells in diameter. Taking these measurements as a guide, we estimated that each gap would produce a spot 1.5 times the area of

a cell, and counted the number of distinct spots our gaps would produce. Where an apoptotic gap and another type of gap would both produce a spot covering the same area, the spot was attributed to the apoptotic cell. The results are shown in Table 2.3. The results for our control monolayers were similar to those of Lin et al. (Lin, Jan et al. 1990) in the rat aorta, where they measured the association of Evans Blue Albumin (EBA) with dead cells identified with IgG. There are no in vivo studies of LDL transport in association with apoptotic or dying cells. However, it is expected that the percentage of leakage sites accounted for by apoptosis would be higher for LDL than for EBA because normal breaks in the tight junction strand are an available transport pathway for EBA but not for LDL. In the case of mitosis, for example, mitotic cells account for 23.1% of EBA leakage sites and 45.3% of LDL leakage sites. With this in mind, the percentage of estimated spots associated with apoptotic cells in our monolayers (28%) seems low. As discussed above, however, many of the gaps not identified as being associated with apoptosis could, directly or indirectly, still be the result of the apoptotic process.

Table 2.3. Association of leakage spots with apoptotic cells and tricellular corners. Leakage spots for the present study were estimated using observations of gaps in cell-cell junctions.

	Apoptotic Cells		**% of Total sites with leakage**		
	Frequency (%)	% with leakage	Apoptotic or Dead	Tricellular	Other
Present study (BAECs)					
Control	0.58	79	28	18	54
TNFα/CHX treated	6.75	84	32	8	60
Lin et al. (rat aorta; dead cells; EBA)	0.48	63	37	-*	63*

* Lin et al. did not look at tricellular corners, therefore the unexplained leakage spots are assigned to the "Other" category.

IV. Discussion

The aims of this study were to test the hypothesis that apoptosis rates dictate, in part, the permeability of endothelial monolayers to LDL under physiologically relevant (convective)

conditions, and to demonstrate that inhibition of apoptosis results in a reduction of LDL permeability. We were able to show this by inducing an elevated rate of apoptosis with TNFα/CHX and then bringing the rate back down with the caspase inhibitor Z-VAD-FMK. TNFα is a proinflammatory ligand which has been shown to induce apoptosis (Polunovsky, Wendt et al. 1994) and endothelial barrier dysfunction (Petrache, Birukova et al. 2003; McKenzie and Ridley 2007) in vascular endothelial cells. Cycloheximide (CHX) is an inhibitor of protein synthesis which can either potentiate or attenuate TNFα induced apoptosis, depending on the timing of exposure in relation to TNFα treatment. Polunovsky et al. (Polunovsky, Wendt et al. 1994) studied the kinetics and synergy of apoptosis induction by TNFα/CHX in bovine aortic endothelial cells *in vitro*. They found that CHX could potentiate TNFα-induced apoptosis if it was added either alongside or after the addition of TNFα, but not if it was added before TNFα. On our BAEC monolayers TNFα/CHX induced between 2 and 5 times more apoptosis than TNFα alone at the same concentration and duration. The rate of apoptosis induced by TNFα/CHX in Polunovsky et al. was five times higher than in the present study (31% vs 5.9%), but it should be noted that the cells in that study were in the log phase of growth when treated, whereas our cells were confluent monolayers with well developed junctions and low, stable growth rates. Previous studies have shown that junctional adhesive proteins transfer intercellular signals that negatively modulate cell proliferation and sensitivity to apoptotic stimuli (Bazzoni, Dejana et al. 1999; Spagnuolo, Corada et al. 2004).

The application of a 10cm-H_2O hydrostatic pressure gradient necessitated a 20-hr recovery period in which TNFα/CHX was removed from the media. Monolayers that were not allowed to recover did not hold up well to the pressure gradient, appearing disrupted after its application (not shown). Monolayers that were allowed to recover for 20 hours remained intact

and confluent after application of the pressure gradient (Figures 2.3 and 2.4). The apoptosis rate remained elevated after the recovery period on cells treated with the apoptosis inducers (Figure 2.1A). The recovery period is likely to be allowing cells to reestablish their junctions enough to withstand the hydrostatic pressure gradient.

TNFα/CHX-treated monolayers were immunostained for the tight junction protein ZO-1. Despite the 20-hr recovery period, a decreased immunoreactivity is clear for treated monolayers (Figures 2.3B and 2.3C). In addition to inducing apoptosis, TNFα has been shown to disrupt the junctional complex in epithelial (Gitter, Bendfeldt et al. 2000; Bruewer, Luegering et al. 2003) and endothelial (Wojciak-Stothard, Entwistle et al. 1998; Petrache, Birukova et al. 2003; McKenzie and Ridley 2007) cells. McKenzie and Ridley (McKenzie and Ridley 2007) showed that TNFα induced a fragmented distribution of ZO-1, loss of occludin from the cell junctions and down-regulation of occludin levels in HUVECs after 24 hr treatment with TNFα. These morphological changes occurred on the same timescale as an increase in permeability of 42 kDa dextran. While apoptosis levels were not measured in McKenzie and Ridley, their results suggest that the TNFα–induced increase in 42 kDa dextran permeability was partly due to the loss of tight junction proteins (McKenzie and Ridley 2007).

CHX could also be altering the endothelial cell junction by its inhibition of protein synthesis. We measured the apoptosis, LDL permeability and water flux of BAEC monolayers treated with CHX alone at the same concentration and duration used when the cells were treated with the combination of TNFα and CHX. We found no effect of CHX on apoptosis, LDL permeability or water flux. The fact that CHX did not increase water flux suggests that it also has no effect on ZO-1 distribution, since water transport occurs primarily though the breaks in

the tight junction strand (Cancel, Fitting et al. 2007). Therefore, it is likely that the reduction in ZO-1 is due to the effects of TNFα that have been previously described.

The main limitations of this study are: 1) it was performed *in vitro* and 2) shear stress was not applied. Endothelial cells *in vivo* are constantly exposed to mechanical forces as a result of the blood flow. These forces have been shown to affect endothelial function (Ogunrinade, Kameya et al. 2002; Li, Haga et al. 2005). Physiological levels of steady shear have been shown to have several atheroprotective effects on the endothelium, some directly affecting its permeability, while disturbed flow seems to have an atherogenic effect on the endothelium (see (Chien 2008) for a review). Steady shear reduces cell proliferation (Chien 2003) and apoptosis (Dimmeler, Haendeler et al. 1996; Cho, Mitchell et al. 1997), both of which would reduce permeability through the leaky junction pathway. In contrast, disturbed flow such as that occurring in branch points and bifurcations in arteries increases cell turnover (mitosis (Chien 2003) and apoptosis (Freyberg, Kaiser et al. 2001)) and activates sterol regulatory element binding proteins (SREBPs), a family of transcription factors involved in receptor-mediated LDL uptake and metabolism (Liu, Chen et al. 2002). Liu et al. showed that activation of SREBPs by shear led to a nearly 2-fold increase in ^{125}I-LDL binding to BAECs *in vitro*. While increased LDL binding through the LDL receptor could potentially increase transendothelial transport, several *in vivo* studies (Wiklund, Carew et al. 1985; Rosengren, Carlsson et al. 2004) as well as our previous *in vitro* study (Cancel, Fitting et al. 2007) have shown that vesicles contribute only a small fraction of the total transport of LDL under convective conditions. Finally, disturbed flow could induce conformational changes that may alter the cell-cell junctions, thus affecting permeability (Chien 2008). BAECs exposed to disturbed flow had discontinuous VE-cadherin staining, indicating the presence of gaps in the cell-cell junction (Miao, Hu et al. 2005).

The apoptosis levels induced in the present study are similar to those observed around human atherosclerotic plaques by Tricot et al. (Tricot, Mallat et al. 2000) This group measured endothelial cell apoptosis upstream and downstream of the plaque stenosis and found a preferential occurrence of apoptosis in the downstream part of the plaque, where shear levels are low. The apoptosis rate was 2.7% in the upstream part of the plaque, and 18.8% in the downstream part. Our maximum apoptosis value was 5.9%.

The decrease in apoptosis obtained with Z-VAD-FMK treatment had no significant effect on water flux (Figure 2.2). This observation can be explained by the fact that water transport occurs primarily through the breaks in the tight junction strand and not through leaky junctions (Cancel, Fitting et al. 2007). As shown in Figure 3C, the discontinuities in ZO-1 staining persist, like the increase in J_v, even after treatment with Z-VAD-FMK. Therefore, it seems that the increase in water flux caused by TNFα/CHX treatment is primarily the result of an overall increase in the area of the breaks (as evidenced by discontinuous ZO-1 staining) rather than an increase in individual leaky junctions resulting from increased apoptosis.

On the other hand, it is unlikely that LDL (22nm diameter) would pass through an altered endothelial junction with discontinuities in the tight junction strand because the widest part of the junction is expected to be about 20nm (Adamson and Michel 1993). Most of the cell-cell junction, i.e. both tight and adherens junctions need to be disrupted to create a large pore that would allow the passage of LDL molecules. This kind of disruption is not evident in our treated monolayers except in places where a cell appears to be detaching from the layer (arrows in Figures 2.3B and 2.3C). These cells are likely to be apoptotic as they exhibit the same morphology as cells identified as apoptotic using the annexin V assay. To confirm this, we co-

stained monolayers for ZO-1 and TUNEL. The results (Figure 2.4) show gaps forming around or near TUNEL positive (apoptotic) cells as they detach from their neighboring cells.

We conclude that the increase in LDL permeability in response to TNFα/CHX is due to leaky junctions created by individual apoptotic cells, and not to a global effect of TNFα on the junctions. We are, therefore, able to show a correlation between apoptosis and LDL permeability in Figure 2.6 (obtained by cross-plotting the data in Figures 2.1A and 2.1B). The Pearson Product Moment Correlation coefficient was calculated to be 0.72, indicating a strong correlation between LDL permeability and apoptosis. This plot shows that in order to increase permeability by 2-fold the apoptosis rate would have to be increased by 5-fold, to about 1.6%. This is less than the increases observed by Tricol et al. (Tricot, Mallat et al. 2000) around human atherosclerotic plaques. It is also close to the 4-fold increase in dead cells observed by Gerrity et al. (Gerrity, Richardson et al. 1977) in atheroprone areas compared to atheroprotected areas in the aortas of young pigs. Our results suggest that permeability in atheroprone and disease areas could increase anywhere from 2 to 10-fold due to observed increases in apoptosis in those areas.

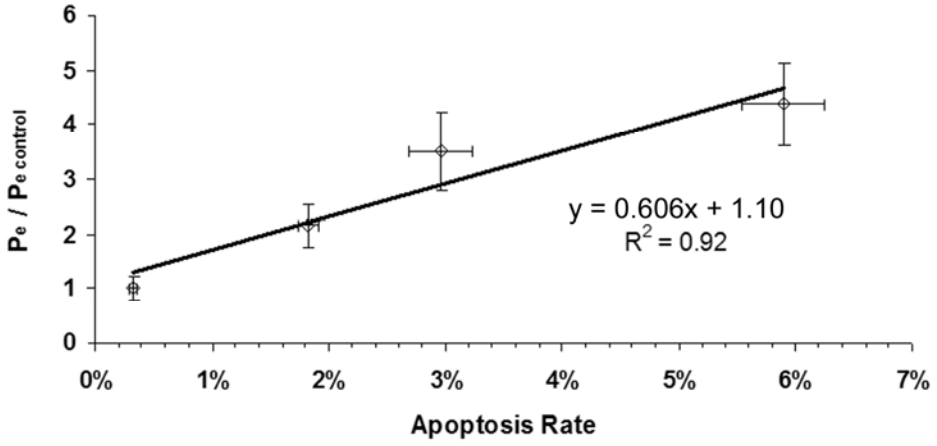

Figure 2.6. Correlation between the normalized LDL permeability and apoptosis rate. The Pearson Product Moment Correlation coefficient was calculated to be 0.72.

In a parallel study in our lab, Francesco Piraino studied the effect of simvastatin on the apoptosis and permeability of BAEC monolayers (Piraino, Cancel et al. under review). Statins are a class of low molecular weight drugs that inhibit 3-hydroxy-3-methylgluraryl-CoA reductase, the rate-limiting enzyme of the mevalonate pathway, thus reducing plasma levels of LDL. Statins have been shown to exert cholesterol-independent effects on the endothelium including: upregulating the expression and activity of endothelial nitric oxide synthase (Laufs, La Fata et al. 1998; Guerard, Rakotoniaina et al. 2006) and reducing or increasing endothelial cell apoptosis depending on the concentration (Kureishi, Luo et al. 2000; Guerard, Rakotoniaina et al. 2006; Luthra, Dong et al. 2008). Using the same methods described in this chapter, apoptosis was induced with TNFα/CHX and simvastatin was introduced as a possible inhibitor of apoptosis. Simvastatin at nanomolar concentrations (1 – 100 nM) was found to inhibit TNFα/CHX-induced apoptosis in a dose-dependent manner, with the lowest concentration (1nM) having the greatest reduction in apoptosis. Using simvastatin at 1nM, we tested whether the reduction in apoptosis would result in a reduction in LDL permeability under convective conditions. We found a strong correlation between the apoptosis rate and the permeability (Figure 2.7). The Pearson Product Moment Correlation coefficient was calculated to be 0.66. This correlation is very similar to the one found previously, when Z-VAD-FMK was used as an inhibitor of apoptosis (dashed line in Figure 2.7). Because two different drugs (simvastatin and Z-VAD-FMK) produced the same effect on LDL permeability, it suggests that other drugs affecting endothelial apoptosis would have similar effects.

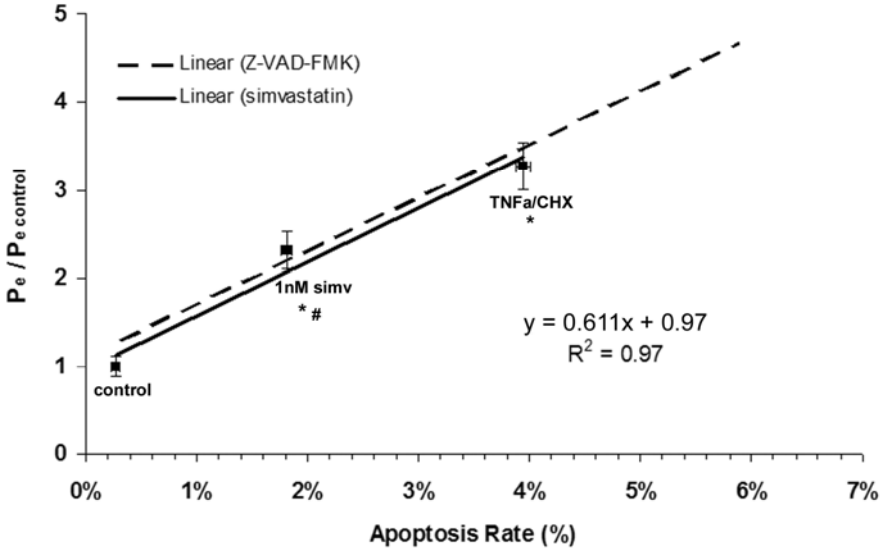

Figure 2.7. Effect of TNFα/CHX and 1nM simvastatin on the convective LDL permeability (P_e). P_e (▪) was normalized by the permeability of controls ($1.83x10^{-6} \pm 1.42x10^{-7}$ cm/s). Data points shown (▪) are mean ± SEM. *p<0.01 versus control. #p<0.01 versus TNFα/CHX. Correlations between normalized LDL permeability and apoptosis rate are shown for simvastatin study (solid line) and Z-VAD-FMK study (dashed line). Equation shown corresponds to simvastatin data. The Pearson Product Moment Correlation coefficient for the present study (simvastatin) was calculated to be 0.66.

These results demonstrate the potential to manipulate endothelial LDL permeability by altering the rate of apoptosis. Because the flux of LDL into the arterial wall (J) is related to its concentration in the blood (C_l) and the endothelial permeability (P_e) by the simple relationship

$$J = Pe \times C_l ,$$

it is clear, for example, that reducing P_e by 50% (by reducing the apoptosis by ~70% - Figure 2.6) would reduce the flux, J, as effectively as reducing C_l by 50%. This has obvious implications in the treatment of atherosclerosis.

Chapter 3: The role of mitosis in LDL transport through cultured endothelial cell monolayers

I. Introduction

The first event in the cascade of processes leading to atherosclerotic lesion formation is lipid infiltration and accumulation within the arterial wall (Schwenke and Carew 1989). A relationship between enhanced endothelial permeability to LDL and the localization of atherosclerotic plaques is well established (Duncan, Buck et al. 1963) (Nielsen, Nordestgaard et al. 1992). There are three potential pathways for transport of macromolecules across the endothelium: transcytosis in vesicles, paracellular transport through the breaks in the tight junction strand, and the leaky junction pathway associated with cells undergoing mitosis or apoptosis. Previous in vivo (Chien, Lin et al. 1988; Lin, Jan et al. 1988; Lin, Jan et al. 1990) and theoretical (Weinbaum, Tzeghai et al. 1985) studies have supported the importance of the leaky junction pathway in LDL and albumin transport across the endothelium. In Lin et al. (Lin, Jan et al. 1989) and Chien et al. (Chien, Lin et al. 1988) aortic sections were stained with hematoxylin in order to identify cells in the M phase of the cell cycle using morphological criteria. Roughly 1 in 3000 cells were found to be mitotic, but nearly all of those had an Evans Blue-albumin (EBA) or Lucifer Yellow-LDL leakage spot associated with it (99% for EBA and 80% for LDL). Mitotic cells accounted for 30% of all EBA leaks and 45% of all LDL leaks.

Observations that hemodynamic factors usually associated with the development of atherosclerosis also affect EC proliferation provide indirect evidence for its importance in atherogenesis. Atherosclerotic plaques tend to be localized in regions of low shear stress and disturbed flow (Ku, Giddens et al. 1985; Frangos, Gahtan et al. 1999; Malek, Alper et al. 1999). Several studies have demonstrated that high levels of steady shear stress reduce the rate of

endothelial cell proliferation (Levesque, Nerem et al. 1990; Gooch, Dangler et al. 1997). Chien (Chien 2003) measured EC proliferation using BrdU incorporation in a step flow chamber. After 24hr of flow at 12 dynes/cm^2 BrdU incorporation was enhanced in the region of disturbed flow, while it was much lower in the downstream laminar flow region.

A recent *in vitro* study in our lab (Cancel, Fitting et al. 2007) demonstrated that leaky junctions are the dominant transport pathway for LDL under convective conditions, when transport is driven by transendothelial water flux induced by the pressure differential across the endothelial layer. We used a model consisting of bovine aortic endothelial cells (BAEC) plated onto porous polyester filters and measured the flux of albumin, water and LDL across the endothelial monolayers under convective conditions. Leaky junctions accounted for 90.9% of LDL transport, the remainder going through vesicles. These results are consistent with the *in vivo* observations that vesicles do not contribute significantly to LDL uptake in arteries (Wiklund, Carew et al. 1985; Rosengren, Carlsson et al. 2004). We also recently showed that the permeability of BAEC monolayers is highly correlated with their rate of apoptosis, and that inhibiting apoptosis lowers the permeability of the monolayers to LDL (Cancel and Tarbell 2010). In the present study we used our *in vitro* model to investigate the role of mitosis in LDL transport under convective conditions. BAEC monolayers were treated with the microtubule stabilizing drug paclitaxel for different periods of time to obtain elevated rates of mitosis. LDL flux was measured using an automated fluorometer system and water flux was measured using a bubble tracker apparatus. We found correlations between the mitosis rate and the convective and diffusive LDL permeabilities (P_e and P_0, respectively) as well as the water flux (J_v) across the monolayers. Our results indicate a linear relationship between the mitosis rate and each of these three transport properties.

II. Materials and Methods

Materials

The following chemicals were obtained from Sigma (St. Louis, MO): minimum essential medium (MEM), fibronectin, bovine serum albumin (BSA), l-glutamine, penicillin-streptomycin, and paclitaxel. Phenol-red free MEM was from Mediatech (Herdon, VA). Fetal bovine serum (FBS) was from Hyclone (Logan, UT). Human LDL tagged with 1,1'-dioctadecyl – 3,3,3',3'-tetramethyl-indocarbocyanine perchlorate (DiI-LDL) was from Biomedical Technologies (Stoughton, MA).

Cell Culture

Bovine aortic endothelial cells (BAECs) were purchased from VEC Technologies, Inc. (Rensselaer, NY) and grown in MEM supplemented with 10% FBS, 1% l-glutamine and 1% penicillin-streptomycin. For transport experiments, cells were plated onto fibronectin-coated Transwell membranes (Corning, Acton, MA) at a density of 1.25×10^5 cells/cm^2. Experiments were carried out on monolayers 4-6 days post-plating.

Cell treatment and measurement of mitosis rates

An increased rate of mitosis was obtained by incubating BAEC monolayers with the microtubule stabilizer paclitaxel at a concentration of 2.5μM for 1.5, 3, 4.5 or 6 hours (Verin, Birukova et al. 2001). Mitosis rates were determined using anti-phospho-Ser/Thr-Pro (MPM-2, Upstate Biotechnology, Lake Placid, NY), a primary antibody that recognizes a variety of proteins that are phosphorylated during mitosis. Briefly, cells were washed with PBS, fixed with 4% paraformaldehyde for 10 min, permeabilized with ice cold methanol for 6 min and blocked with 1% BSA in PBS. After washing 2X with PBS, monolayers were incubated with primary antibody (MPM-2, 1:200 in blocking solution) for 2hr at room temperature or overnight at 4°C.

The monolayers were then washed 2X with PBS and incubated with the secondary antibody (Alexa Fluor 488 rabbit anti-mouse, 1:200 in PBS) for 1.5 hr at room temperature. The monolayers were washed 3X in PBS before imaging. The mitosis rate was defined as the number of MPM-2 positive cells divided by the total number of cells on the filter.

To check that paclitaxel treatment did not induce apoptosis, the In situ cell death detection kit (TMR red) from Roche (Indianapolis, IN) was used. This assay uses the TdT-mediated dUTP nick end labeling (TUNEL) technique to identify apoptotic cells. Cells were fixed with 4% paraformaldehyde for 1hr, permeabilized with 0.1% Triton X-100 in 0.1% sodium citrate for 2min, then incubated with the TUNEL reaction mixture for 1hr at 37 ºC. Cells were then washed 3X with PBS before imaging.

All imaging was conducted with a Nikon Eclipse TE2000-E microscope. Images were taken with a Photometrics Cascade 650 CCD camera from Roper Scientific (Tucson, AZ).

Immunostaining of Junction Proteins

BAEC monolayers were grown in the same manner as for transport experiments. Monolayers were washed 2X with PBS, fixed in 1% paraformaldehyde for 10 min, permeabilized with 0.2% Triton X-100 in PBS for 10 min and blocked with 10% bovine serum albumin (BSA) and 0.1% Triton X-100 in PBS for 1 hr. After washing with PBS, the monolayers were incubated with primary antibody for VE-cadherin (3:200; Cell Signaling, Beverly, MA) for 3 hrs at room temperature or overnight at 4°C. The monolayers were then washed 5X with PBS and incubated with secondary antibody, Alexa Fluor 594 goat anti-rabbit IgG (Invitrogen, Carlsbad, CA), for 1 hr at room temperature. The monolayers were washed 4X in PBS and re-fixed with 4% paraformaldehyde for 10 min. The MPM-2 assay described above was then performed to co-stain for mitotic cells.

Measurement of solute and water flux

DiI-LDL flux was measured using an automated fluorometer system previously developed in our laboratory (Antonetti, Wolpert et al. 2002) and extensively described (Cancel, Fitting et al. 2007) (Cancel and Tarbell 2010). Briefly, a Transwell filter containing the BAEC monolayer was sealed within a transport chamber to form a luminal (top) and abluminal (bottom) compartment. An aluminum support ring and an o-ring helped create a tight seal within the chamber. The abluminal compartment was connected to a fluid reservoir via tygon tubing and borosilicate glass. The reservoir could be lowered to apply a hydrostatic pressure differential across the monolayer. Both the luminal compartment and abluminal reservoir were continuously supplied with 5% CO_2-95% air to maintain the medium at physiological pH. The experimental apparatus, excluding the laser source and the emission detector were housed inside a Plexiglas box. A hairdryer attached to a temperature controller maintained the air temperature inside the box at 37°C.

Each filter was rinsed twice with experimental medium (1% BSA in phenol red free MEM) prior to inserting into the chambers. A solution of 5μg/mL DiI-LDL was added to the luminal compartment. Each transport experiment consisted of a one hour equilibration period, followed by application of a 10-cm H_2O pressure differential (to drive convective flux) and data collection for one hour, and finally two hours of data collection under diffusive conditions. The permeability was calculated as

$$P_e\ ,\ P_o = \frac{\left(\Delta C_a / \Delta t\right) \times V_a}{C_l \times A} \quad (1)$$

where P_e (P_o) is the convective (diffusive) permeability, $\Delta C_a / \Delta t$ is the change in abluminal concentration with respect to time, V_a is the fluid volume in the abluminal compartment, C_l is the concentration in the luminal compartment, and A is the area of the filter.

The water flux was measured simultaneously with solute flux. When a 10-cm H_2O differential pressure was applied, the water flux (J_v) was measured by tracking the position of an air bubble that was inserted into the glass tubing. The bubble was monitored using a spectrophotometer which followed the air-liquid interface in the glass tube.

The bubble displacement data was used to compute J_v values using the following equation

$$J_V = \frac{\Delta d}{\Delta t} \times \frac{F}{A} \quad (2)$$

where $\Delta d/\Delta t$ is the bubble displacement per unit time, and F is a tube calibration factor (fluid volume per unit length of tubing).

Statistical Analysis

Minitab (Minitab; State College, PA) was used to calculate linear regressions between mitosis and permeability values. Correlations were evaluated using the Pearson Product Moment Correlation Coefficient also calculated in Minitab.

III. Results

Effect of paclitaxel on mitosis rate and LDL permeability

The convective (P_e) and diffusive permeability (P_o) of control and paclitaxel treated monolayers were measured using our transport system. After each transport experiment, the monolayers were fixed with 4% paraformaldehyde and the mitosis assay was performed. The

mitosis rate of each BAEC monolayer was plotted against its corresponding permeability (Figures 3.1 and 3.2).

The mitosis rate of BAEC monolayers maintained in growth media (10%FBS-MEM) ranged between 0.008% and 0.093% on day 5 after plating. To increase mitosis rates, BAEC monolayers were incubated with paclitaxel at a concentration of 2.5μM for 1.5, 3, 4.5 or 6 hours. Paclitaxel does not induce additional mitosis, but instead arrests the cells in M-phase by hyper-stabilizing the structure of microtubules. Therefore the increase in mitosis greatly depended on the basal rate of mitosis at the time of incubation as well as on the duration of the incubation period. For this reason, results from each incubation period were not pooled together and averaged but instead plotted individually against the permeability measured for each particular monolayer. When treated with paclitaxel at the indicated times, the mitosis rate ranged between 0.099% and 1.03% (Figures 3.1 and 3.2). Because paclitaxel has been shown to induce apoptosis, we also measured apoptosis rates on paclitaxel-treated monolayers. The apoptosis rate was 0.47% $\pm$ 0.03%, 0.45% $\pm$ 0.03%, and 0.50% $\pm$ 0.06% for control monolayers, and monolayers treated with paclitaxel for 4.5hr and 6hr, respectively. There was no significant difference between these apoptosis rates ($p>0.6$).

The average diffusive permeability of control monolayers was $2.8\text{x}10^{-7} \pm 2.5\text{x}10^{-8}$ cm/s, similar to previous measurements (Cancel, Fitting et al. 2007; Cancel and Tarbell 2010). Increasing the mitosis rate had a small but significant effect on the diffusive permeability to LDL as shown in the correlation in Figure 3.1. The Pearson correlation coefficient was calculated to be 0.696 with a *p*-value <0.0005.

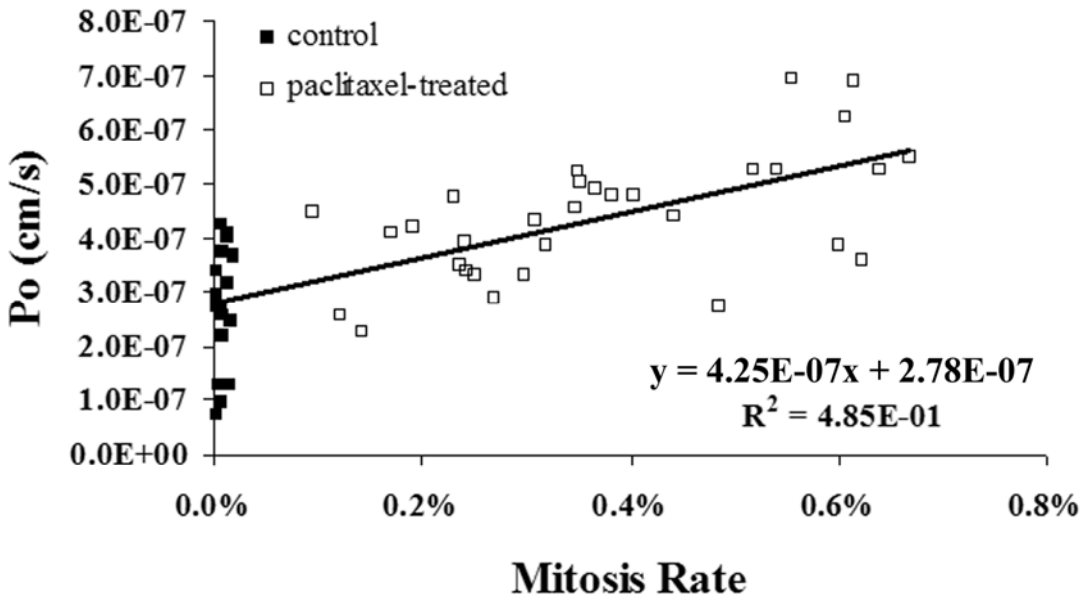

Figure 3.1. Correlation between mitosis rate and difussive permeability (P_o). Plot shows the mitosis rate and P_o for control monolayers (■) and monolayers treated with paclitaxel (□) for 1.5, 3, 4.5 or 6 hrs. The Pearson Product moment correlation coefficient = 0.696, $p<0.0005$.

The average convective permeability of control monolayers was $1.71 \times 10^{-6} \pm 1.50 \times 10^{-7}$ cm/s, consistent with previous measurements (Cancel, Fitting et al. 2007; Cancel and Tarbell 2010). P_e was significantly increased by increasing mitosis rates with paclitaxel as shown in Figure 3.2. The Pearson correlation coefficient was 0.774 with a *p*-value <0.0005.

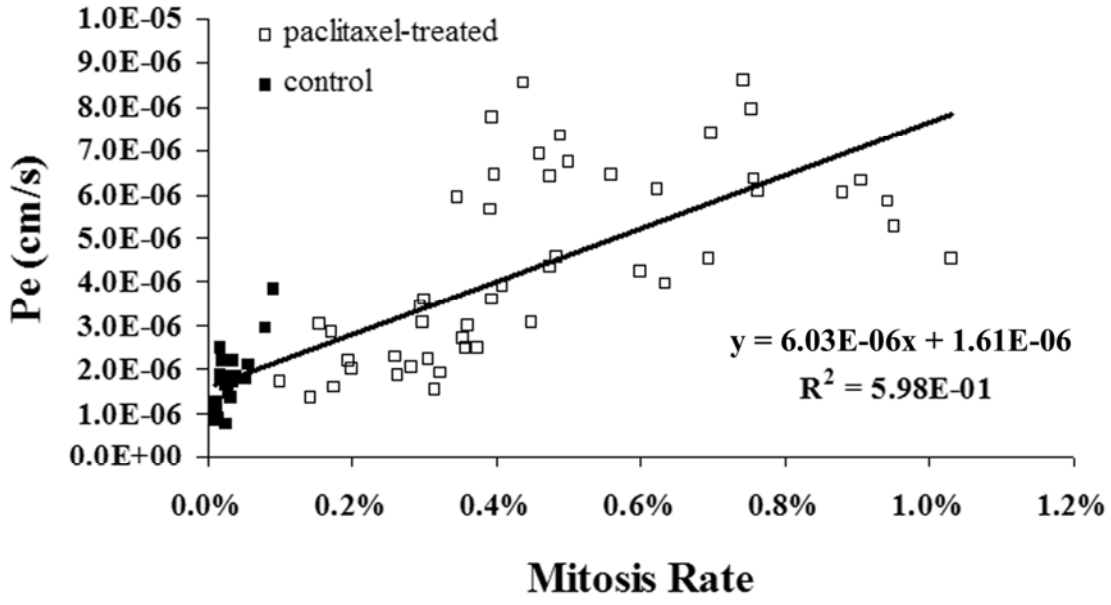

Figure 3.2. Correlation between mitosis rate and convective permeability (P_e). Plot shows the mitosis rate and P_e for control monolayers (■) and monolayers treated with paclitaxel (□) for 1.5, 3, 4.5 or 6 hrs. The Pearson Product moment correlation coefficient = 0.774, $p<0.0005$.

Effect of paclitaxel on water flux

The flux of water (J_v) across control and paclitaxel-treated monolayers was measured simultaneously with permeability, as described in the methods. Figure 3.3 shows the effect of paclitaxel on water flux. Control monolayers had an average J_v of $3.24 \times 10^{-6} \pm 2.39 \times 10^{-7}$ cm/s. Increasing the mitosis rate significantly increased the water flux, as shown on Figure 3.3. The Pearson correlation coefficient was 0.795 with a *p*-value <0.0005.

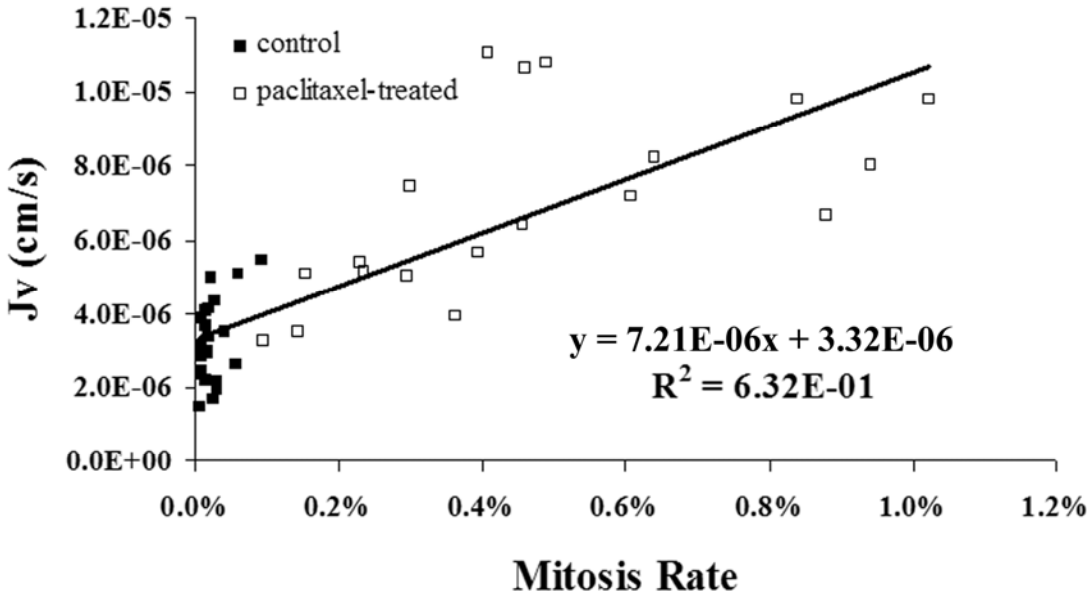

Figure 3.3. Correlation between mitosis rate and water flux (J_v). Pearson Product Moment correlation coefficient = 0.795, $p<0.0005$.

Co-localization of endothelial gap formation with mitosis

BAEC monolayers were immunostained for the adherens junction protein VE-cadherin and co-stained for mitosis to assess the co-localization of gaps in the cell-cell junction with mitosis. Representative photomicrographs are shown in Figure 3.4. Mitotic cells in control monolayers appear, in most cases, to be spread-out and flattened whereas paclitaxel-treated mitotic cells appear rounded. This rounded morphology is characteristic of cells during metaphase (Boucrot and Kirchhausen 2008). Consistent with these results, paclitaxel-treated cells have been shown to arrest in metaphase (Jordan, Toso et al. 1993) because the spindle-assembly checkpoint ensures that cells do not enter anaphase until all chromosomes are attached to both poles of the spindle, a process highly dependent on microtubule dynamics (Alberts, Johnson et al. 2002).

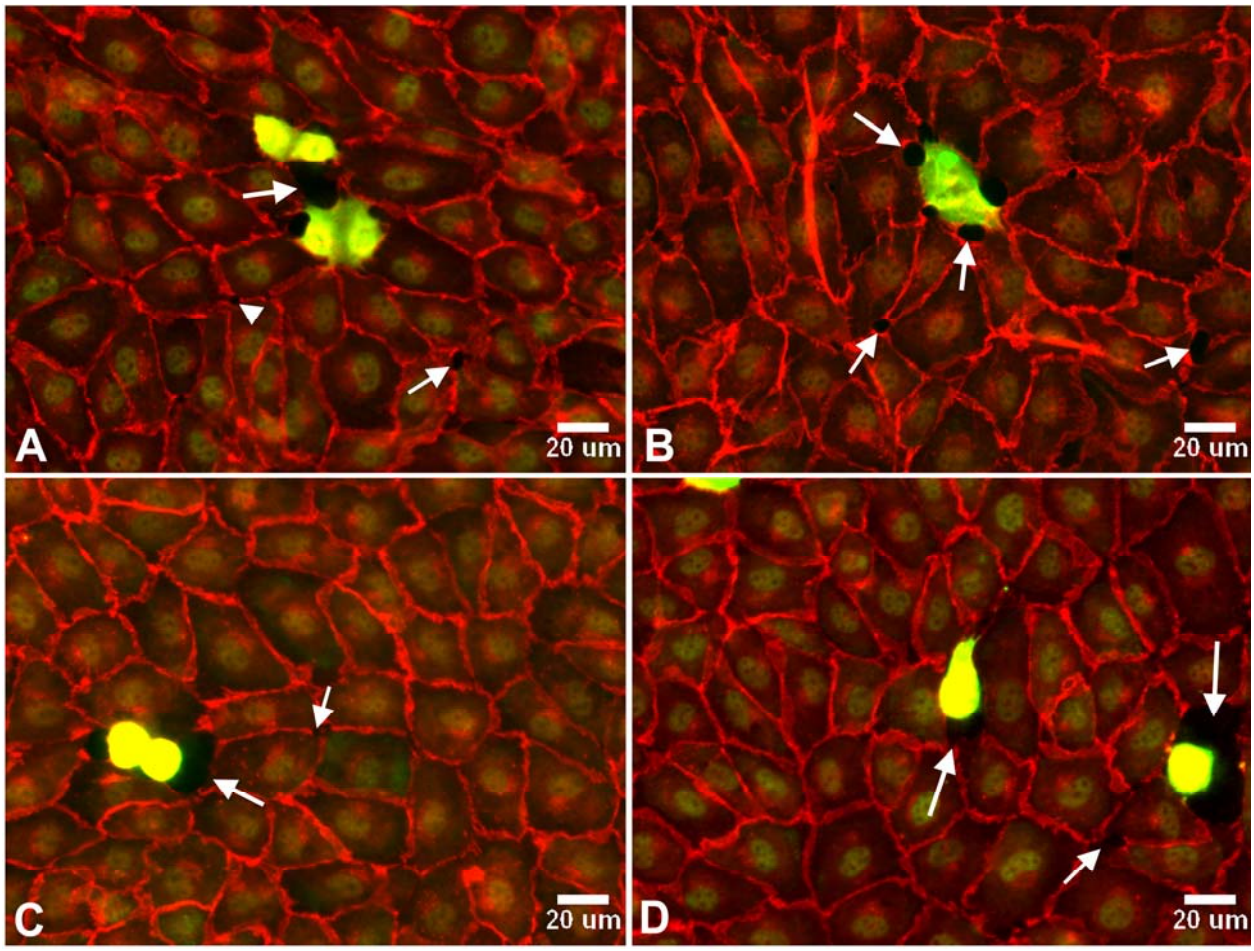

Figure 3.4. VE-Cadherin staining (red) for cell-cell junction and MPM-2 staining (green) for M phase. A and B are controls; C and D are treated with paclitaxel for 3hrs. Arrows denote gaps in cell-cell junctions. Arrowhead in A denotes a tricellular corner gap. Note that paclitaxel-treated mitotic cells appear rounded, while controls are more spread out. This is likely due to paclitaxel arresting cells in metaphase, when cells normally assume this spherical shape.

The total number of mitotic cells and gaps in 15 fields per monolayer ($0.044mm^2$ per field) was quantified for two controls (one with a normal mitosis rate and one with a slightly high rate) and one paclitaxel-treated monolayer. A gap was defined as a clear opening in the cell-cell junction, normally appearing as a dark region between cells (arrows in Figure 3.4). In addition to quantifying gaps associated with mitotic cells, we also identified tricellular corners, which occur where three cells meet (arrowhead in Figure 3.4A), as well as other gaps. The

results are shown in Table 3.1 and 3.2 for control monolayers, and Table 3.3 for a paclitaxel-treated monolayer.

The mitosis rate for each monolayer was obtained from a count of all mitotic cells in each filter. Since most camera fields (~60 cells/field) analyzed contained at least one mitotic cell, the rate obtained from adding up these fields is artificially high. Most mitotic cells were found to co-localize with an endothelial gap (82%, 88% and 95% for control and paclitaxel-treated monolayers, respectively). However, most gaps did not co-localize with a mitotic cell. Tricellular corners accounted for 25%, 17% and 12% of all the gaps in control and paclitaxel-treated monolayers, respectively. Gaps that did not co-localize with mitotic cells or tricellular corners accounted for the majority of the gaps found (53%, 61% and 55%).

Table 3.1. Quantification of gaps in association with mitosis and tricellular corners in a control monolayer.

	Cells			Gaps			
Field	**Mitotic**	**Total**	**Cell Density (cells/cm^2)**	**Mitosis**	**Tricellular**	**Other**	**Total**
1	2	70	1.6 x10^5	2	1	2	5
2	0	68	1.5 x10^5	0	0	1	1
3	0	75	1.7 x10^5	0	0	2	2
4	0	81	1.8 x10^5	0	1	0	1
5	1	64	1.5 x10^5	1	1	1	3
6	1	73	1.7 x10^5	1	1	3	5
7	1	68	1.5 x10^5	1	2	1	4
8	1	79	1.8 x10^5	0	0	1	1
9	1	66	1.5 x10^5	0	0	0	0
10	1	62	1.4 x10^5	1	0	3	4
11	1	81	1.8 x10^5	1	2	0	3
12	1	77	1.7 x10^5	1	0	4	5
13	1	68	1.5 x10^5	1	0	2	3
14	0	74	1.4 x10^5	0	0	1	1
15	0	68	1.5 x10^5	0	2	0	2
Total	11	1074	-	9	10	21	40

Mitosis rate: 0.161%
Mitotic cells with gap: 82%

Gaps associated with Mitotic cells: 23%
Gaps associated with tricellular corners: 25%
Other gaps: 53%

Table 3.2. Quantification of gaps in association with mitosis and tricellular corners in a control monolayer.

	Cells			Gaps			
Field	**Mitotic**	**Total**	**Cell Density (cell/cm^2)**	**Mitosis**	**Tricellular**	**Other**	**Total**
1	1	61	1.4 x10^5	0	1	1	2
2	1	63	1.4 x10^5	1	1	2	4
3	1	63	1.4 x10^5	1	0	0	1
4	1	58	1.3 x10^5	1	0	2	3
5	1	63	1.4 x10^5	1	1	3	5
6	1	63	1.4 x10^5	1	2	1	4
7	1	66	1.5 x10^5	1	1	0	2
8	0	62	1.4 x10^5	0	1	0	1
9	0	64	1.5 x10^5	0	0	1	1
10	0	63	1.4 x10^5	0	0	2	2
11	0	68	1.5 x10^5	0	2	5	7
12	0	62	1.4 x10^5	0	0	4	4
13	0	60	1.4 x10^5	0	0	1	1
14	1	65	1.5 x10^5	1	0	1	2
15	0	63	1.4 x10^5	0	0	2	2
Total	8	944	-	7	9	25	41

Mitosis rate: %0.058
Mitotic cells with gap: 88%

Gaps associated with Mitotic cells: 17%
Gaps associated with tricellular corners: 22%
Other gaps: 61%

Table 3.3. Quantification of gaps in association with mitosis and tricellular corners in a paclitaxel-treated monolayer.

	Cells			Gaps			
Field	**Mitotic**	**Total**	**Cell Density (cells/cm^2)**	**Mitosis**	**Tricellular**	**Other**	**Total**
1	2	60	1.4 x10^5	2	1	3	6
2	1	60	1.4 x10^5	1	0	1	2
3	0	59	1.3 x10^5	0	2	2	4
4	1	62	1.4 x10^5	1	0	2	3
5	0	64	1.5 x10^5	0	0	7	7
6	0	76	1.7 x10^5	0	0	1	1
7	1	72	1.6 x10^5	1	0	0	1
8	1	64	1.5 x10^5	1	0	1	2
9	0	72	1.6 x10^5	0	1	3	4
10	1	63	1.4 x10^5	1	1	2	4
11	1	65	1.5 x10^5	1	1	1	3
12	2	64	1.5 x10^5	2	0	2	4
13	3	78	1.8 x10^5	3	0	2	5
14	1	63	1.4 x10^5	1	1	4	6
15	6	66	1.5 x10^5	5	0	1	6
Total	20	988	-	19	7	32	58

Mitosis rate: 0.690%
Mitotic cells with gap: 95%

Gaps associated with Mitotic cells: 33%
Gaps associated with tricellular corners: 12%
Other gaps: 55%

In order to compare our gap counts to leakage spot co-localization studies in the literature, we estimated the number of distinct spots our gaps would produce. Lin et al. (Lin, Jan et al. 1989) reported Lucifer Yellow LDL leakage spots around mitotic cells to be slightly larger than the size of one cell. Truskey et al. (Truskey, Roberts et al. 1992) observed focal regions of increased ^{125}I-LDL permeability, some around mitotic cells, to be two or three cells in diameter. Taking these observations as a guide, we estimated that each gap would produce a spot 1.5 times the surface area of a cell, and counted the number of distinct spots our gaps would produce.

Where a mitotic gap and another type of gap would both produce a spot covering the same area, the spot was assigned to the mitotic cell. The results are shown in Table 3.4.

Table 3.4. Association of leakage spots or increased Pe with mitotic cells and tricellular corners. Leakage spots for the present study were estimated using observations of gaps in cell-cell junctions.

	Mitotic Cells		**% of Total sites with leakage**		
	Frequency (%)	% with leakage	Mitotic	Tricellular	Other
Present study (BAECs; estimated leakage spots)					
control 1	0.161	73	27.6	24.1	48.3
control 2	0.058	100	25.8	22.6	51.6
paclitaxel treated	0.690	70	34.1	12.2	53.7
Truskey et al. (rabbit aorta; increased Pe)	0.011	65	25	-*	75*
Lin et al. (rat aorta; leakage spots)	0.034	80.5	45.3	-*	54.7*

* Truskey et al. and Lin et al. did not look at tricellular corners, therefore the unexplained leakage spots are assigned to the "Other" category.

IV. Discussion

The aim of this study was to show that, as part of the leaky junction pathway, mitosis rates dictate in part the permeability of endothelial cell monolayers to LDL under convective conditions. To this end, we used paclitaxel to induce elevated rates of mitosis. Paclitaxel is a taxane used in the treatment of lung, ovarian and breast cancer (Rowinsky 1997), and in the prevention of restenosis of coronary stents (Colombo, Drzewiecki et al. 2003; Stone, Ellis et al. 2004). Paclitaxel binds microtubules (Schiff and Horwitz 1980) thus hyper-stabilizing the microtubule network and arresting cells in M phase (Jordan, Toso et al. 1993). Verin et al. (Verin, Birukova et al. 2001) exposed bovine pulmonary artery endothelial cells to paclitaxel at 2.5μM for up to 4 hours and found it had no effect on the transendothelial electrical resistance (TER) of cell monolayers. In the same study, the microtubule-disrupting agents nocodazole and

vinblastine were shown to increase TER and stress fiber formation, resulting in cell contraction and the formation of gaps between cells. These effects were attenuated by the addition of paclitaxel (Verin, Birukova et al. 2001). These results suggest that paclitaxel does not affect the junctional complex between endothelial cells.

Paclitaxel has also been shown to induce apoptosis in certain cells types, including endothelial cells, depending on the concentration used and the exposure time (Wang, Wang et al. 2000; Pasquier, Carre et al. 2004). Apoptosis in paclitaxel-treated cells is thought to occur through multiple mechanisms. Mitotic arrest can induce apoptosis through the spindle-assembly checkpoint. The activation of the mitotic spindle-assembly checkpoint has recently been shown to inhibit the anti-apoptotic proteins Bcl-xL and Bcl-2 through CDK1-mediated phosphorylation (Terrano, Upreti et al.). In addition, activation of other cyclin-dependent kinases (cdks) and the c-Jun N-terminal kinase/stress-activated protein kinase (JNK/SAPK) have been shown to be involved in paclitaxel-induced apoptosis (Wang, Wang et al. 2000). To check that our treatment did not induce apoptosis in BAECs, we used the TUNEL technique to measure apoptosis of cells treated with paclitaxel (2.5μM) for 4.5 and 6 hours (the longest exposure times). We found that paclitaxel did not induce apoptosis above control levels under these conditions.

As in our apoptosis study (Cancel and Tarbell 2010), we sought to observe the co-localization of endothelial gap formation with mitotic cells. BAEC monolayers were co-stained with the adherens junction protein VE-cadherin to identity gaps and MPM-2 for mitotic cells (Figure 3.4). Despite the small number of cells analyzed (about 1000 each for control and paclitaxel-treated monolayers) the results were similar to previous in vivo studies of the association of LDL leakage with mitosis (Table 3.4). Truskey et al (Truskey, Roberts et al. 1992) studied the associations of mitotic cells with increased permeability of ^{125}I-LDL in the

rabbit aorta. They found that 65% of mitotic cells had increased permeability, accounting for 25% of all permeable areas. Lin et al. (Lin, Jan et al. 1989) studied the association of Lucifer Yellow LDL (LY-LDL) with mitosis in the rat aorta. In that study 80.5% of mitotic cells were found to co-localize with LY-LDL leakage spots, accounting for 45.3% of all leakage spots. In our control monolayers, 84% (average of two controls) of mitotic cells were associated with estimated leakage spots accounting for 26.7% of all leaks. In paclitaxel-treated monolayers 70% of mitotic cells were associated with gaps, accounting for 34% of all gaps. There is no point of comparison for these paclitaxel-treated cells because all in vivo co-localization studies have been done on the straight portion of the normal rat or rabbit aorta, where mitotic rates are low. For atheroprone areas, co-localization in vivo are nearly impossible to analyze because these areas generally present a diffuse staining pattern covering a large area, making it difficult to correlate the leaks (the so-called blue areas in experiments with EBA) with individual mitotic cells.

The main results from the present study are the correlations obtained for the association of mitosis with P_e, P_0 and J_v. In Figure 3.5 these correlations have been normalized by the average permeabilities and mitosis rates for each set. As expected, the main effect of mitosis is in the convective permeability (P_e) of LDL, while there is little effect on the diffusive permeability (P_0). This plot also shows that in order to increase each transport property by 2-fold the mitosis rate would have to be increased by 10-, 18-, and 77-fold for P_e, J_v, and P_0, respectively.

Few studies have measured mitosis rates in atheroprone areas of the vasculature. Wright (Wright 1972) measured the incorporation of [^{3}H]thymidine over the length of the aorta of guinea pigs. The mitotic index varied between 0.54 and 1.23%, with the highest mitotic index found to be in the aortic arch. Around the mouths of branches, [^{3}H]thymidine uptake was

significantly higher, by 1.7-fold, than in control areas at the same level but remote from the branch. When a silver clip was used to create an arterial constriction, a 3.7-fold increase in thymidine uptake was found in the stenosed area. Caplan and Schwartz (Caplan and Schwartz 1973) found a 1.4-fold increase in [^{3}H]thymidine labeling index in areas of EBA uptake in the pig aorta. Schwartz measured [^{3}H]-thymidine uptake in the rat aorta and found clusters of replicating cells (Schwartz and Benditt 1976). While not all of these clusters were correlated with areas of disturbed flow, the clusters had an average mitotic index that was twice that of the entire population average. Since [^{3}H]thymidine incorporates into the nuclei of cells in the DNA synthesis phase (S-phase), these rates cannot be directly compared to our M-phase rates. In addition, cells in S-phase are not likely to yet be leaky. However these results do show that atheroprone areas exhibit higher cell turnover rates than protected areas such as the straight part of the aorta.

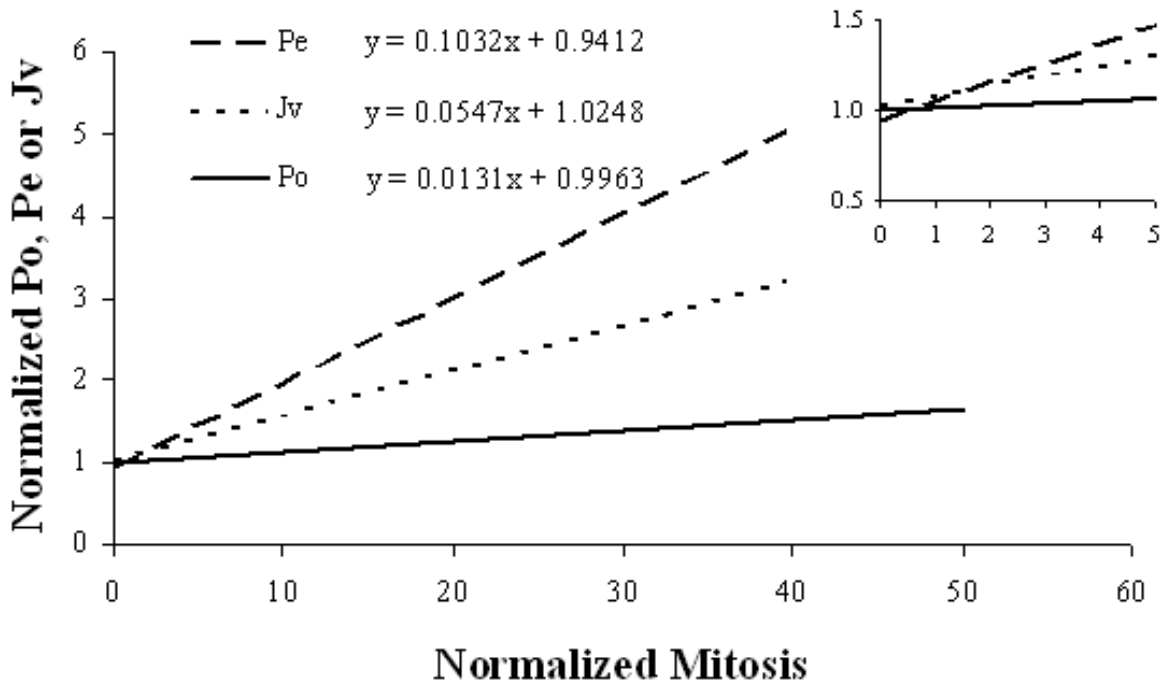

Figure 3.5. Effect of mitosis rate on transport properties. The data in Figures 3.1, 3.2, and 3.3 was normalized by the average control values for each set. Inset shows detail at the low range of (normalized) mitosis.

Better studies are needed to determine the fraction of cells in M-phase (when the junctions are likely to be leaky) in atheroprone areas of the aorta, as well as during early lesion formation. However the results summarized above seem to indicate that the increase in mitosis rates in these areas would likely be lower than 10-fold. If we consider a range of increase in mitosis between 2- and 5-fold above control, our results indicate increases in permeability between 15 and 47% (inset in Figure 3.5). These results are in good agreement with the previous in vivo study of Truskey et al. in which they found that permeable areas associated with mitotic cells had LDL permeability 26 to 47% higher than regions not associated with mitotic cells (Truskey, Roberts et al. 1992). In experiments with ^{131}I-albumin and ^{131}I-fibrinogen, the blue

areas associated with increased cell turnover had permeabilities 66% and 64% higher, respectively, than white areas (Bell, Adamson et al. 1974; Bell, Gallus et al. 1974).

In conclusion, we have found a strong linear relationship between the mitosis rate of endothelial cells monolayers and their convective permeability to LDL. The predicted increases in LDL permeability are in agreement with values observed in vivo in areas of increased cell turnover. The increase in permeability obtained by increasing mitosis is about half of that obtained in our previous study (Cancel and Tarbell 2010) by increasing apoptosis rate by the same amount. This is due in part to the fact that the baseline mitosis rate is an order of magnitude lower than the baseline apoptosis rate. However if we take into account the physiological (and pathological) ranges of mitosis and apoptosis rates, we find that apoptosis increases much more than mitosis in diseased areas. The highest apoptosis rates are found around the plaque stenosis (Tricot, Mallat et al. 2000) and can reach up to 50 times the baseline. Several studies of cell proliferation in plaques have reported increased mitosis of smooth muscle cells, as well as other cells of undetermined type in the intima, but not of the luminal endothelial cells covering the plaque (Cavallero, Turolla et al. 1971). Increased mitosis rates are found in atheroprone areas before any lesion has formed and are about 2 to 4 times the baseline rate, as summarized above. Apoptosis rates in these areas are also about 4-fold greater than in protected areas (Gerrity, Richardson et al. 1977). Taken together these results indicate that, while endothelial cell mitosis may play a role in the initial infiltration of LDL into the artery wall, the progression of atherosclerosis might be more closely correlated with endothelial cell apoptosis.

Chapter 4: 3-pore model analysis of apoptosis and mitosis data

I. Introduction

In our previous study of LDL transport under convective conditions (Cancel, Fitting et al. 2007) we used a 3-pore model to analyze the fluxes of LDL, albumin and water measured using our transport system. That study allowed us to identify the leaky junction as the dominant pathway for LDL transport under physiologically relevant convective conditions. In this chapter, we use the model to analyze the fluxes of LDL and water obtained when apoptosis and mitosis were increased or decreased pharmacologically.

II. Methods

3-pore model

Solute transport through a single pathway can be described using the following relationships (Patlak, Goldstein et al. 1963)

$$P_e = P_0 Z + (1-\sigma) J_V \quad (1)$$

where P_0 is the diffusive permeability, P_e is the apparent permeability and it has been assumed that the concentration in the abluminal side of the endothelium is much less than that on the luminal side. The first term is the diffusive contribution and the second term is convective. The relative importance of diffusion to convection is determined by Z, defined as

$$Z = \frac{N_{P_e}}{\exp N_{P_e} - 1} \quad (2)$$

where N_{Pe} is the Peclet number defined as

$$N_{P_e} = \frac{J_V (1-\sigma)}{P_0} \quad (3)$$

If we allow for vesicular transport that is strictly diffusive (i.e. no water flux through vesicles), and two convective pathways: a pathway through the breaks in the tight junction (pore 2) and a leaky junction pathway (pore 3), then the following 3-pore model equations arise

$$J_V = J_{V2} + J_{V3} \quad (4)$$

$$P_e = P_{0v} + P_{02}Z_2 + J_{V2}(1-\sigma_2) + P_{03}Z_3 + J_{V3}(1-\sigma_3) \quad (5)$$

$$P_0 = P_{0v} + P_{02} + P_{03} \quad (6)$$

J_{vi} is the water flux through pore i ; P_{0v} is the diffusive permeability of the vesicular pathway ; P_{0i} is the diffusive permeability of pore i ; σ_i is the reflection coefficient of pore i and Z_i is defined by equations (2) and (3) with the appropriate subscripts for pore i. It is assumed here, as by Fu et al. (Fu, Curry et al. 1997), that the tight junction pathway (not the breaks) is so small that it not only excludes LDL but also blocks water flux because of its elevated hydraulic resistance. Therefore all the water is assumed to pass through pores 2 and 3. To further simplify these expressions we assume that pore 2 does not allow LDL transport ($\sigma_2 = 1$; $P_{02} = 0$) and that pore 3 allows unrestricted passage of LDL ($\sigma_3 = 0$). With these assumptions we are left with the following three equations:

$$J_V = J_{V2} + J_{V3} \quad (4)$$

$$P_e = P_{0v} + P_{03}Z_3 + J_{V3} \quad (5)$$

$$P_0 = P_{0v} + P_{03} \quad (6)$$

These three equations can be solved for the three unknowns: J_{v2}, J_{v3}, P_{03}. The data and correlations obtained for J_v, P_e and P_0 in chapters 2 (as a function of apoptosis) and 3 (as a function of mitosis) were used to determine the unknowns. P_{0v} was determined using the methods described below.

Cell fixation and receptor blocking experiments

To eliminate trancytosis in vesicles from the overall transport process, BAECs were fixed with 1% paraformaldehyde for 10 minutes before performing the transport experiment. To test the role that LDL receptors play in transport across the endothelium, we ran experiments in which an excess of untagged native LDL was added to saturate the receptors. Native LDL was added at 50 times the concentration of tagged (DiI) LDL and the standard transport experiment was performed. In both of these sets of experiments, only diffusive permeability was measured. The results are shown in Table 4.1.

Table 4.1. Diffusive LDL permeability of fixed and receptor-blocked monolayers. From Cancel et al. 2007

P_0 cm/s x 10^{-7}	$P_{0,fixed}$ cm/s x 10^{-7}	$P_0 / P_{0,fixed}$
1.79 ± 0.29	0.69 ± 0.18	2.59 ± 0.80
P_0 cm/s x 10^{-7}	**$P_{0,excess\ LDL}$ cm/s x 10^{-7}**	**$P_0 / P_{0,excess\ LDL}$**
1.16 ± 0.50	0.51 ± 0.09	2.28 ± 1.10

There was no significant difference between the permeability of fixed and receptor-blocked monolayers (or between controls for each set) and, therefore, the average of the two sets was used for calculations. Note that, for LDL, $P_{0,fixed/excess\ LDL}$ is equal to P_{03}, since only these two pathways are available. For the purpose of using these results to analyze the apoptosis and mitosis data it will be beneficial, however, to instead solve for the fraction of total diffusive permeability that is accounted for by the transcytosis component (P_{0v}) as follows:

$$\frac{P_{0v}}{P_0} = \frac{P_0 - P_{0,\,fixed\,/\,excessLDL}}{P_0} = 1 - \frac{P_{0,\,fixed\,/\,excessLDL}}{P_0} \quad (7)$$

For the results in Table 4.1 we find that 59% of the diffusive transport goes through vesicles (Cancel, Fitting et al. 2007). In the analysis that follows, we first assumed that this fraction

stayed the same for our control monolayers, and calculated P_{0v} accordingly. We then assumed that none of the drugs used to treat the cells had an effect on vesicular transport, that is, any change in P_0 is due to changes in the leaky junction (P_{03}) not in vesicular transport (P_{0v}).

III. Results and Discussion

Comparison of 3-pore model parameters for control monolayers

Table 4.2 shows the results of the 3-pore model analysis on the control monolayers for the three separate experimental sets. The only statistically significant difference among these three sets is in the J_v of the mitosis control set, which is about 40% lower than for the other two sets. Note that since the LDL permeability is similar for all three sets, the amount of water going through the leaky junction calculated using our model (J_{v3}) is not significantly changed. The main difference between the sets is in J_{v2}, suggesting that some sets of cells formed tighter junctions than others. Another possibility, not considered in our model, is that some sets of cells expressed more or less aquaporin than others. In our experience, the range of J_v in Table 4.2 is within the normal variation between different batches of cells. Clearly, this difference has not affected the results as far as LDL in concerned. However it is important to consider these variations when assessing the percentage contribution of each pore to water flux.

The contribution of vesicles to the total diffusive permeability was only measured for the first set of controls (Cancel, Fitting et al. 2007) as indicated above. However, since the diffusive permeability to LDL is not significantly different between sets our assumption that the fraction P_{0v}/P_0 does not change seems reasonable.

Table 4.2. Transport parameters and contribution of each pore to the overall LDL or water transport for control monolayers in the three experimental sets. Permeability and water flux given in units of cm/s x 10^{-6}. The numbers in parenthesis are the percentage contribution of each pore to the overall transport.

Expt. Set				Pore Contribution to Overall Transport			
				Water		LDL	
	J_v	P_e	P_0	J_{v2}	J_{v3}	vesicles	Pore 3
Control (Cancel et al. 2007)	5.39	1.31	0.208	4.19 (77.7%)	1.2 (22.3%)	0.12 (9.1%)	1.20 (90.9%)
Control (apoptosis)	5.05	2.07	0.260	3.14 (62%)	1.9 (38%)	0.15 (8%)	1.91 (92%)
Control (mitosis)	3.24	1.71	0.279	1.70 (52%)	1.5 (48%)	0.16 (9%)	1.55 (91%)

3-pore model analysis of apoptosis data

Table 4.3 shows the results for the 3-pore model analysis on the apoptosis data. As discussed in Chapter 2, the only value that was significantly different from control and between treatments was the convective permeability (P_e). The diffusive permeability (P_0), while slightly higher, was not significantly different from control for any of the treatments. We calculated P_{0v} as 59% of P_0 for control monolayers and assumed that this value stayed constant for all treatments, as indicated in the Methods.

J_v of treated monolayers was significantly different from control, but not from each other. The results in Table 4.3 show that J_v increases much more than what can be explained by an increase in leaky junctions. There are at least two possible explanations for this observation. One possibility, as discussed in Chapter 2, is that the drugs used to induce apoptosis have an adverse effect on the cell-cell junctions. Previous studies have shown that TNFα disrupts the junctional complex of endothelial cells (Wojciak-Stothard, Entwistle et al. 1998; Petrache, Birukova et al. 2003; McKenzie and Ridley 2007), producing a fragmented distribution of ZO-1 and loss of occludin. Our own experiments (Chapter 2) showed decreased ZO-1

immunoreactivity in treated monolayers, even those where apoptosis was inhibited by Z-VAD-FMK. These disruptions to the tight junction strand would affect water flux without an increase in LDL permeability.

A second way in which water flux could increase while LDL transport does not is if there is a gradual widening of the junctions as the cells become apoptotic. The gaps around a dying cell would initially allow more water but not more LDL to pass through. Similarly, as the neighboring cells gradually close the gaps opened by the apoptotic cell, the junction would be leaky to water for a longer period than to LDL. Chen et al. (Chen, Jan et al. 1995) studied the ultrastructure of the junctions around dying endothelial cells and found gaps around the cells ranging from 15nm to 1000nm. Chien and coworkers (Chien, Lin et al. 1988) found that only 63% of dying cells associated with an EBA leakage spot, suggesting that some of the dying cells do not have gaps big enough to allow even the 7nm diameter EBA molecule. Together with our immunostaining experiments (Chapter 2) these results suggest that both processes, TNFα effect on junctions and gradual widening of junctions, are in play and contribute to the observed increase in water flux.

Table 4.3. Transport parameters and contribution of each pore to the overall LDL or water transport for apoptosis data. Permeability and water flux given in units of cm/s x 10^{-6}. The numbers in parenthesis are the percentage contribution of each pore to the overall transport.

Expt. Set				Pore Contribution to Overall Transport			
				Water		LDL	
	J_v	P_e	P_0	J_{v2}	J_{v3}	vesicles	Pore 3
Control	5.05	2.07	0.260	3.14 (62%)	1.9 (38%)	0.15 (8%)	1.91 (92%)
TNFα/CHX + 100μM Z-VAD-FMK	11.7	4.47	0.322	7.40 (63%)	4.31 (37%)	0.15 (3%)	4.31 (97%)
TNFα/CHX + 50μM Z-VAD-FMK	15.6	7.27	0.456	8.51 (54%)	7.11 (46%)	0.15 (2%)	7.11 (98%)
TNFα/CHX	13.7	9.09	0.452	4.78 (35%)	8.94 (65%)	0.15 (2%)	8.94 (98%)

3-pore model analysis of mitosis data

Using our 3-pore model and the correlations obtained (Figures 3.1, 3.2 and 3.3), we determined the amount of water and LDL that is transported through each pore as a function of the mitosis rate. Figure 4.1 shows the results of these calculations for the water flux. The plot shows that the amount of water going through the leaky junction (J_{v3}) increases nearly in parallel with the overall increase in J_v. There is a small increase in the amount of water going through the break in the tight junction strand, J_{v2}. J_{v3} increases by 5.12-fold over the entire range of mitosis rates, while J_{v2} increases by 1.64-fold. As in the case of apoptosis above, this small increase in the amount of water passing through the break in the tight junction strand could be due to a gradual widening of the junctions as cells enter mitosis, which initially allows more water but not more LDL transport. Lin et al (Lin, Jan et al. 1989) found that 80% of mitotic cells were associated with an LDL leakage spot, while this number was 99% for EBA, suggesting that the gaps around mitotic cells are not always large enough to allow LDL transport.

It is also possible that paclitaxel treatment could be having a small adverse effect on the junctions, independent of cell cycle arrest. A previous study showed no effect of paclitaxel on the TER of BAECs over a 4hr incubation (Verin, Birukova et al. 2001), however our highest mitosis rates were obtained with 6hrs of incubation. Nevertheless the increase in J_{v2} is relatively small compared to the increase in the water flux through the leaky junction pathway (J_{v3}).

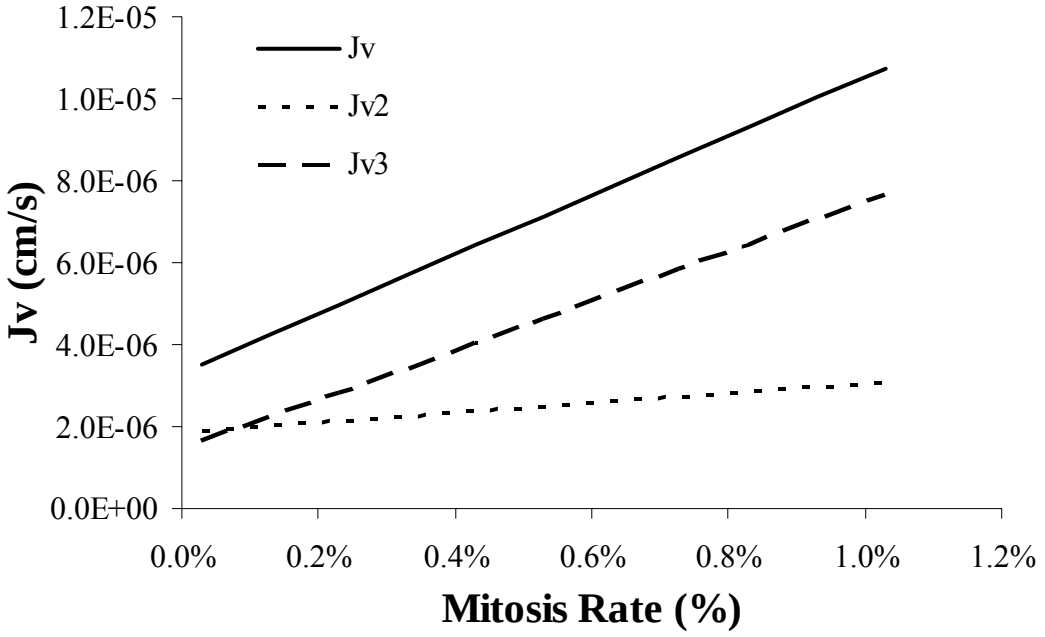

Figure 4.1. 3-pore model analysis of mitosis results. Water flux values show the increase of total flux (J_v), flux through break in tight junction strand (J_{v2}) and flux through the leaky junction (J_{v3}).

Figure 4.2 shows the results of the 3-pore model calculations for LDL transport. Once again we assumed P_{0v} is 59% of P_0 for control monolayers, or 1.64×10^{-7} cm/s, and that this value does not change with paclitaxel treatment. The diffusive permeability is shown on the left axis of Figure 4.2. Since P_{0v} was assumed to remain constant with increasing mitosis rate, the entire increase in P_0 is calculated to go through the leaky junction (P_{03}). The vesicular transport initially accounts for 9.5% of the total LDL transport (dashed line, right axis on Figure 4.2). As

the LDL flux increases with higher mitosis rates, the vesicular contribution accounts for a smaller portion of the total flux (2.2% at the highest mitosis rate).

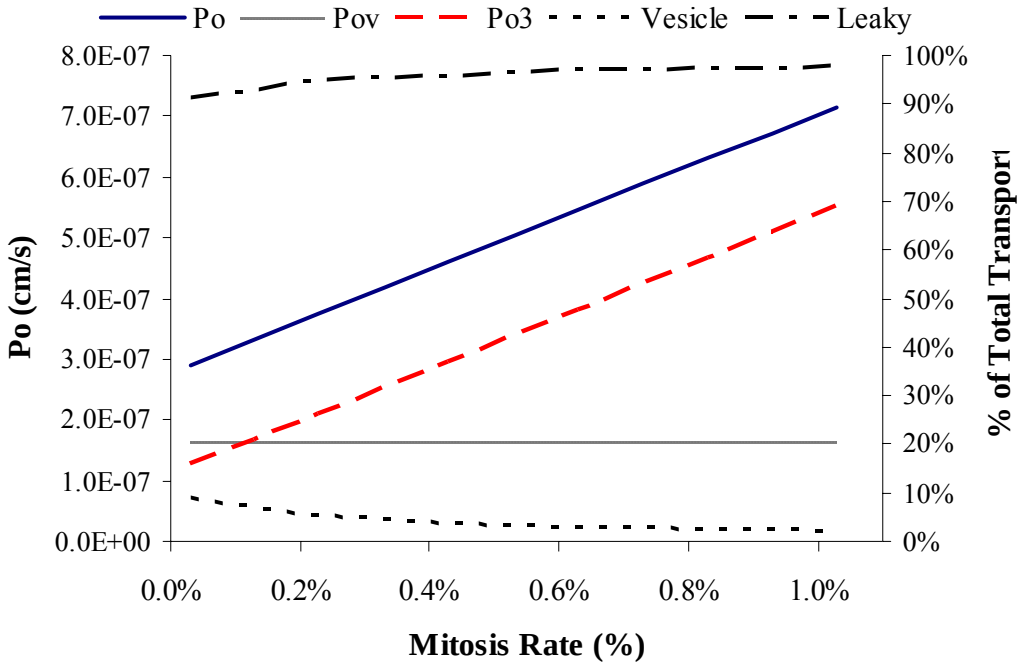

Figure 4.2. 3-pore model analysis of mitosis results. On the left axis, P_0 values show the increase of total diffusive transport (P_0), transport through vesicles (P_{0v}) and diffusive transport through the leaky junction (P_{03}). On the right axis the percentage of the total convective transport (P_e) that goes through vesicles (dashed line) and the leaky junction (dash-dot line) is shown.

IV. Conclusions

The main result of the analysis performed in this chapter is the insight gained into the pathways that carried water when apoptosis and mitosis rates were altered pharmacologically (Chapters 2 and 3, respectively). It is clear from the results that while the major increase in water flux is through the leaky junction (J_{v3}), there is also some increase through the break in the

tight junction strand pathway (J_{v2}). In the case of apoptosis, the increase in J_{v2} is comparable to the increase in J_{v3}. In this case, the large increase in J_{v2} is likely due to the adverse effect TNFα has on the endothelial cell-cell junctions. We have also hypothesized that J_v could increase as a result of a gradual widening of the junctions as the cells enter mitosis or apoptosis. This is more likely to be the case for mitosis, where we observe only a small increase in J_{v2} at the higher mitosis rates.

Chapter 5: Summary and Future Work

A relationship between increased endothelial permeability and localization of atherosclerosis is well established (Duncan, Buck et al. 1963; Somer and Schwartz 1971; Bell, Somer et al. 1972; Nielsen, Nordestgaard et al. 1992; Fry, Herderick et al. 1993). Despite this, controlling endothelial permeability to LDL pharmacologically is not currently a strategy in the treatment of atherosclerosis. Previous in vivo (Chien, Lin et al. 1988; Lin, Jan et al. 1988; Lin, Jan et al. 1990) and theoretical (Weinbaum, Tzeghai et al. 1985) studies supported the importance of leaky junctions associated with dying or dividing cells in the transport of LDL across the endothelium. A recent in vitro study in our lab demonstrated that leaky junctions are the dominant transport pathway for LDL under convective conditions, accounting for more than 90% of the transport (Cancel, Fitting et al. 2007). Building on these results, the objective of the present study was to directly probe the roles of mitosis and apoptosis in LDL transport across endothelial monolayers in order to assess the feasibility of developing drugs that reduce endothelial permeability to LDL.

In Chapter 2 we showed a strong correlation between LDL permeability and apoptosis using TNFα and cycloheximide to induce apoptosis and the broad caspase inhibitor Z-VAD-FMK to inhibit apoptosis. TNFα is an inflammatory cytokine secreted by stimulated macrophages and a major inflammatory modulator in atherosclerosis (Ross 1993). In addition to inducing apoptosis of endothelial cells, TNFα increases binding of LDL to endothelial and smooth muscle cells resulting in further inflammation (Ross 1999). A key molecule triggering the initial endothelial dysfunction leading to the inflammatory response in atherosclerosis is oxidized LDL (oxLDL) (Ross 1993). OxLDL has been shown to induce apoptosis in cultured

endothelial cells (Dimmeler, Haendeler et al. 1997; Harada-Shiba, Kinoshita et al. 1998; Kamiyama, Kishimoto et al. 2009) and to injure endothelial cells in vivo (Rangaswamy, Penn et al. 1997). Moving forward with our study, it would be important to explore the effects of oxLDL on LDL permeability, and to determine whether the correlation between apoptosis and permeability shown in Chapter 2 would still hold when oxLDL is used as the inducer of apoptosis.

Equally important would be to find and test drugs that could act as inhibitors of apoptosis for therapeutic use. In the present study we used the broad caspase inhibitor Z-VAD-FMK to inhibit apoptosis. Originally developed as a drug, Z-VAD-FMK was found to metabolize in vivo into the cytotoxic compound fluoroacetate (Van Noorden 2001), which made it unsuitable for clinical use. A number of apoptosis inhibitors are currently FDA approved or undergoing clinical development (see Green and Kroemer (Green and Kroemer 2005) for a list of compounds as of 2005). Some of these compounds target the inducers of apoptosis (e.g. TNFα and reactive oxygen species (ROS)), while others target the molecular machinery of apoptosis (e.g. caspases, PARP). It is interesting to note that most of these compounds are used for the treatment of inflammatory diseases such as rheumatoid arthritis. Evaluating the efficacy of these drugs in reducing endothelial permeability to LDL in our in vitro model would be an important first step in determining their potential as therapeutic agents for the treatment of atherosclerosis.

In a parallel study in our lab, Piraino et al. (Piraino, Cancel et al. under review) showed that simvastatin inhibits apoptosis and LDL permeability and found a correlation between these two values similar to the one obtained when Z-VAD-FMK was used as the inhibitor of apoptosis. Statins are low molecular weight drugs that reduce blood cholesterol levels by inhibiting 3-

hydroxy-3-methylgluraryl-CoA reductase, the rate-limiting enzyme of the mevalonate pathway. Statins are currently the most widely prescribed medications, however it is important to remember that statins are not prescribed for the inhibition of apoptosis and therefore their dosage is not optimized for this use. In fact statins have been shown to have a bi-phasic effect on endothelial cell apoptosis, with high doses resulting in increased apoptosis while low doses reduce apoptosis (Kureishi, Luo et al. 2000; Dulak and Jozkowicz 2005; Guerard, Rakotoniaina et al. 2006; Luthra, Dong et al. 2008). In addition, the efficacy of different statins as inhitors of apoptosis would also have to be evaluated.

In Chapter 3 we showed a strong correlation between LDL permeability and the mitosis rate. However, the effect of mitosis on permeability was about half that of apoptosis. Taking also into account that apoptosis rates increase much more than mitosis in diseased areas, we concluded that the progression of atherosclerosis is probably more closely correlated with endothelial apoptosis. Future efforts to reduce permeability of the endothelium to LDL should therefore be geared towards reducing endothelial cell apoptosis.

Using immunocytochemistry techniques, we attempted to correlate the formation of gaps (and potential leaks) between endothelial cells with both mitosis and apoptosis. In Chapter 2 we found that for control monolayers 28.2% of all potential leaks were associated with apoptotic cells and 17.9% were associated with tricellular corners. The majority of potential leaks (53.8%) were not associated with either apoptosis or tricellular corners. However, some of these leaks could be associated with mitotic cells, which could not be stained simultaneously. In Chapter 3 we found that 26.7% of all potential leaks were associated with mitotic cells while 23.3% were associated with tricellular corners. In this case, half of the potential leaks were not associated with either mitosis or tricellular corners, but could be associated with apoptosis. Combining the

results of the two experiment sets, we find that 55% of potential leaks are associated with apoptotic or mitotic cells, and 21% are associated with tricellular corners. The remaining 24% of potential leaks cannot be accounted for by any of these processes. However, as was discussed in Chapter 2, many of the gaps not directly associated with apoptotic cells could still have been formed as a consequence of apoptosis, either by the stretching of nearby cells to push away an apoptotic cell, by an early apoptotic cell that is not stained by the TUNEL technique, or by an apoptotic cell that has just detached from the monolayer (or is washed away during the immunostaining process) leaving only the gaps between its neighbors as evidence. It is also important to note that it is not clear whether tricellular corners would constitute a pore through which solutes can cross the endothelium. Walker et al. found that the tricellular regions were organized such that an overlapping flap provided by one of the cells covered the junctional discontinuity between the other two adjacent cells (Walker, MacKenzie et al. 1994).

Building on the results of the present study, the next step should be to confirm the role of apoptosis in LDL permeability in an animal model by establishing a correlation like the one found in Chapter 2. Methods to measure leakage of macromolecules (e.g. HRP, EBA, LDL), their permeability, and their co-localization with dying or dividing cells in blood vessels in vivo are well established (Chien, Lin et al. 1988; Lin, Jan et al. 1989; Lin, Jan et al. 1990; Truskey, Roberts et al. 1992; Chen, Jan et al. 1997; Shou, Jan et al. 2007). Inducing apoptosis in an animal model could be accomplished, as we have done in vitro, with the use TNFα. Studies of the pharmacokinetics of TNFα in rats (Zahn and Greischel 1989) and monkeys (Greischel and Zahn 1989) show that, at doses similar to the ones we have used in vitro, TNFα is quickly bound, internalized, and degraded via its receptor. Therefore an intravenous injection of TNFα should quickly deliver the drug to the endothelium and induce endothelial cell apoptosis. In

addition, apoptosis could be induced in vivo using oxLDL. Interestingly, while a previous study (Rangaswamy, Penn et al. 1997) demonstrated that oxLDL induces endothelial injury and increased permeability in vivo, a direct correlation such as the one found in Chapter 2 has not been established for oxLDL-induced apoptosis and permeability. Once these correlations are established in vivo, drugs found to be effective in reducing apoptosis and LDL permeability in vitro can be tested in the animal model. If successful, these steps will take us closer to the development of a new approach to the treatment of atherosclerosis.

References

(1994). "Randomised trial of cholesterol lowering in 4444 patients with coronary heart disease: the Scandinavian Simvastatin Survival Study (4S)." Lancet **344**(8934): 1383-1389.

(1998). "Prevention of cardiovascular events and death with pravastatin in patients with coronary heart disease and a broad range of initial cholesterol levels. The Long-Term Intervention with Pravastatin in Ischaemic Disease (LIPID) Study Group." N Engl J Med **339**(19): 1349-1357.

Adamson, R. H. and C. C. Michel (1993). "Pathways through the intercellular clefts of frog mesenteric capillaries." J Physiol **466**: 303-327.

Alberts, B., A. Johnson, J. Lewis, M. Raff, K. Roberts and P. Walter (2002). Molecular biology of the cell. New York, Garland Science.

Antonetti, D. A., E. B. Wolpert, L. DeMaio, N. S. Harhaj and R. C. Scaduto, Jr. (2002). "Hydrocortisone decreases retinal endothelial cell water and solute flux coincident with increased content and decreased phosphorylation of occludin." J Neurochem **80**(4): 667-677.

Barath, P., M. C. Fishbein, J. Cao, J. Berenson, R. H. Helfant and J. S. Forrester (1990). "Detection and localization of tumor necrosis factor in human atheroma." Am J Cardiol **65**(5): 297-302.

Bazzoni, G., E. Dejana and M. G. Lampugnani (1999). "Endothelial adhesion molecules in the development of the vascular tree: the garden of forking paths." Curr Opin Cell Biol **11**(5): 573-581.

Bell, F. P., I. L. Adamson and C. J. Schwartz (1974). "Aortic endothelial permeability to albumin: focal and regional patterns of uptake and transmural distribution of 131I-albumin in the young pig." Exp Mol Pathol **20**(1): 57-68.

Bell, F. P., A. S. Gallus and C. J. Schwartz (1974). "Focal and regional patterns of uptake and the transmural distribution of 131-I-fibrinogen in the pig aorta in vivo." Exp Mol Pathol **20**(2): 281-292.

Bell, F. P., J. B. Somer, I. H. Craig and C. J. Schwartz (1972). "Patterns of aortic Evans blue uptake in vivo and in vitro." Atherosclerosis **16**(3): 369-375.

Boucrot, E. and T. Kirchhausen (2008). "Mammalian cells change volume during mitosis." PLoS One **3**(1): e1477.

Bratzler, R. L., G. M. Chisolm, C. K. Colton, K. A. Smith and R. S. Lees (1977). "The distribution of labeled low-density lipoproteins across the rabbit thoracic aorta in vivo." Atherosclerosis **28**(3): 289-307.

Bruewer, M., A. Luegering, T. Kucharzik, C. A. Parkos, J. L. Madaro, A. M. Hopkins and A. Nusrat (2003). "Proinflammatory Cytokines Disrupt Epithelial Barrier Function by Apoptosis-Independent Mechanisms." The Journal of Immunology **171**: 6164-6172.

Bundgaard, M. (1984). "The three-dimensional organization of tight junctions in a capillary endothelium revealed by serial-section electron microscopy." J Ultrastruct Res **88**(1): 1-17.

Burns, A. R., D. C. Walker, E. S. Brown, L. T. Thurmon, R. A. Bowden, C. R. Keese, S. I. Simon, M. L. Entman and C. W. Smith (1997). "Neutrophil transendothelial migration is independent of tight junctions and occurs preferentially at tricellular corners." J Immunol **159**(6): 2893-2903.

Cancel, L. M., A. Fitting and J. M. Tarbell (2007). "In vitro study of LDL transport under pressurized (convective) conditions." Am J Physiol Heart Circ Physiol **293**(1): H126-132.

Cancel, L. M. and J. M. Tarbell (2010). "The role of apoptosis in LDL transport through cultured endothelial cell monolayers." Atherosclerosis **208**(2): 335-341.

Caplan, B. A. and C. J. Schwartz (1973). "Increased endothelial cell turnover in areas of in vivo Evans Blue uptake in the pig aorta." Atherosclerosis **17**(3): 401-417.

Cavallero, C., E. Turolla and G. Ricevuti (1971). "Cell proliferation in the atherosclerotic plaques of cholesterol-fed rabbits. 1. Colchicine and (3H)thymidine studies." Atherosclerosis **13**(1): 9-20.

Chen, J., J. L. Mehta, N. Haider, X. Zhang, J. Narula and D. Li (2004). "Role of Caspases in Ox-LDL-Induced Apoptotic Cascade in Human Coronary Artery Endothelial Cells." Circulation Research **94**: 370-376.

Chen, Y. L., K. M. Jan, H. S. Lin and S. Chien (1995). "Ultrastructural studies on macromolecular permeability in relation to endothelial cell turnover." Atherosclerosis **118**(1): 89-104.

Chen, Y. L., K. M. Jan, H. S. Lin and S. Chien (1997). "Relationship between endothelial cell turnover and permeability to horseradish peroxidase." Atherosclerosis **133**(1): 7-14.

Chien, S. (2003). "Molecular and mechanical bases of focal lipid accumulation in arterial wall." Prog Biophys Mol Biol **83**(2): 131-151.

Chien, S. (2008). "Effects of disturbed flow on endothelial cells." Ann Biomed Eng **36**(4): 554-562.

Chien, S., S. J. Lin, S. Weinbaum, M. M. Lee and K. M. Jan (1988). "The role of arterial endothelial cell mitosis in macromolecular permeability." Adv Exp Med Biol **242**: 59-73.

Cho, A., L. Mitchell, D. Koopmans and B. L. Langille (1997). "Effects of changes in blood flow rate on cell death and cell proliferation in carotid arteries of immature rabbits." Circ Res **81**(3): 328-337.

Choy, J. C., D. J. Granville, D. W. C. Hunt and B. M. McManus (2001). "Endothelial Cell Apoptosis: Biochemical Characteristics and Potential Implications for Atherosclerosis." Journal of Molecular and Cellular Cardiology **33**: 1673-1690.

Colombo, A., J. Drzewiecki, A. Banning, E. Grube, K. Hauptmann, S. Silber, D. Dudek, S. Fort, F. Schiele, K. Zmudka, G. Guagliumi and M. E. Russell (2003). "Randomized study to assess the effectiveness of slow- and moderate-release polymer-based paclitaxel-eluting stents for coronary artery lesions." Circulation **108**(7): 788-794.

Corfe, B. M., C. Dive and D. R. Garrod (2000). "Changes in intercellular junctions during apoptosis precede nuclear condensation or phosphatidylserine exposure on the cell surface." Cell Death Differ **7**(2): 234-235.

Csiszar, A., Z. Ungvari, A. Koller, J. G. Edwards and G. Kaley (2004). "Proinflammatory phenotype of cronary arteries promotes endothelial apoptosis in aging." Physiological Genomics **17**: 21-30.

Dejana, E., M. G. Lampugnani, O. Martinez-Estrada and G. Bazzoni (2000). "The molecular organization of endothelial junctions and their functional role in vascular morphogenesis and permeability." Int J Dev Biol **44**(6): 743-748.

DeMaio, L., J. M. Tarbell, R. C. Scaduto, Jr., T. W. Gardner and D. A. Antonetti (2004). "A transmural pressure gradient induces mechanical and biological adaptive responses in endothelial cells." Am J Physiol Heart Circ Physiol **286**(2): H731-741.

Deveraux, Q. L. and J. C. Reed (1999). "IAP family proteins--suppressors of apoptosis." Genes Dev **13**(3): 239-252.

Dimmeler, S., J. Haendeler, J. Galle and A. M. Zeiher (1997). "Oxidized low-density lipoprotein induces apoptosis of human endothelial cells by activation of CPP32-like proteases. A mechanistic clue to the 'response to injury' hypothesis." Circulation **95**(7): 1760-1763.

Dimmeler, S., J. Haendeler, V. Rippmann, M. Nehls and A. M. Zeiher (1996). "Shear stress inhibits apoptosis of human endothelial cells." FEBS Lett **399**(1-2): 71-74.

Dulak, J. and A. Jozkowicz (2005). "Anti-angiogenic and anti-inflammatory effects of statins: relevance to anti-cancer therapy." Curr Cancer Drug Targets **5**(8): 579-594.

Duncan, L. E., Jr., K. Buck and A. Lynch (1963). "Lipoprotein Movement Through Canine Aortic Wall." Science **142**: 972-973.

Ekert, P. G., J. Silke and D. L. Vaux (1999). "Caspase Inhibitors." Cell Death and Differentiation **6**: 1081-1086.

Esterbauer, H., J. Gebicki, H. Puhl and G. Jurgens (1992). "The role of lipid peroxidation and antioxidants in oxidative modification of LDL." Free Radic Biol Med **13**(4): 341-390.

Fabbro, D., S. Ruetz, E. Buchdunger, S. W. Cowan-Jacob, G. Fendrich, J. Liebetanz, J. Mestan, T. O'Reilly, P. Traxler, B. Chaudhuri, H. Fretz, J. Zimmermann, T. Meyer, G. Caravatti, P. Furet and P. W. Manley (2002). "Protein kinases as targets for anticancer agents: from inhibitors to useful drugs." Pharmacol Ther **93**(2-3): 79-98.

Ferrara, N. and T. Davis-Smyth (1997). "The biology of vascular endothelial growth factor." Endocr Rev **18**(1): 4-25.

Frangos, S. G., V. Gahtan and B. Sumpio (1999). "Localization of atherosclerosis: role of hemodynamics." Arch Surg **134**(10): 1142-1149.

Freyberg, M. A., D. Kaiser, R. Graf, J. Buttenbender and P. Friedl (2001). "Proatherogenic flow conditions initiate endothelial apoptosis via thrombospondin-1 and the integrin-associated protein." Biochem Biophys Res Commun **286**(1): 141-149.

Fry, D. L., E. E. Herderick and D. K. Johnson (1993). "Local intimal-medial uptakes of 125I-albumin, 125I-LDL, and parenteral Evans blue dye protein complex along the aortas of normocholesterolemic minipigs as predictors of subsequent hypercholesterolemic atherogenesis." Arterioscler Thromb **13**(8): 1193-1204.

Fu, B., F. R. Curry, R. H. Adamson and S. Weinbaum (1997). "A model for interpreting the tracer labeling of interendothelial clefts." Ann Biomed Eng **25**(2): 375-397.

Gerrity, R. G., M. Richardson, J. B. Somer, F. P. Bell and C. J. Schwartz (1977). "Endothelial cell morphology in areas of in vivo Evans blue uptake in the aorta of young pigs. II. Ultrastructure of the intima in areas of differing permeability to proteins." Am J Pathol **89**(2): 313-334.

Gillis, P., U. Savla, O. V. Volpert, B. Jimenez, C. M. Waters, R. J. Panos and N. P. Bouck (1999). "Keratinocyte growth factor induces angiogenesis and protects endothelial barrier function." J Cell Sci **112 (Pt 12)**: 2049-2057.

Gitter, A. H., K. Bendfeldt, J.-D. Schulzke and M. Fromm (2000). "Leaks in the epithelial barrier caused by spontaneous and TNF-α-induced single-cell apoptosis." The FASEB Journal **14**: 1749-1753.

Gooch, K. J., C. A. Dangler and J. A. Frangos (1997). "Exogenous, basal, and flow-induced nitric oxide production and endothelial cell proliferation." J Cell Physiol **171**(3): 252-258.

Green, D. R. and G. Kroemer (2005). "Pharmacological manipulation of cell death: clinical applications in sight?" J Clin Invest **115**(10): 2610-2617.

Greischel, A. and G. Zahn (1989). "Pharmacokinetics of recombinant human tumor necrosis factor alpha in rhesus monkeys after intravenous administration." J Pharmacol Exp Ther **251**(1): 358-361.

Grotte, G. (1956). "Passage of dextran molecules across the blood-lymph barrier." Acta Chir Scand Suppl **211**: 1-84.

Guerard, P., Z. Rakotoniaina, F. Goirand, L. Rochette, M. Dumas, F. Lirussi and M. Bardou (2006). "The HMG-CoA reductase inhibitor, pravastatin, prevents the development of monocrotaline-induced pulmonary hypertension in the rat through reduction of endothelial cell apoptosis and overexpression of eNOS." Naunyn Schmiedebergs Arch Pharmacol **373**(6): 401-414.

Harada-Shiba, M., M. Kinoshita, H. Kamido and K. Shimokado (1998). "Oxidized low density lipoprotein induces apoptosis in cultured human umbilical vein endothelial cells by common and unique mechanisms." J Biol Chem **273**(16): 9681-9687.

Hengartner, M. O. (2000). "The biochemistry of apoptosis." Nature **407**: 770-776.

Hogg, N., J. Browning, T. Howard, C. Winterford, D. Fitzpatrick and G. Gobe (1999). "Apoptosis in Vascular Endothelial Cells Caused by Serum Deprivation, Oxidative Stress and Transforming Growth Factor-β." Endothelium **7**(1): 35-49.

Hong, F. D., J. Chen, S. Donovan, N. Schneider and P. D. Nisen (1999). "Taxol, vincristine or nocodazole induces lethality in G1-checkpoint-defective human astrocytoma U373MG cells by triggering hyperploid progression." Carcinogenesis **20**(7): 1161-1168.

Hu, X., R. H. Adamson, B. Liu, F. E. Curry and S. Weinbaum (2000). "Starling forces that oppose filtration after tissue oncotic pressure is increased." Am J Physiol Heart Circ Physiol **279**(4): H1724-1736.

Hu, X. and S. Weinbaum (1999). "A new view of Starling's hypothesis at the microstructural level." Microvasc Res **58**(3): 281-304.

Huang, A. L., K. M. Jan and S. Chien (1992). "Role of intercellular junctions in the passage of horseradish peroxidase across aortic endothelium." Lab Invest **67**(2): 201-209.

Jordan, M. A., R. J. Toso, D. Thrower and L. Wilson (1993). "Mechanism of mitotic block and inhibition of cell proliferation by taxol at low concentrations." Proc Natl Acad Sci U S A **90**(20): 9552-9556.

Kamiyama, M., Y. Kishimoto, M. Tani, K. Utsunomiya and K. Kondo (2009). "Effects of equol on oxidized low-density lipoprotein-induced apoptosis in endothelial cells." J Atheroscler Thromb **16**(3): 239-249.

Kedem, O. and A. Katchalsky (1958). "Thermodynamic analysis of the permeability of biological membranes to non-electrolytes." Biochim Biophys Acta **27**(2): 229-246.

Ku, D. N., D. P. Giddens, C. K. Zarins and S. Glagov (1985). "Pulsatile flow and atherosclerosis in the human carotid bifurcation. Positive correlation between plaque location and low oscillating shear stress." Arteriosclerosis **5**(3): 293-302.

Kureishi, Y., Z. Luo, I. Shiojima, A. Bialik, D. Fulton, D. J. Lefer, W. C. Sessa and K. Walsh (2000). "The HMG-CoA reductase inhibitor simvastatin activates the protein kinase Akt and promotes angiogenesis in normocholesterolemic animals." Nat Med **6**(9): 1004-1010.

Laufs, U., V. La Fata, J. Plutzky and J. K. Liao (1998). "Upregulation of endothelial nitric oxide synthase by HMG CoA reductase inhibitors." Circulation **97**(12): 1129-1135.

Lefkowitz, R. J. and J. T. Willerson (2001). "Prospects for cardiovascular research." Jama **285**(5): 581-587.

Levesque, M. J., R. M. Nerem and E. A. Sprague (1990). "Vascular endothelial cell proliferation in culture and the influence of flow." Biomaterials **11**(9): 702-707.

Li, H., M. I. Cybulsky, M. A. Gimbrone, Jr. and P. Libby (1993). "Inducible expression of vascular cell adhesion molecule-1 by vascular smooth muscle cells in vitro and within rabbit atheroma." Am J Pathol **143**(6): 1551-1559.

Li, Y. S., J. H. Haga and S. Chien (2005). "Molecular basis of the effects of shear stress on vascular endothelial cells." J Biomech **38**(10): 1949-1971.

Lin, S.-J., K.-m. Jan and S. Chien (1990). "Role of Dying Endothelial Cells in Transendothelial Macromolecular Transport." Arteriosclerosis **10**: 703-709.

Lin, S.-J., K.-M. Jan, G. Schuessler, S. Weinbaum and S. Chien (1988). "Enhanced Macromolecular Permeability of Aortic Endothelial Cells in Association with Mitosis." Atherosclerosis **73**: 223-232.

Lin, S. J., K. M. Jan, S. Weinbaum and S. Chien (1989). "Transendothelial transport of low density lipoprotein in association with cell mitosis in rat aorta." Arteriosclerosis **9**(2): 230-236.

Liu, Y., B. P. Chen, M. Lu, Y. Zhu, M. B. Stemerman, S. Chien and J. Y. Shyy (2002). "Shear stress activation of SREBP1 in endothelial cells is mediated by integrins." Arterioscler Thromb Vasc Biol **22**(1): 76-81.

Lizard, G., S. Monier, C. Cordelet, L. Gesquiere, V. Deckert, S. Gueldry, L. Lagrost and P. Gambert (1999). "Characterization and comparison of the mode of cell death, apoptosis versus necrosis, induced by 7beta-hydroxycholesterol and 7-ketocholesterol in the cells of the vascular wall." Arterioscler Thromb Vasc Biol **19**(5): 1190-1200.

Luthra, S., J. Dong, A. L. Gramajo, M. Chwa, D. W. Kim, A. Neekhra, B. D. Kuppermann and M. C. Kenney (2008). "7-Ketocholesterol activates caspases-3/7, -8, and -12 in human microvascular endothelial cells in vitro." Microvasc Res **75**(3): 343-350.

Malek, A. M., S. L. Alper and S. Izumo (1999). "Hemodynamic shear stress and its role in atherosclerosis." Jama **282**(21): 2035-2042.

McKenzie, J. A. and A. J. Ridley (2007). "Roles of Rho/ROCK and MLCK in TNF-alpha-induced changes in endothelial morphology and permeability." J Cell Physiol **213**(1): 221-228.

Miao, H., Y. L. Hu, Y. T. Shiu, S. Yuan, Y. Zhao, R. Kaunas, Y. Wang, G. Jin, S. Usami and S. Chien (2005). "Effects of flow patterns on the localization and expression of VE-cadherin at vascular endothelial cell junctions: in vivo and in vitro investigations." J Vasc Res **42**(1): 77-89.

Michel, C. C. (1997). "Starling: the formulation of his hypothesis of microvascular fluid exchange and its significance after 100 years." Exp Physiol **82**(1): 1-30.

Michel, C. C. and F. E. Curry (1999). "Microvascular permeability." Physiol Rev **79**(3): 703-761.

Michel, C. C. and M. E. Phillips (1987). "Steady-state fluid filtration at different capillary pressures in perfused frog mesenteric capillaries." J Physiol **388**: 421-435.

Nguyen, T., J. Toussaint, K. M. Jan and D. Rumschitzki (2007). The Effect Of Altered Aquaporin-1 Expression In Chronically Hypertensive Vessels. BMES 2007 Fall Meeting, Los Angeles, CA.

Nielsen, L. B. (1996). "Transfer of low density lipoprotein into the arterial wall and risk of atherosclerosis." Atherosclerosis **123**(1-2): 1-15.

Nielsen, L. B., B. G. Nordestgaard, S. Stender and K. Kjeldsen (1992). "Aortic permeability to LDL as a predictor of aortic cholesterol accumulation in cholesterol-fed rabbits." Arterioscler Thromb **12**(12): 1402-1409.

O'Connor, D. S., J. S. Schechner, C. Adida, M. Mesri, A. L. Rothermel, F. Li, A. K. Nath, J. S. Pober and D. C. Altieri (2000). "Control of apoptosis during angiogenesis by survivin expression in endothelial cells." Am J Pathol **156**(2): 393-398.

Ogunrinade, O., G. T. Kameya and G. A. Truskey (2002). "Effect of fluid shear stress on the permeability of the arterial endothelium." Ann Biomed Eng **30**(4): 430-446.

Pang, Z. and J. M. Tarbell (2003). "In vitro study of Starling's hypothesis in a cultured monolayer of bovine aortic endothelial cells." J Vasc Res **40**(4): 351-358.

Pappenheimer, J. R., E. M. Renkin and L. M. Borrero (1951). "Filtration, diffusion and molecular sieving through peripheral capillary membranes; a contribution to the pore theory of capillary permeability." Am J Physiol **167**(1): 13-46.

Pasquier, E., M. Carre, B. Pourroy, L. Camoin, O. Rebai, C. Briand and D. Braguer (2004). "Antiangiogenic activity of paclitaxel is associated with its cytostatic effect, mediated by the initiation but not completion of a mitochondrial apoptotic signaling pathway." Mol Cancer Ther **3**(10): 1301-1310.

Patlak, C. S., D. A. Goldstein and J. F. Hoffman (1963). "The flow of solute and solvent across a two-membrane system." J Theor Biol **5**(3): 426-442.

Petrache, I., A. Birukova, S. I. Ramirez, J. G. N. Garcia and A. D. Verin (2003). "The Role of the Microtubules in Tumor Necrosis Factor-α-Induced Endothelial Cell Permeability " American Journal of Respiratory Cell and Molecular Biology **28**: 574-581.

Piraino, F., L. M. Cancel and J. M. Tarbell (under review). "Effect of simvastatin on the apoptosis and convective permeability of endothelial cell monolayers." Atherosclerosis.

Polunovsky, V. A., C. H. Wendt, D. H. Ingbar, M. S. Peterson and P. B. Bitterman (1994). "Induction of Endothelial Cell Apoptosis by TNFα: Modulation by Inhibitors of Protein Synthesis." Experimental Cell Research **214**: 584-594.

Predescu, S. A., D. N. Predescu and A. B. Malik (2007). "Molecular determinants of endothelial transcytosis and their role in endothelial permeability." Am J Physiol Lung Cell Mol Physiol **293**(4): L823-842.

Rangaswamy, S., M. S. Penn, G. M. Saidel and G. M. Chisolm (1997). "Exogenous oxidized low-density lipoprotein injures and alters the barrier function of endothelium in rats in vivo." Circ Res **80**(1): 37-44.

Raymond, G. M., M. M. Jumblatt, S. P. Bartels and A. H. Neufeld (1986). "Rabbit corneal endothelial cells in vitro: effects of EGF." Invest Ophthalmol Vis Sci **27**(4): 474-479.

Rippe, B., B. I. Rosengren, O. Carlsson and D. Venturoli (2002). "Transendothelial transport: the vesicle controversy." J Vasc Res **39**(5): 375-390.

Rosamond, W., K. Flegal, G. Friday, K. Furie, A. Go, K. Greenlund, N. Haase, M. Ho, V. Howard, B. Kissela, S. Kittner, D. Lloyd-Jones, M. McDermott, J. Meigs, C. Moy, G. Nichol, C. J. O'Donnell, V. Roger, J. Rumsfeld, P. Sorlie, J. Steinberger, T. Thom, S. Wasserthiel-Smoller and Y. Hong (2007). "Heart disease and stroke statistics--2007 update: a report from the American Heart Association Statistics Committee and Stroke Statistics Subcommittee." Circulation **115**(5): e69-171.

Rosenblatt, J., M. C. Raff and L. P. Cramer (2001). "An epithelial cell destined for apoptosis signals its neighbors to extrude it by an actin- and myosin-dependent mechanism." Curr Biol **11**(23): 1847-1857.

Rosengren, B. I., O. Carlsson, D. Venturoli, O. al Rayyes and B. Rippe (2004). "Transvascular passage of macromolecules into the peritoneal cavity of normo- and hypothermic rats in vivo: active or passive transport?" J Vasc Res **41**(2): 123-130.

Ross, R. (1993). "The pathogenesis of atherosclerosis: a perspective for the 1990s." Nature **362**(6423): 801-809.

Ross, R. (1993). "Rous-Whipple Award Lecture. Atherosclerosis: a defense mechanism gone awry." Am J Pathol **143**(4): 987-1002.

Ross, R. (1999). "Atherosclerosis--an inflammatory disease." N Engl J Med **340**(2): 115-126.

Ross, R. and J. A. Glomset (1976). "The pathogenesis of atherosclerosis (second of two parts)." N Engl J Med **295**(8): 420-425.

Rowinsky, E. K. (1997). "The development and clinical utility of the taxane class of antimicrotubule chemotherapy agents." Annu Rev Med **48**: 353-374.

Schiff, P. B. and S. B. Horwitz (1980). "Taxol stabilizes microtubules in mouse fibroblast cells." Proc Natl Acad Sci U S A **77**(3): 1561-1565.

Schwartz, C. J., J. L. Kelley, R. M. Nerem, E. A. Sprague, M. M. Rozek, A. J. Valente, E. H. Edwards, A. R. Prasad, J. J. Kerbacher and S. A. Logan (1989). "Pathophysiology of the atherogenic process." Am J Cardiol **64**(13): 23G-30G.

Schwartz, S. M. and E. P. Benditt (1976). "Clustering of replicating cells in aortic endothelium." Proc Natl Acad Sci U S A **73**(2): 651-653.

Schwenke, D. C. and T. E. Carew (1989). "Initiation of atherosclerotic lesions in cholesterol-fed rabbits. I. Focal increases in arterial LDL concentration precede development of fatty streak lesions." Arteriosclerosis **9**(6): 895-907.

SenBanerjee, S., Z. Lin, G. B. Atkins, D. M. Greif, R. M. Rao, A. Kumar, M. W. Feinberg, Z. Chen, D. I. Simon, F. W. Luscinskas, T. M. Michel, M. A. Gimbrone, Jr., G. Garcia-Cardena and M. K. Jain (2004). "KLF2 Is a novel transcriptional regulator of endothelial proinflammatory activation." J Exp Med **199**(10): 1305-1315.

Shang, W., I. Konidari and D. W. Schomberg (2001). "2-Methoxyestradiol, an endogenous estradiol metabolite, differentially inhibits granulosa and endothelial cell mitosis: a potential follicular antiangiogenic regulator." Biol Reprod **65**(2): 622-627.

Shepherd, J., S. M. Cobbe, I. Ford, C. G. Isles, A. R. Lorimer, P. W. MacFarlane, J. H. McKillop and C. J. Packard (1995). "Prevention of coronary heart disease with pravastatin in men with hypercholesterolemia. West of Scotland Coronary Prevention Study Group." N Engl J Med **333**(20): 1301-1307.

Shou, Y., K. M. Jan and D. S. Rumschitzki (2007). "Transport in rat vessel walls. II. Macromolecular leakage and focal spot size growth in rat arteries and veins." Am J Physiol Heart Circ Physiol **292**(6): H2881-2890.

Silverthorn, D. U. (2000). Human Physiology: An Integrated Approach, Benjamin-Cummings Publishing Company.

Simionescu, M. (2007). "Implications of early structural-functional changes in the endothelium for vascular disease." Arterioscler Thromb Vasc Biol **27**(2): 266-274.

Simionescu, N., M. Siminoescu and G. E. Palade (1975). "Permeability of muscle capillaries to small heme-peptides. Evidence for the existence of patent transendothelial channels." J Cell Biol **64**(3): 586-607.

Somer, J. B. and C. J. Schwartz (1971). "Focal 3 H-cholesterol uptake in the pig aorta." Atherosclerosis **13**(3): 293-304.

Spagnuolo, R., M. Corada, F. Orsenigo, L. Zanetta, U. Deuschle, P. Sandy, C. Schneider, C. J. Drake, F. Breviario and E. Dejana (2004). "Gas1 is induced by VE-cadherin and vascular endothelial growth factor and inhibits endothelial cell apoptosis." Blood **103**(8): 3005-3012.

Spyridopoulos, I., E. Brogi, M. Kearney, A. B. Sullivan, C. Cetrulo, J. M. Isner and D. W. Losordo (1997). "Vascular Endothelial Growth Factor Inhibitis Endothelial Cell Apoptosis Induced by Tumor Necrosis Factor-α: Balance Between Growth and Death Signals." Journal of Molecular and Cellular Cardiology **29**: 1321-1330.

Sridhar, J., N. Akula and N. Pattabiraman (2006). "Selectivity and potency of cyclin-dependent kinase inhibitors." Aaps J **8**(1): E204-221.

Stemerman, M. B. (1981). "Effects of moderate hypercholesterolemia on rabbit endothelium." Arteriosclerosis **1**(1): 25-32.

Stemerman, M. B., E. M. Morrel, K. R. Burke, C. K. Colton, K. A. Smith and R. S. Lees (1986). "Local variation in arterial wall permeability to low density lipoprotein in normal rabbit aorta." Arteriosclerosis **6**(1): 64-69.

Stone, G. W., S. G. Ellis, D. A. Cox, J. Hermiller, C. O'Shaughnessy, J. T. Mann, M. Turco, R. Caputo, P. Bergin, J. Greenberg, J. J. Popma and M. E. Russell (2004). "A polymer-based, paclitaxel-eluting stent in patients with coronary artery disease." N Engl J Med **350**(3): 221-231.

Tarbell, J. M. (2003). "Mass transport in arteries and the localization of atherosclerosis." Annu Rev Biomed Eng **5**: 79-118.

Tarbell, J. M. and M. Y. Pahakis (2006). "Mechanotransduction and the glycocalyx." J Intern Med **259**(4): 339-350.

Terrano, D. T., M. Upreti and T. C. Chambers "Cyclin-dependent kinase 1-mediated Bcl-xL/Bcl-2 phosphorylation acts as a functional link coupling mitotic arrest and apoptosis." Mol Cell Biol **30**(3): 640-656.

Tricot, O., Z. Mallat, C. Heymes, J. Belmin, G. Leseche and A. Tedgui (2000). "Relation Between Endothelial Cell Apoptosis and Blood Flow Direction in Human Atherosclerotic Plaques." Circulation **101**: 2450-2453.

Truskey, G. A., W. L. Roberts, R. A. Herrmann and R. A. Malinauskas (1992). "Measurement of endothelial permeability to 125I-low density lipoproteins in rabbit arteries by use of en face preparations." Circ Res **71**(4): 883-897.

Tuma, P. L. and A. L. Hubbard (2003). "Transcytosis: crossing cellular barriers." Physiol Rev **83**(3): 871-932.

Van Noorden, C. J. (2001). "The history of Z-VAD-FMK, a tool for understanding the significance of caspase inhibition." Acta Histochem **103**(3): 241-251.

Vasile, E., M. Simionescu and N. Simionescu (1983). "Visualization of the binding, endocytosis, and transcytosis of low-density lipoprotein in the arterial endothelium in situ." J Cell Biol **96**(6): 1677-1689.

Verin, A. D., A. Birukova, P. Wang, F. Liu, P. Becker, K. Birukov and J. G. Garcia (2001). "Microtubule disassembly increases endothelial cell barrier dysfunction: role of MLC phosphorylation." Am J Physiol Lung Cell Mol Physiol **281**(3): L565-574.

Verkman, A. S. (2006). "Aquaporins in endothelia." Kidney Int **69**(7): 1120-1123.

Walker, D. C., A. MacKenzie and S. Hosford (1994). "The structure of the tricellular region of endothelial tight junctions of pulmonary capillaries analyzed by freeze-fracture." Microvasc Res **48**(3): 259-281.

Wang, N., H. Miao, Y. S. Li, P. Zhang, J. H. Haga, Y. Hu, A. Young, S. Yuan, P. Nguyen, C. C. Wu and S. Chien (2006). "Shear stress regulation of Kruppel-like factor 2 expression is flow pattern-specific." Biochem Biophys Res Commun **341**(4): 1244-1251.

Wang, T. H., H. S. Wang and Y. K. Soong (2000). "Paclitaxel-induced cell death: where the cell cycle and apoptosis come together." Cancer **88**(11): 2619-2628.

Ward, B. J., K. F. Bauman and J. A. Firth (1988). "Interendothelial junctions of cardiac capillaries in rats: their structure and permeability properties." Cell Tissue Res **252**(1): 57-66.

Weinbaum, S. (1998). "1997 Whitaker Distinguished Lecture: Models to solve mysteries in biomechanics at the cellular level; a new view of fiber matrix layers." Ann Biomed Eng **26**(4): 627-643.

Weinbaum, S., J. M. Tarbell and E. R. Damiano (2007). "The structure and function of the endothelial glycocalyx layer." Annu Rev Biomed Eng **9**: 121-167.

Weinbaum, S., G. Tzeghai, P. Ganatos, R. Pfeffer and S. Chien (1985). "Effect of Cell Turnover and Leaky Junctions on Arterial Macromolecular Transport." American Journal of Physiology **248**: H945-H958.

Wiklund, O., T. E. Carew and D. Steinberg (1985). "Role of the low density lipoprotein receptor in penetration of low density lipoprotein into rabbit aortic wall." Arteriosclerosis **5**(2): 135-141.

Wojciak-Stothard, B., A. Entwistle, R. Garg and A. J. Ridley (1998). "Regulation of TNF-alpha-induced reorganization of the actin cytoskeleton and cell-cell junctions by Rho, Rac, and Cdc42 in human endothelial cells." J Cell Physiol **176**(1): 150-165.

Wright, H. P. (1972). "Mitosis patterns in aortic endothelium." Atherosclerosis **15**(1): 93-100.

Wu, J., C. Parungo, G. Wu, P. M. Kang, R. J. Laham, F. W. Sellke, M. Simons and J. Li (2004). "PR39 Inhibits Apoptosis in Hypoxic Endothelial Cells: Role of Inhibitor Apoptosis Protein-2." Circulation **109**: 1660-1667.

Zahn, G. and A. Greischel (1989). "Pharmacokinetics of tumor necrosis factor alpha after intravenous administration in rats. Dose dependence and influence of tumor necrosis factor beta." Arzneimittelforschung **39**(9): 1180-1182.